EXPERIMENTAL ANALYSIS OF WELDING PARAMETERS OF WELDING JOINT OF AUSTENATIC STEEL (300 SERIES) BY TIG WELDING

Author

MUHAMMAD ASAD DAR

Regn Number

00000273727

Supervisor

DR. SADAQAT ALI

SCHOOL OF MECHANICAL & MANUFACTURING ENGINEERING

NATIONAL UNIVERSITY OF SCIENCES AND TECHNOLOGY

ISLAMABAD

JULY, 2022

Experimental Analysis of Welding Parameters of Welding Joints of Austenitic Steel (300 Series) by TIG Welding

Author

MUHAMMAD ASAD DAR

Regn Number

00000273727

A thesis submitted in partial fulfillment of the requirements for the degree of

MS Mechanical Engineering

Thesis Supervisor:

Dr. SADAQAT ALI

Thesis Supervisor‟s Signature: _____

DEPARTMENT

SCHOOL OF MECHANICAL & MANUFACTURING ENGINEERING

NATIONAL UNIVERSITY OF SCIENCES AND TECHNOLOGY,

ISLAMABAD

JULY,2022

1.1.1 Declaration

I certify that this research work titled "*Experimental Analysis of Welding Parameters of Welding Joints of Austenitic Steel (300 Series) by TIG Welding"* is my own work. The work has not been presented elsewhere for assessment. The material that has been used from other sources it has been properly acknowledged / referred.

Signature of Student

Muhammad Asad Dar

2018-NUST-MS-Mech-00000273727

1.1.2 Plagiarism Certificate (Turnitin Report)

This thesis has been checked for Plagiarism. Turnitin report endorsed by Supervisor is attached.

Signature of Student
Muhammad Asad Dar
00000273727

Signature of Supervisor
Dr.Sadaqat Ali

1.1.3 Copyright Statement

- Copyright in text of this thesis rests with the student author. Copies (by any process) either in full, or of extracts, may be made only in accordance with instructions given by the author and lodged in the Library of NUST School of Mechanical & Manufacturing Engineering (SMME). Details may be obtained by the Librarian. This page must form part of any such copies made. Further copies (by any process) may not be made without the permission (in writing) of the author.
- The ownership of any intellectual property rights which may be described in this thesis is vested in NUST School of Mechanical & Manufacturing Engineering, subject to any prior agreement to the contrary, and may not be made available for use by third parties without the written permission of the SMME, which will prescribe the terms and conditions of any such agreement.
- Further information on the conditions under which disclosures and exploitation may take place is available from the Library of NUST School of Mechanical & Manufacturing Engineering, Islamabad.

1.1.4 Acknowledgements

I am thankful to my Creator Allah Subhana-Watala who has guided me throughout this work, at every step and for every new thought which emerged in my mind. Indeed I could have done nothing without your eternal help and guidance. Whosoever helped me throughout the course of my thesis, whether my parents or any other individual was your will, so indeed none be worthy of praise but you.

I am truly thankful to my loving parents, who reared me from the time I was unable to walk and have continued to support me in every aspect of my life.

I would also like to express special thanks to my supervisor, respectable Dr.Sadaqat Ali, for his supervision, continuous support, encouragement, research approach and expertise in this research work.

I would also like to pay special thank for his efforts and valuable guidance of Dr. Sadaqat Ali who made it possible for me not only to serve the purpose but also to enhance my research skills as well. I am very grateful for his inspiration and guidance throughout the research work. I am highly obliged to the invaluable help and guidance of Dr. Emad Ud Din for the finalization of all the MS thesis/degree requirements as a supervisor in place of Dr.Sadaqat Ali tremendous support and cooperation. Each time I got stuck in something, he came up with the solution. Without his help I wouldn‟t have been able to complete my thesis. I appreciate his patience and guidance throughout the whole thesis.

My deep gratitude also goes to my Research Committee members, comprising of Dr. Emad ud Din, Dr. Aamir Mubashir and Dr. Adnan Munir for their support, guidance and encouragement during the research work.

Finally, I would like to express my gratitude to all the individuals who have rendered valuable assistance to my study.

Dedicated to my exceptional parents, sister, brother, wife and children's whose tremendous support and cooperation led me to this wonderful accomplishment

Abstract

After the advent of welding as a joining method, welding technology was employed as a key joining technique in hi-tech industry for the welding of AISI 321 structures such as pressure vessels and aerospace applications. Due to their high strength and low weight ratio, stainless steel AISI 321 is extensively used for various applications in a number of industries including nuclear, aerospace, chemical, petrochemical, fertilizer, and food processing industries and in many other major industrial operations. Manufacturing industry has taken advantages of tungsten Inter gas (TIG) welding to join structures. High quality weld for stainless steels and non-ferrous alloys are also obtained with this technique. However, in comparison to arc welding processes the TIG welding has lower productivity due to shallow penetration, which confines its application. From industrial point of view, stainless steel AISI 321 is very commonly used material due to its improved corrosion resistance, low weight ratio and better creep rupture strength.

In this experimental work, the main objectives are to analyze and optimize the joining of stainless steel AISI 321 sheet by tungsten Inter Gas (TIG) welding using Taguchi experimental design. The current, voltage, gas flow rate and filler rod are the variable parameters in this study. The properties namely ultimate tensile strength (UTS), yield strength, % elongation, joint quality and hardness of stainless steel AISI 321 are investigated by using filler material 316L and 308L at varying current, voltage and gas flow rate.

Key Words: *Tungsten Inter Gas Welding, Ultimate tensile strength, % elongation and AISI 321*

Table of Contents

List of Table

List of Figures

CHAPTER 1 INTRODUCTION

1.1 INRODUCTION

GTAW (Gas Tungsten Arc Welding), also known as Tungsten Inert Gas welding (TIG) is a fusion welding technique that uses a non-oxidizing gas to shield the weld area from oxidation [1]. The required heat for welding is generated by arc between electrode (tungsten) and the workpiece. In TIG welding filler material is injected onto weld area, either manually or automatically, and filler wire is liquefied with base metal. All types of steel are easily welded using GTAW, and it can be used to weld austenitic steel with an insert or support ring. TIG welding is extensively utilized in shell to tube heat exchangers to attach tubes on sheets [1].

1.2 PROBLEM STATEMENT

According to the available literature, the welding of AISI321 stainless steel is preferred with filler wire 347. It is pertinent to mention here that 347 filler wire is a controlled item due to its utilization in aerospace industry and is not easily available in market. In many instances, grades 304 and 316L have been used [2] for welding of AISI 321. Therefore, current comparative study of Welding parameters (current, voltage and gas flow rate) and filler metal (308L and 316L wires) on TIG welding of AISI321 is conducted to find out the optimal mechanical properties.

1.3 AIM AND OBJECTIVE

For austenitic steel AISI321, experimental investigation was performed to find appropriate welding parameters such as current, voltage, filler and gas flow. The optimal welding parameters and filler rod will be created based on the results received.

The objective of the experimental study was:

1. Literature study on welding of AISI321 was performed.
2. Experimental study to define the influence of multiple weld setting and filler wire on mechanical performance of AISI321 Stainless steel welds.

3. Experimental data was analyzed using MINITAB.
4. On the basis of results of current study conclusions and recommendations were drawn.

1.4 HYPOTHESIS

The compatibility of welding parameters such as current, voltage, gas flow & filler material on mechanical performance of austenitic steel AISI321 was investigated. During said work ER316L and ER308L filler metal rods were used. Hypothesis of this work states "Optimizing TIG welding parameters for AISI 321 through experimental evaluation"

1.5 METHODOLOGY

This experimental study is based on determining the micro-structure, surface roughness, hardness, yield strength and tensile strength of austenitic steel AISI 321 with different welding parameters and filler material. Tests were performed on 3mm AISI 321 stainless steel sheet weld with ER308L and ER316L filler wire. Nine samples (60 x 60 x 3 mm) of each filler rod were made and tested at various welding parameters before the ideal welded arrangement was chosen.

1.6 SIGNIFICANCE

Stainless steel AISI321 is normally utilized in automotive and aerospace industries due its corrosion resistance, good strength and weight saving. Austenitic steel AISI321 is a unique grade of steel because of its ability to withstand corrosion. This experiment yielded reliable results with welding of AISI 321 with ER316L and ER308L filler wire.

1.7 OUTLINE OF RESEARCH

Chapter no.1 includes Introduction, problem statement, purpose and objectives, hypothesis, methodology, and importance of research.

Chapter no.2 presents literature assessment on TIG welding parameters for austenitic steel. This chapter also contains the results of earlier research on the subject topic. In the current analysis, this experiment was used as a reference. It serves as a starting point for the experiments.

Chapter no.3 depicts the experimental setup for the experiments conducted in the current study. It also covers the findings of the experiments that were conducted.
Chapter no.4 contains results from experimental data and welding parameters optimization using MINITAB.

Chapter no. 5 discusses conclusions and future recommendations.

CHAPTER 2: LITERATURE REVIEW

2.1 INTRODUCTION

Current study is dedicated on predicting strength and other mechanical properties of various types of steels that have been welded using tungsten arc welding (TIG). The available literature was reviewed and same is discussed in chapter. The available literature is divided into the following categories:

- Current study is focused on welding process employing Tungsten Arc Welding (TIG)
- Control parameter and its impact on welding quality
- Control on mechanical Properties of Steel by using ER316L and ER308L filler
- Parameters optimization through ANOVA methodology

2.2 WELDING PROCESS

Welding is the process of fusing metal by bringing them in proximity and heating the places of contact to a state of fusion. The process of welding is categorized in two sets i.e. fusion welding and forge welding. heat-based joining technique is known as fusion welding whereas forge welding is a process of fusing metals using pressure and heat [3].

2.2.1 Forge Welding

In this welding, initially the job is heated in a furnace to a specific temperature, afterwards they are hammered together. Electric-Resistance, Seam, Spot, Upset Welding, Projection, and Flash welding are various methods that uses heat and pressure to join metals together [3].

2.2.2 Fusion Welding

In this process work is held in placed while the molten metal is delivered to the joint is known as fusion welding. Base metal or filler metal is used for provision of molten metal. Upon the solidification or fusion of molten metal joint is formed [3]. Thermite, gas and arc welding are the examples of fusion welding.

2.3 ARC WELDING

To create an arc between the electrodes, an electrical power supply is utilized and the work-piece metals to be connected, resulting in the melting of the work-piece metals at the interface in order to complete the weld [3]. The arc welding method utilize either an AC or DC power supply. In arc welding, electrodes can be either consumable or non consumable. External filler material can be employed for non consumable electrodes. Different type of for arc welding processes[3] are enlisted as:

- Carbon Arc Welding (CAW)
- Shielded Metal Arc Welding (SMAW)
- Flux Cored Arc Welding (FCAW)
- Gas Tungsten Arc Welding (GTAW)
- Gas Metal Arc Welding (GMAW)
- Plasma Arc Welding (PAW)
- Atomic Hydrogen Welding (AHW)
- Electro slag Welding (ESW)
- Stud Arc Welding (SAW)

2.3.1 Stainless Steel Weld Technique

Welding of stainless steel is performed by Gas Tungsten Arc Welding (GTAW or TIG), Plasma Arc Welding (PAW), Shielded Metal Arc Welding (SMAW or MMA), Gas Metal Arc Welding (GMAW or MIG/MAG), Fluxed Core Arc Welding (FCAW or FCW), Submerged Arc Welding (SAW), Electric Resistance Welding (ERW) and LASER Welding.

2.3.1.1 Gas Tungsten Arc Welding

Welding process that uses tungsten electrode is known as Gas tungsten arc welding (GTAW) or tungsten inert gas (TIG) welding. Shielding gas (helium, Argon) is used for protection of the weld area from atmospheric contamination, and filler rod is used for welding of work piece. Constant current welding power source supply the energy which is directed across the arc through a column of high ionized gas[4]. Alloys of Non ferrous metals and thin sheets of stainless steel are commonly weld by tungsten inert gas (TIG) welding.

2.3.1.2 Plasma Arc Welding

It uses a built-in nozzle system to create a thin, concentrated transferred plasma arc with deep penetration properties [5]. Automatic welding plants uses this process where speed and productivity is required. PAW can weld sheet up to 8mm thickness. Blend of PAW / TIG with filler rod is used for welding of heavier square-edged butt joint. Argon backing during welding protect the bead from corrosion [5].

2.3.1.3 Shield Metal Arc Welding

In this welding process, the arc is hit among the electrode (flux coated) and the workpiece, which causes the melting of the surface of both generating the weld pool [5]. The instantaneous melting of the flux layer produces gas and slag on the rod, it protects the weld joint from the environment.

2.3.1.4 Gas Metal Arc Welding

It is a partial automatic welding process, which uses an argon-rich shielding gas and solid wire electrode. It is used for mass production. By adding the oxygen, helium, or carbon dioxide in the gas mixture stability of the arc stability and features weld bead can be improved [6].

2.3.1.5 Submerged Arc Welding

It is a completely automated wire and flux powder shielded arc technique capable of high rate deposition, quick travel speeds, and high weld quality (refer Figure 2-3). It is applied in continuous down hand fillet and butt welds in thicker section plate, pipe, vessels, and stainless steel casing of carbon steel components [4].

2.3.1.6 Electric Resistance Welding

It involves heating of metal pieces through electric current and melting the metal at the joint. It is commonly employed in the manufacturing of steel tubing and vehicle bodies assemblies [7].

2.3.1.7 LASER Welding

It uses a laser beam to fuse two or more pieces of material together. The ends of the work piece are heated and melted through beam thus making a joint. LBW is used in the electronics components manufacturing and aerospace industries [3].

2.3.2 Gas Tungsten Arc (GTA) or Tungsten Inert Gas (TIG) Welding

It is a fusion welding technique that uses an inert gas for shielding of weld zone from atmospheric effect and an electric arc for heating and melting of tungsten electrode and the work piece as shown in figure 2-1. This technique was introduced in World War II, for welding of magnesium and aluminum in aircraft industry [8]. Stainless steel pipes and sheet can easily weld with GTAW or TIG with or without an insert or backing ring and it is also used for joining tubes and sheets in shell and tube heat exchangers.

Manually feeding the filler metal results in slow welding of thick components. Automating the feeding of filler metal and heating it using resistance heating, hot-wire GTAW may increase welding speed and achieve greater deposition rates.

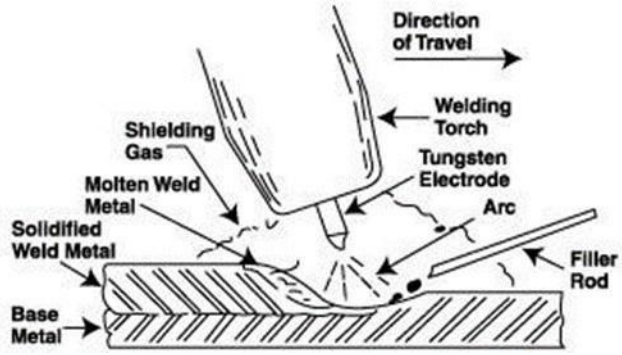

Figure 2-1: GTAW Basic Working Principal [9]

The Tungsten Inert Gas (TIG) welding setup includes a welding torch, a non consumable tungsten electrode, constant current power supply and a shielded gas source as shown in figure 2-2.

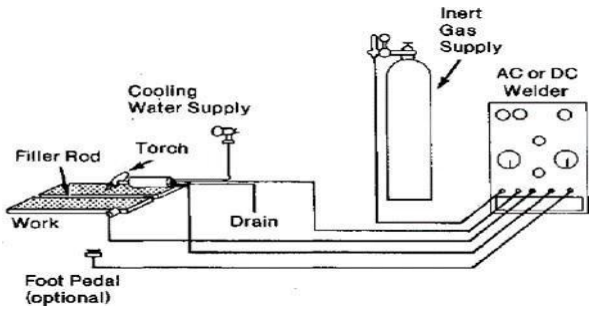

Figure 2-2: GTAW setup [9]

2.3.2.1 Advantages of TIG Welding

Depending on the superiority of weld and strength of joints it has some advantages on other welding techniques [4] such as:

- No flux required
- Improved resistance to corrosion
- Not any Slag formation
- High deposit rate
- Penetration at deep rate
- Welding of all ferrous and non ferrous metals

2.3.2.2 Disadvantages of TIG welding

Some of the disadvantages of the TIG welding [4] are:

- Equipment used is more expensive and less portable
- Welding on sharp corner is difficult
- Continuous exposure of radiation during welding causes harmful effects
- Frequent grinding of non consumable electrode is required

2.4 TIG WIRES

The selection of TIG wires depends on the following parameters [10] :

- Material composition of weld
- Mechanical characteristics of the weld material and base material
- Corrosion resistance of weld and base metal

- Design of Joint
- Base material thickness
- Economical

2.5 WELD DESIGN

Selection of accurate weld joint design is the most important element in fabrication process. Poorly welded joint design can negate most optimum welding condition. The main consideration in weld joint design is the appropriate material, cost effective joint design, minimum welding, accessibility and space for movement of electrode, filler and inspection. The weld joints have five basic types.

2.5.1 Butt Joint

Two sheets lying in the same plane are joint together through butt joint.

2.5.2 Corner Joint

Two members lying approximately at right angles to each other are welded through corner joint.

2.5.3 T-Joint

Two sheets lying at right angle to each other in the form of T are joined through T joint.

2.5.4 Lap Joint

Overlapping members are welded through lap joint.

2.5.5 Edge Joint

Parallel sheets are join together through edge joint.

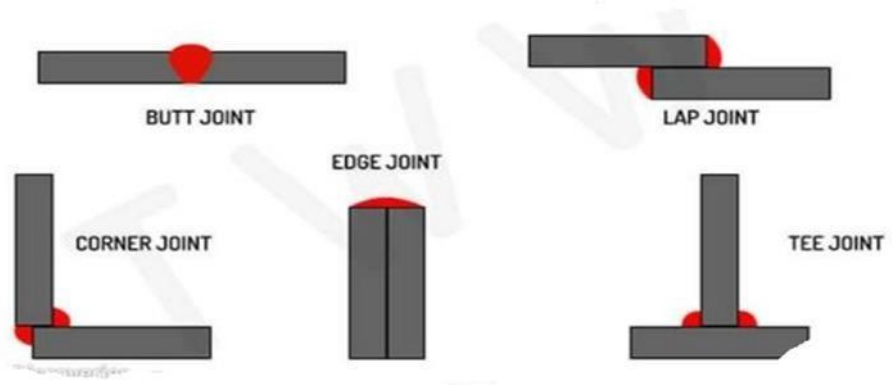

Figure 2-3:**Welding Joint Types [8]**

2.6 WELDIND DEFECTS

A rejectable discontinuity is referred to as defect. Discontinuities can be observed in weld metal, heat effected zone, or base metal of many weldments. During welding a certain number of discontinuities may exist within the weld. These include porosity, cracks, slag inclusions etc.

2.6.1 Porosity

Gas entrapment during solidification results in hole formation known as porosity. Porosity in welding shows that welding process is not properly controlled, or base metal or filler metal is not clean properly or filler rod is not compatible.

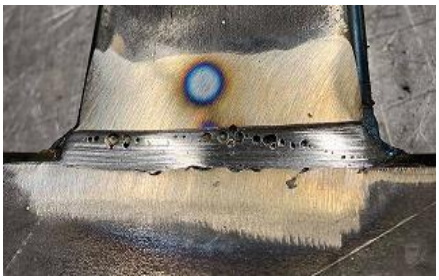

Figure 2-4: **Porosity**

2.6.2 Slag Inclusion

Entrapment of non-metallic solids in weld metal is known as slag inclusions. The solid slag represents a portion of weld where the metal is not fused properly. Slag inclusion can be removed through properly cleaning the base metal and filler rod before welding so that dust, oil, and moisture is removed from the surface.

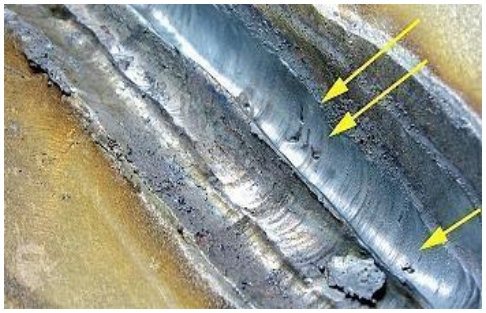

Figure 2-5: Slag Inclusions

2.6.3 Overlap

It occurs due to the poor control of welding process or improper selection of welding material. Overlap is surface fault that form mechanical notch and consider reject able. With care and practice overlap defect can be eliminated. If overlap occurs during welding it is corrected by carefully grinding of defected surface.

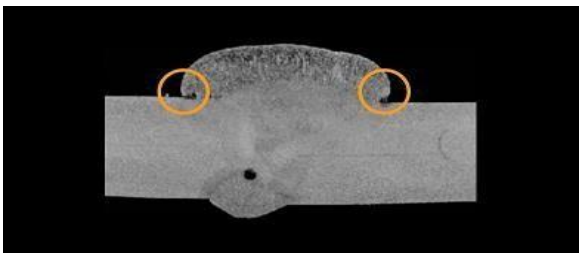

Figure 2-6: overlap

2.6.4 Undercut

Undercut is considered as a defect. It occurs due to improper welding techniques, weld parameters, or selecting excessive welding current or voltage. Undercut can be removed by grinding the weld. Undercuts are not easy to avoid in welding even though with lot of time and practice.

Figure 2-7: Undercut

2.6.5 Cracks

Cracks occur during welding when localize stresses exceeds the ultimate strength of the metal. They can be classified into hot and cold cracks. Cold cracks grow after solidification and hot cracks develop at high temperature.

Figure 2-8: Cracks

2.7 PROCESS PARAMETERS AND THEIR EFFECT ON WELDING PROPERTIES

Reduction in welding defects of SS-304 sheet by increasing the strength and durability of hoarding structures were studied by M saha [11]. The tests were planned to use the design of experiments technique. For increased ultimate tensile strength and hardness, optimal welding parameters were determined. Mechanical testing, both destructive and nondestructive, validated the selection of optimal values. Quality of the weld joint is mainly affected by the current, flow rate of gas, welding speed and electrode diameter. The best parameter combinations for ultimate tensile strength and hardness is the current value. For optimal ultimate tensile strength, a greater current value (180 amp) was found to be suitable, however, a low current value (150 amp) was found optimal for desired hardness.

To adjust the process parameters i.e current, voltage, root gap and gas flow rate for making welding of thin sheet easier and more compatible PKumar [12] proposed a design. Based on the design of the experiment, twenty-seven pairs of specimens were weld using the gas tungsten arc welding procedure. AISI304 sheet of 200 x 50 x 3 mm size is butt welded by gas tungsten arc welding. Filler rod 308L was used as an electrode in GTAW process. Voltage is the most effective parameter for hardness and bending strength. The maximum hardness was achieved at 70A current, 50V voltage, 0.5mm root gap and 16 l/min gas flow rate. Whereas maximum bending strength was found at 70A current, 40V voltage, 0.5m root gap and 20 l/min gas flow rate. Hence, voltage is important factor for changing the mechanical properties of weld joints.

A. Singh and R. Mitta [13] studied the effect of welding parameters on the mechanical and microstructural behavior of the dissimilar SS304 - SS202 welded with TIG welding and Inconel 625 filler rod of 3.2 mm diameter. Current, speed, and gas flow rate were set as input parameter for welding. Impact toughness and bending strength were chosen as mechanical qualities. The data was collected based on the L9 orthogonal array Taguchi Method's. Bending strength increases by increasing the current from 95 A to 115A and after that the bending

strength decrease with an increase in current due to grain growth and decreasing the grain boundaries. Whereas with an increase in speed of welding, bending strength increase due to change in structural weld joint.

N. Karunakaran [14] conducted TIG welding of AISI 304L stainless steel, and the weld bead shapes for constant and pulsed current settings were compared. The effect of current on the tensile strength, hardness, microstructure, and residual stress distribution of steel samples' welding zones were investigated. During said study, Welding currents of 100~180 Amp, welding speed of 118.44 mm / min, and frequency of 6 Hertz were selected. The magnitude of residual stress was determined to be lower in welding through pulsed current compared to continuous current welding. The use of pulsed current results in better tensile strength and hardness of the joints by forming finer grains and breaking dendrites.

2.8 EFFECT ON MECHANICAL PROPERTIES OF STEEL BY SHIELDING GAS

G. B. Joseph and T. N. Valarmathi [15] presented, the effect of shield gas on weld shape, angular distortion, and hardness when employing the Automatic GTAW method to weld 3mm thick AISI304L stainless steel plates was investigated. Nondestructive testing (NDT), destructive testing (DT), and metallography tests were used in the evaluations. After carefully evaluating the mechanical properties, micro structural experimental tests, and residual stress measurement, welding parameters with appropriate shielding gas for welding of AISI 304L on the Automatic GTAW machine were optimized. according to microstructure study, the base metal is austenite and weld metal exhibits dendrite development. Due to the additional hydrogen in the shield media, heat affected zone (HAZ) clearly shows a growth of dendritic structure, resulting in the larger grains of the weld metal due to increased heat input. The argon plus hydrogen specimen has a homogeneous hardness across the weld center and heat affected area (HAZ) when no filler wire welding is used. The argon plus hydrogen specimen has lower delta ferrite content.

A. Durgutlu [16] evaluated the effect of hydrogen and argon as a shielding gas on TIG welding of 316L steel. The mechanical properties, microstructure and penetration of the material were investigated. Stainless steel plates specimens of 200 x 80 x 4 mm dimension were used, and welding was performed with tungsten electrode of 2.4 mm, a 10 l/min gas flow rate, a welding current of 115 Amp, and a welding speed of 100 mm/min, with pure argon, 1.5 percent Hyd-Argon, and 5 percent Hyd-Argon as shielding gas. To determine the effect of shielding, bending tests, tensile tests, and microstructure analyses were performed. results of the test show that

a. The best tensile strength is achieved with 1.5 percent Hyd-Argon gas shielding.
b. No cracks, tears, or surface flaws were visible with the naked eye on specimens welded through all three shield media
c. Weld metal has a lower hardness than HAZ and base metal for all shielding mediums. Examining penetration profiles for all three shield media reveals that penetration depth and width of weld bead increase as hydrogen content rises.
d. The weld metal's mean grain size grows as the hydrogen level rises. Weld metal grain orientation shifted as the hydrogen level increased.

2.9 PARAMETERS OPTIMIZATION THROUGH ANOVA METHODOLOGY

N. Ghosh, P. K. Pal, and G. Nandi [17] conducted visual inspection and X-ray radiography to detect surface and sub-surface faults in weld specimens of AISI 316L austenitic stainless steels. It was investigated through experiments and analysis, the effect of current, gas flow rate, and nozzle to plate distance on weld quality in metal inter gas arc welding of AISI 316L austenitic stainless steel. Different level of current, gas flow rate, and nozzle to plate distance were used to create butt welded joints. The yield strength, ultimate tensile strength, and percentage of elongation of the welded specimens were used to assess the weld quality. Current was one of the most important factors in comparison to gas flow rate and plate to nozzle distance in determining the weld joint strength. Taguchi method was utilized for optimization of welding parameters best results obtained at current 100 Amp, 20 l/sec gas flow rate and nozzle to plate distance of 15 mm.

A. Kumar and S. Sundarrajan [18] analyzed the pulse TIG welding parameters on dilution and mechanical properties such as notch tensile strength, hardness, and impact toughness of welded Al-Mg-Si alloy of 250 mm x 150 mm x 3.14 mm w dimensions. Because of microstructure characteristics in the inter dendritic network, pulsed TIG welds have low notch tensile strength and impact toughness than the source metal. For enhancing the mechanical properties of heat treated aluminium alloy weldments, the Taguchi method was employed to optimise the pulsed TIG welding parameters. The notch tensile strength and impact toughness have been found to have an inverse relation.

K. Sittichai, N. Santirat, and P. Sompong [19] in his experimental study evaluated the effect of welding current (80, 90 & 100 A), welding speed (250, 300 & 350 mm/min) & shielding gas mixture, on mechanical properties of AISI 304 steel was determined. The significant factors were identified using statistical data such as mean, standard error of mean, and analysis of variance (ANOVA). AISI 304 specimen of 65 mm x 80 mm x 3 mm dimension was used as the raw material. They concluded that the shielding media had the greatest impact on Tensile strength, with the best results of 954.81 N/mm is obtained with a mixture of 70% Argon + 25% Carbon mono oxide + 5% Oxygen, compared to other mixtures.

2.10 MICROSTRUCTURE BEHAVIOR

K. Nakata, M. Ozawa, and K. Kamo [20] had studed, TIG welding with 308L filler to test the weldability of neutron exposed stainless steel (SS 304) specimen of 60 mm X 100 mm X 10 mm size, imitating the repair of reactor components. At a heat input of 0.4 MJ/m, no obvious flaws emerged in the specimen during build-up welding of a groove.

S. Mamat [21] investegated, Low carbon steel with dimensions of 10 mm x 10 mm x 55 mm was utilized as the raw material with welding parameters of voltage 20V, 25V, and 30 V, current 130Amp and 180 Amp, filler rod of diameter 1 mm, welding speed of 40 cm/min, and CO2 as the shielding gas. According to the results of the experiment, grain size number reduced from 12.4 to 9.8 when the voltage was increased from 20 to 30 V. Fine grain austenite were

produced in the weld metal at high temperatures, high heat input and quick cooling rates which resulted in the development of fine grained polygonal ferrites at room temperature. Grain coarsening, which was more prominent in the HAZ, as well as a reduction in impact energy and toughness, were all caused by the high heat input. The hardness in the HAZ was reduced from 160 to 148 HBN by increasing the heat input from 5 to 8 KJ/cm. This is thought to be due to a decrease in dislocation density and microstructural coarsening.

2.11 OBJECTIVE OF THE STUDY

The goal of this experimental work is to see how tungsten inert gas welding parameters i.e. current, voltage, gas flow rate and filler rod (316L & 308L) affect Ultimate Tensile Strength, % elongation and hardness of welded AISI 321 sheet of size 100 mm x 100 mm x 3 mm. The process parameters were optimized using Taguchi Design of Experiment. The TIG welding was used in this study, which include three welding levels i.e. current, voltage, and gas flow rate with 316L and 308L filler wire. The following tests were conducted to analyze the weld quality.

a) Chemical analysis of base and filler wire metal
b) Dye Penetration test
c) X-ray of welded seam
d) Ultimate tensile strength
e) Percentage Elongation
f) Hardness
g) Optical analysis

CHAPTER 3: METHODOLOGY

3.1 INTRODUCTION

In this chapter we discuss objective of the experiment, parameter optimization, manufacture of the tensile samples, and the experimental methods used. The procedures and testing standards employed are analyzed and provided. The welding, cutting, and machining of AISI321, as well as the parameters employed and the safety precautions used, are all covered. Also discussed are the material characterizations used.

3.2 AIM OF EXPERIMENT

The study was performed to discover the optimal welding parameters for welding of AISI321 with ER316L and ER308L filler wire, which was accomplished through microstructural analysis and mechanical testing of welded samples.

3.3 MATERIALS DESCRIPTION

In this experiment AISI321 sheet of 3 mm thickness was used as a base metal. ER316L and ER308L filler rod were used to weld the AISI321 sheet at different welding parameters. The AISI321 sheet is shown in Figure 3-1.

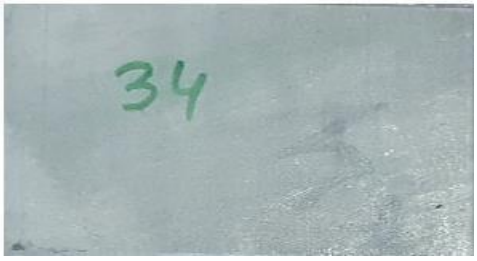

Figure 3-1: AISI321 Test Sheet

3.4 PREPERATION OF SAMPLES

3.4.1 Experimental Matrix

Table 3.1 and table 3.2 show the experimental matrix for this investigation. There were total of fifty-four test samples, each with a thickness of 3mm were evaluated. Various welding parameters i.e. current, voltage and gas flow rate and filler rod ER316L and ER308L were employed.

Table 3.1: 316L Filler Rod Experimental Matrix

Filler Metal: ER316L	Thickness=3mm								
Tensile Testing	S-1	S-2	S-3	S-4	S-5	S-6	S-7	S-8	S-9
Hardness Testing	S-1	S-2	S-3	S-4	S-5	S-6	S-7	S-8	S-9
Microstructure	S-1	S-2	S-3	S-4	S-5	S-6	S-7	S-8	S-9

Table 3.2: 308L Filler Rod Experimental Matrix

Filler Metal: ER308L	Thickness=3mm								
Tensile Testing	S-A	S-B	S-C	S-D	S-E	S-F	S-G	S-H	S-I
Hardness Testing	S-A	S-B	S-C	S-D	S-E	S-F	S-G	S-H	S-I
Microstructure	S-A	S-B	S-C	S-D	S-E	S-F	S-G	S-H	S-I

3.4.2 Design of Experiment

In current experimental setup, Taguchi design has been utilized for optimizing the welding parameters as it reduces the number of iterations. In this study three level with three welding parameters were selected which is shown in table 3.3.

Table 3.3: Welding parameters and levels

Sr.No	Parameters	Units	Level - 1	Level - 2	Level - 3
1	Current	A	80	90	100
2	Voltage	V	15	16	17
3	Gas Flow Rate	l/min	8	9	10

In order to get a suitable orthogonal array the degrees of freedom (DOF) must be determined. DOF is defined as the number of process variables comparisons that must be performed in order to determine which level is good and, more important. One DOF is represented by two level process parameter. DOF must be greater than, or equal to, the process parameters DOF. In this experimental investigation Taguchi L9 orthogonal array with three columns and three rows was used. Nine welding parameter combinations were examined after that welding parameters were allotted to column. As a result, the L9 orthogonal array was used to examine the complete welding parameter space in only nine experiments. Table 3-3 shows the experimental arrangement for welding settings using the L9 orthogonal array.

3.4.3 Welding

Welding is to be carried out on Tungsten inter gas welding machine as shown in figure 3.2. Important parts of the machine are electrode gun, control panel, regulator for gas and inert gas cylinder. The welding current is to be controlled and showed on the welding machine's control panel which has range of 0-400 A Gas regulator controlled the flow of argon gas. The machine is completely manual, and it must be handled by an experienced operator.

Figure 3-2: TIG Welding Setup

The parameters used for welding of AISI321 stainless steel sheet with ER316L and ER308L filler rods are mentioned in Procedure Qualification Record (PQR) in A-2 and A-3. Figure 3-3 displays welded samples of AISI321 using ER316L and ER308L filler rods.

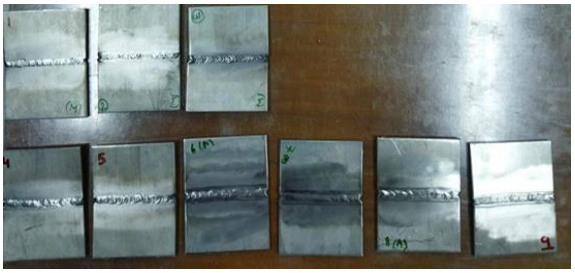

(a)

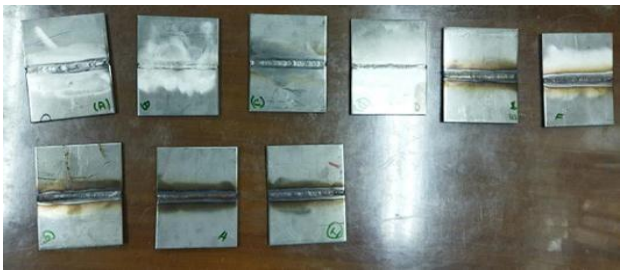

(b)

Figure 3-3: Specimens welding (a) AISI321/ER316L Filler (b) AISI321/ER308L Filler

3.4.4 Welding Plate Cutting

After welding, the specimens were made for cutting and machining to the specified requirement. On both end of welded sample a 15mm portion was cut. After that, four 20mm samples were cut for tensile testing (x9) from each plate, and one sample was taken for microstructure and hardness testing.

Figure 3-4: Cutting of Tensile sample

3.4.5 Tensile Test Sample

The specimens were turn into testing specimens using a milling machine. The specimens were machined to the shape and dimensions, as per the ASTM E8/E8M standard [22] shown in figure 3-5.

Figure 3-5: Specimens for Testing

3.4.6 Preparation of Microstructure Samples

3.4.6.1 Specimens Machining

The test pieces were subsequently divided into smaller segments at the cut off machine for microstructure and hardness testing, as shown in Figure 3-6.

Figure 3-6: Cut-off Machine

3.4.6.2 Hot Mounting

Molding the welded parts for improved handling during microstructure and hardness testing was done to further prepare the microstructure samples. The resin utilized for hot mounting was Polyfast. As shown in Figure 3-7, the samples that had been prepared were put into the mounting machine, which was then closed and started after being coated with resin (Polyfast) powder. 180°C temperature and 30MPa pressure was maintained during placement

of the sample. It was heated for 4.5 minutes and cooled for 2.5 minutes, for a total mounting time of 7 minutes. The mounted samples are shown in figures 3-7 and 3-8.

Figure 3-7: Mounted Sample (ER316L)

Figure 3-8: Mounted Sample (ER308L)

3.4.6.3 Grinding

Specimens were cleaned and prepared for microstructure with the Struers polishing machine and grinding papers grades 220, 800, and 1200, as shown in figure 3-9. The grinding technique was carried out according to table 3-4.

Table 3.4: Stainless Steel Cleaning Guideline

	1st Step	2nd Step	3rd Step
Waterproof Silicon Paper	P#220	P#800	P#1200
Lubricant	Water	Water	Water
RPM	300	300	300
Load in Newton	30	25	25
Time in minutes	Until Plane	5	5

Figure 3-9: Polishing Machine

3.4.6.4 Polishing of samples

The microstructure samples were cleaned on the polishing machine once again, as per techniques listed in table 3-5. Self-lubricating monocrystalline (DiaMaxx Mono 3 m) was used as a primary polishing step. Colloidal silica 50nm alkaline was used for the final polishing with antidying agent [23].

Figure 3-10: Stainless Steel Polishing Guidelines [23]

3.4.6.5 Etching

The samples were etched with an austenitic stainless steel etchant as AISI321 is an austenitic stainless steel (V2A etchant: 100ml H2O, 100ml.H2SO4, and 10ml HNO3). The samples were subsequently subjected to microstructural examination and hardness testing.

3.5 TESTING

This section goes through the various tests that were carried out during the experiment.

3.5.1 Microstructure

Olympus BX51 optical microscope is use to investigate the specimen as illustrated in figure 3-10. In Chapter 4, the results and findings are reported.

Figure 3-11: Olympus BX51 Optical Microscope

3.5.2 Hardness Test

After microscopic analysis, the specimens were ground and re-polished. The hardness test was carried out according to the ASTM E384-11 standard [22]. Indentations were created with a diamond indenter at a spacing of 0.5 mm and a dwell time of 15 seconds with a 300gf. The Vickers micro hardness tester is shown in figure 3-11. Hardness result is discussed in chapter 4.

Figure 3-12: Vickers Micro Hardness Tester

3.5.3 Tensile Test

Tensile testing was performed using the Instron 1195 universal tensile testing machine, as shown in figure 3-12 as per ASTM E8/E8M–15a [24]. The tensile test results were presented in chapter 4.

Figure 3-13: Tensile Test Machine

3.6 SUMMARY

This chapter contains information about the experiment's purpose, the materials utilized, the fabrication process, and the measuring techniques employed. The production parameters were recorded, and the investigated parameters (current, voltage, gas flow rate, and filler rods) were changed for the different samples produced. The experimental technique employed in this inquiry, as well as the equipment and testing standards used, were all detailed. The conclusions of the study are detailed in chapter 4.

CHAPTER 4: RESULTS AND DISCUSSION

In this chapter optimization of TIG welding parameters and characteristics of the single V- Butt Joint stainless steel AISI321 TIG welded with ER316L and ER308L are discussed. Aim of this experimental work is to assess effect of TIG welding parameters on mechanical properties of AISI 321 weld.

4.1 SURFACE ROUGHNES

Surface roughness of welded metals is of prime importance as the service life of the welded material is dependent on it. The welded joints surface roughness was measured longitudinally at bead face. For all the samples surface roughness at Weld Bead (WB) and Heat Affected Zone (HAZ) was calculated and average of three values was chosen. Surface roughness of each welded sample are tabulated below in table 4-1 and 4-2. The value of surface roughness of welded joint at HAZ with filler wire ER316L and ER308L ranged 0.37-2.3 µm and 0.6-3.8 µm respectively. Whereas the value of surface roughness of welded joint at WB with filler wire ER316L and ER308L ranged between 7.1-26.5 µm and 8.1-24.5 µm respectively.

Table 4.1: Surface Roughness values of weld bead with ER316L

Sample No	Current (A)	Voltage (V)	Gas Flow Rate (l/min)	Average Surface Roughness Ra (µm)	
				WB	HZA
S-1.	80	15	8	15.4	0.35
S-2.	80	16	9	14.5	0.40
S-3.	80	17	10	11.0	1.90
S-4.	90	15	9	7.1	0.80
S-5.	90	17	10	8.5	0.74
S-6.	90	17	8	12.1	1.65
S-7.	100	15	10	12.5	2.30
S-8.	100	16	8	21.0	2.20
S-9.	100	17	9	26.5	2.30

Table 4-1 depicts the effect of welding parameters on surface roughness of different weld samples. It is to be noted that maximum and minimum value of surface roughness was oberved for sample no 9 & sample no 4 respectively. Good quality surface finish is achieved at moderate values of current, gas flow rate and lower value of voltage. Highest value of surface roughness is achieved at higher values of current, voltage and moderate value of gas flow rate.

Table 4.2: Surface Roughness values of weld bead with ER308L

Sample No	Current. (A)	Voltage. (V)	Gas.Flow.Rate (l/min)	Average Surface Roughness Ra (µm)	
				WB	HZA
S-A	80	15	8	21.0	1.5
S-B	80	16	9	17.1	2.2
S-C	80	17	10	19.5	3.4
S-D	90	15	9	9.5	1.9
S-E	90	17	10	8.1	1.1
S-F	90	17	8	12.0	0.6
S-G	100	15	10	14.3	2.8
S-H	100	16	8	13.6	3.5
S-I	100	17	9	24.5	3.8

Effect of varying the welding parameters on the surface features are shown in table 4-2. At weld bead maximum value of surface roughness of 24.5µm was obtained for sample No I, whereas minimum value of surface roughness of 8.1 µm was obtained for sample No E. It is noteworthy that better surface finish is observed at moderate values of current and gas low rate and higher value of voltage. Highest values of surface roughness are obtained at higher values of current and voltage and moderate value of gas flow rate.

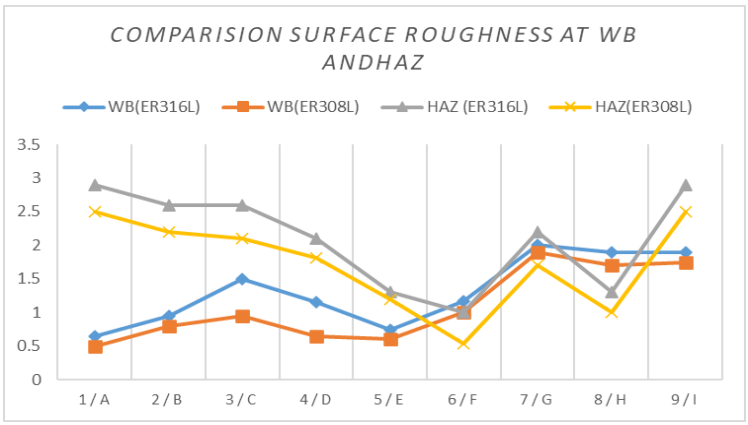

Figure 4-1: Surface roughness comparison of AISI321/ER316L and AISI321/ER308L

The surface roughness of welded joints AISI321/ER316L and AISI321/ER308L at WB and HAZ was compared in Figure 4-1. It is to be noted in the graph that the welded joint AISI321/ER316L at WB has a good surface finish than AISI321/ER308L and similar trend was noted in HAZ of AISI321/ER316L.The Ra value of AISI321/ER316L is lower than that of AISI321/ER308L.

4.2 Main Effect Plot

`A mean effect plot represents the mean response value for a design parameter or process variable at each level. This plot is used to compare the strength of effect of different factors. If the result of process parameter is positive, it average response is higher at higher level of parameter setting. Whereas if the process parameter result is negative, it average response is low level setting is more than at higher level. Figure 4.2 show the main effect plot for S/N ratio.

4.3 ANOVA FOR EXPERIMENTAL STUDY

On each of the resultant parameters, analysis of variance was done. Software Minitab was used for this analytical study. The ANOVA test is used to carry out the statistical analysis of process characteristics that influence responses. This is done by dividing the overall variability of the S/N ratios, which is calculated as the sum of the squared deviations from the total mean of the S/N ratio. P test was performed to determine the essential parameters affecting the output.Each response variable was analyzed independently in this experimental study.

4.3.1 EVALUATION OF AISI321/316LON SURFACE ROUGHNESS (ER316L)

4.3.1.1 Main Effect Plot for Surface Roughness

Surface roughness is one the response that was measured after experimental study. Figure 4.2 show the main effect plot for S/N ratio. In this plot there are three input variables. From plot it is seen that surface roughness is minimum when current is at 90A, voltage is at 16V and gas flow rate is at 10 liters/min. whereas surface roughness is maximum at current of 100A, Voltage of 17V and gas flow rate 8 liter/min

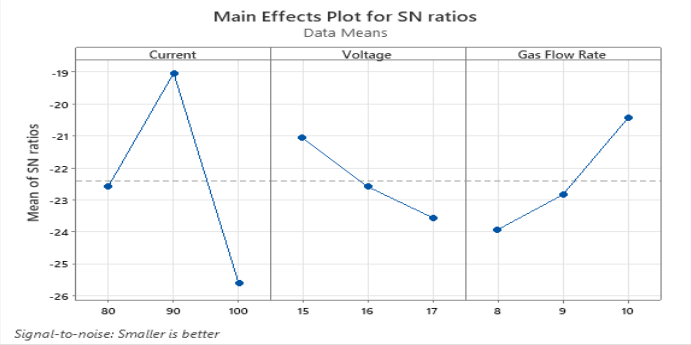

Figure 4-2: S/N ratio graph for current, voltage & gas flow rate for surface roughness (ER316L)

Table 4.3 shows the S/N ration response table for different parameters level. We can see from above table 4.4 and fig. 4.2 that current is most contributing factor. The surface roughness of the specimens is kept to a minimum, when the arc current is kept at 90 A, the voltage is kept at 15 V, and the gas flow rate is kept at 10 liter/min, making these parameters the best for this experiment.

Table 4.3: S/N ratio for surface roughness (ER316L)

Level	Current	Voltage	Gas Flow Rate
1	-22.57	-21.06	-23.93
2	-19.03	-22.59	-22.84
3	-25.62	-23.56	-20.44
Delta	6.59	2.50	3.49
Rank	1	3	2

4.3.1.2 ANOVA for Surface Roughness (ER316L)

Experimental run were compiled for surface roughness. table 4.4 show the results of ANOVA versus the factors used in study. In this experimental study P-value is one of the important measuring value for finding the significance of input parameters. It provided convincing evidence that the risk assumed for this experimental investigation is not greater than 5%, meaning that there is only a 5% chance that the elements in the experimental study will not actually have an impact. From table 4.5 it is shown that all three factor current, voltage and gas flow rate are significant for surface roughness as all three input parameters has P value less than 0.05. Current is the most contributing factor in this experiment and its contribution is 60.54% as its P value is 0.000 second most contributing factor is gas flow rate and its contribution is about 19.06% with P value 0. 007.The error was found to be 8.22%. Pareto chart graphically represent the most important significant parameter. Current is the most important factor which is shown in petro chart in figure 4.3(a).

Table 4.4: Result of ANOVA surface roughness using data from S/N ratio (ER316L)

Source	DF	Seq SS	Contribution	Adj SS	Adj MS	F-Value	P-Value
Current	2	345.821	60.54%	345.821	172.911	40.49	0.000
Voltage	2	69.524	12.17%	69.524	34.762	8.14	0.007
Gas Flow Rate	2	108.868	19.06%	108.868	54.434	12.75	0.001
Error	11	46.978	8.22%	46.978	4.271	-	-
Lack-of-Fit	2	45.818	8.02%	45.818	22.909	177.74	0.000
Pure Error	9	1.160	0.20%	1.160	0.129	-	-
Total	17	571.191	100.00%	-	-	-	-

According to Figure 4-3(b), the ANOVA analysis revealed that the data points were almost exactly in a straight line. The model only included major components, and the error was distributed normally along a straight line. The model points were not closed, and the data was presented in a strewn pattern in the vs fits plots, as seen in Figure 4.3 (c). No outliner was found in figure 4.3 (d). The histogram in Figure 4.3 (e) presented distribution of data within the limits and the data frequently lied on the central line. So the model was adequate for conducting this experimental study.

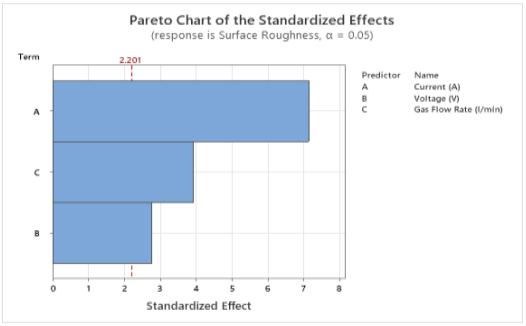

(a)

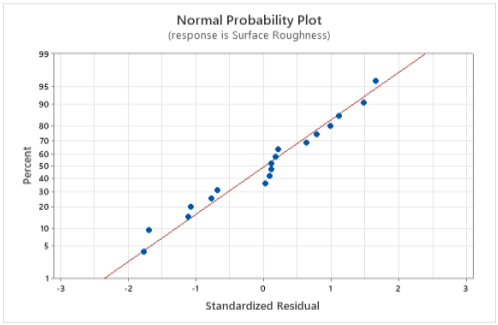

(b)

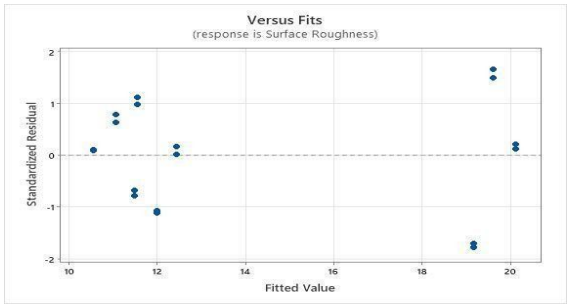

(b)

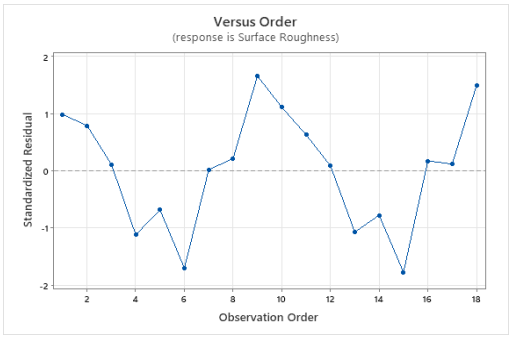

(d)

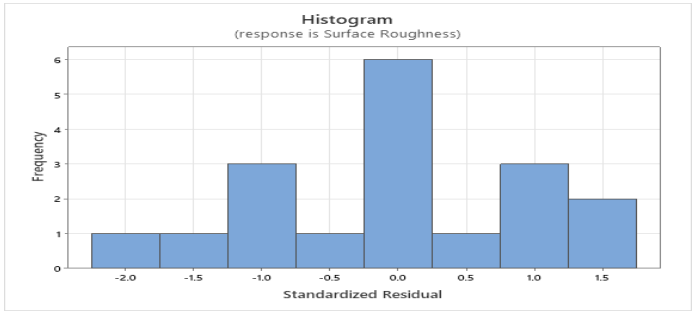

(e)`

Figure 4-3 (a) Pareto Chart (b) Normal Probability Chart (c) Histogram (d) Residual VS Fitted (e) Versus Order

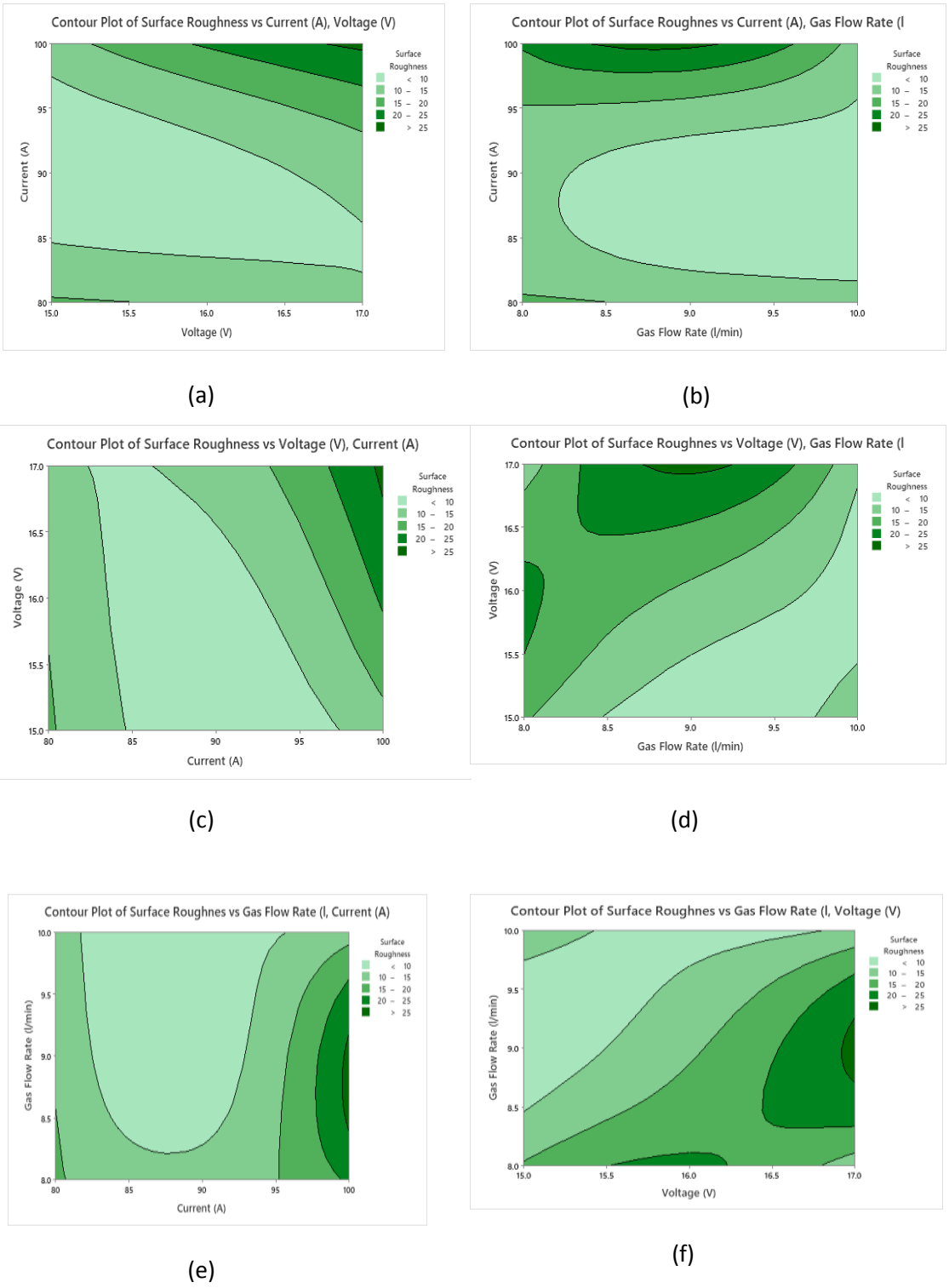

Figure 4-4: Contour Plot of Surface Roughness (316L) (a) Current vs Voltage (b) Current vs Gas flow rate(c) Voltage vs current (d) Voltage vs Gas flow rate (e) Gas Flow rate vs Current (f) Gas Flow rate vs Voltage

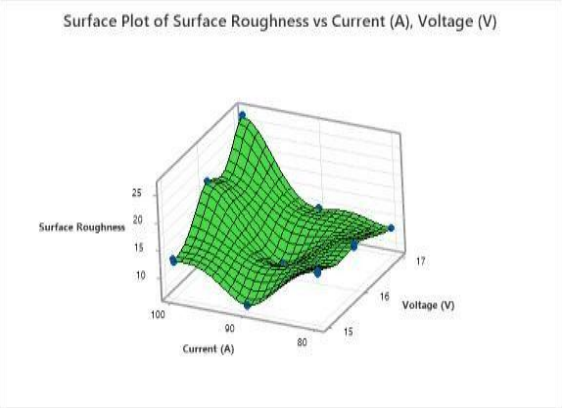

(a)

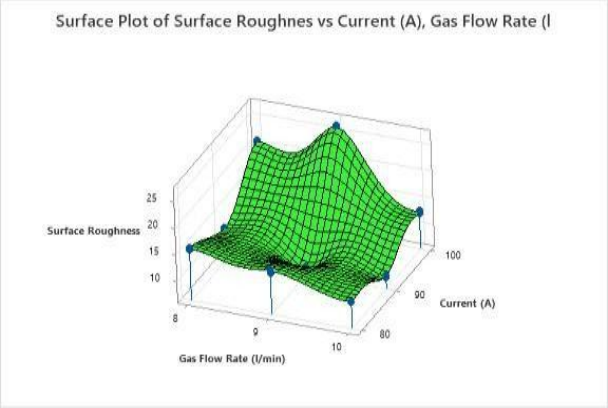

(b)

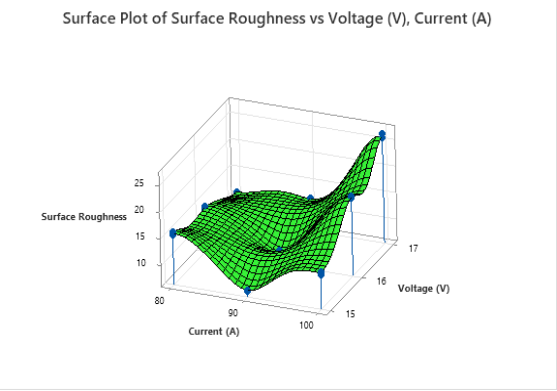

(c)

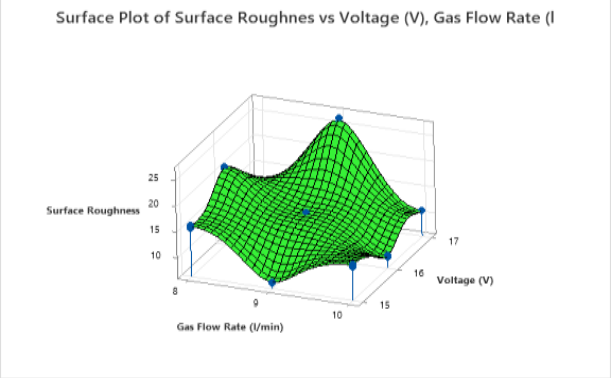

(d)

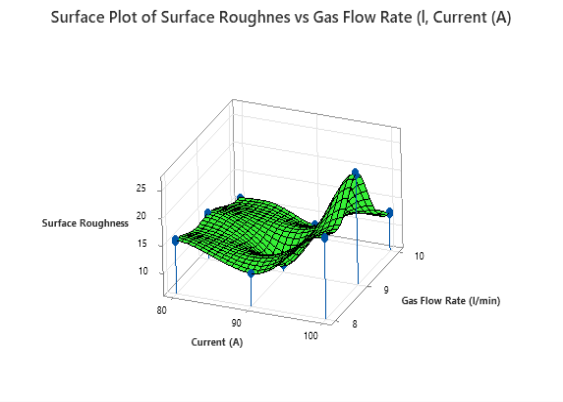

(e)

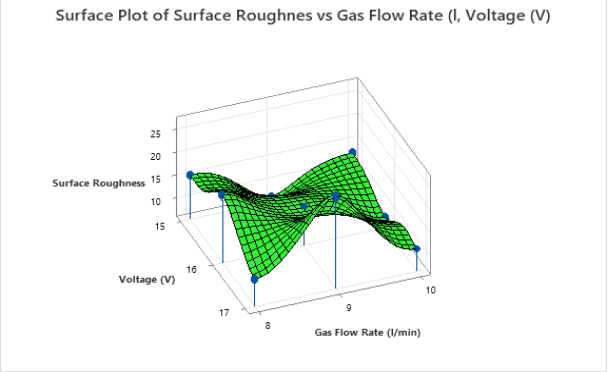

(f)

Figure 4-5: Surface plot of Surface Roughness (316L) (a) Current vs Voltage (b) Current vs Gas flow rate(c) Voltage vs current (d) Voltage vs Gas flow rate (e) Gas Flow rate vs Current (f) Gas Flow rate vs Voltage

4.3.2 EVALUATION OF SURFACE ROUGHNESS OF AISI321/308L

4.3.2.1 Main Effect Plot for Surface Roughness (ER308L)

From table 4.2 it can be seen that sample no E had minimum value of surface roughness, whereas the sample no I had maximum surface roughness in welded joint of AISI321/308L. The surface roughness of samples (A to I) were measured through diavite roughness tester. The surface roughness of sample no I is significantly rougher than sample no E. Changes in surface roughness of AISI321/ER308L samples are due to varing welding parameters. Figure 4.3 shows a main effect plot for S/N Ratio at different welding parameters of AISI321/ER308L for surface roughness.

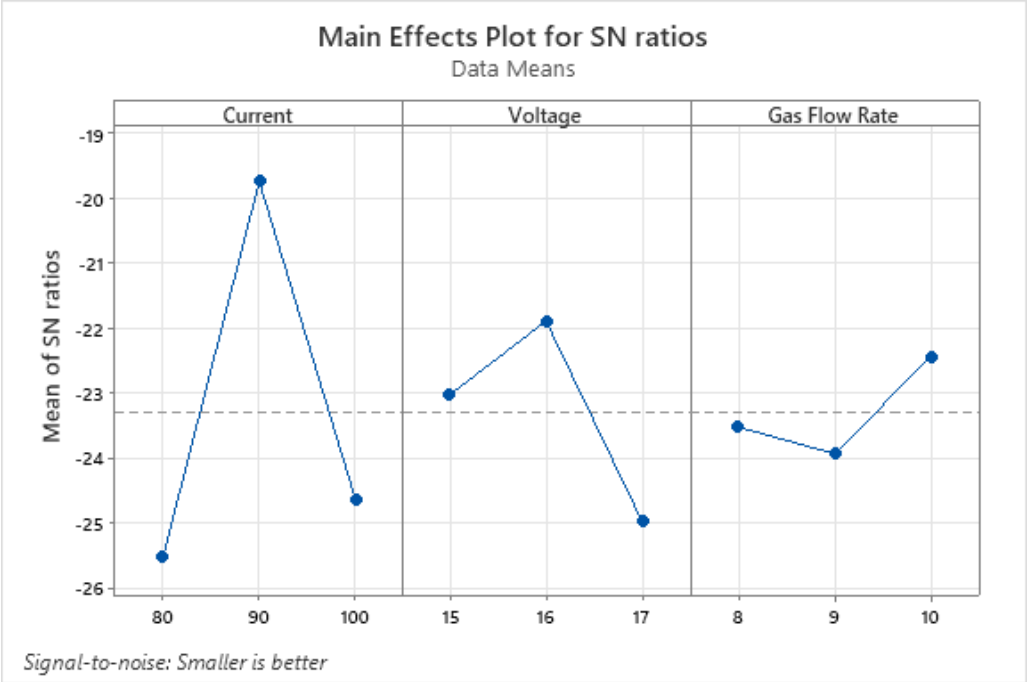

Figure 4-6 :S/N ratio graph for current, voltage & gas flow rate for surface roughness (ER308L)

In this plot there are three input welding parameter. From the plot it is seen that surface roughness is minimum at 90A, 16V and 10 liter/min. Thus these setting are optimal for current experimental study.

Table 4.5: Response table for S/N ratio (ER308L)

Level	Current	Voltage	Gas Flow Rate
1	-25.53	-23.03	-23.52
2	-19.73	-21.89	-23.94
3	-24.64	-24.99	-22.44
Delta	5.79	3.10	1.50
Rank	1	2	3

Table 4.5 shows the S/N ration response table for different parameters level. We can see from above table 4.5 and figure 4.6 that current and voltage is most contributing factor. The surface roughness of the specimens is kept to a minimum, when the arc current is kept at 90 A, the voltage is kept at 16 V, and the gas flow rate is kept at 10 liter/min.

4.3.2.2 ANOVA Analysis of Surface Roughness (ER308L)

Most important factor influencing the surface roughness of welded samples is evaluated by using P test. The Smaller the P value, the greater the influence on performance attributes. ANOVA results for surface roughness are shown in Table 4.6.

Table 4.6: Result of ANOVA using data from signal to noise ratio for surface roughness (ER308L)

Source	DF	Seq SS	Contribution	Adj SS	Adj MS	F-Value	P-Value
Current	2	296.084	61.89%	296.084	148.042	28.10	0.000
Voltage	2	97.981	20.48%	97.981	48.991	9.30	0.004
Gas Flow Rate	2	26.408	5.52%	26.408	13.204	2.51	0.127
Error	11	57.944	12.11%	57.944	5.268		
Lack-of-Fit	2	56.964	11.91%	56.964	28.482	261.57	0.000
Pure Error	9	0.980	0.20%	0.980	0.109		
Total	17	478.418	100.00%				

Above table depicts that P value of current and voltage is less than 0.05 so current and voltage is the most influencing factor for surface roughness of AISI321/ER308L welded joint. Current is the most important factor which is shown in petro chart in figure 4.7(a). According to figure 4.7(b), the ANOVA analysis revealed that the data points were almost exactly in a straight line. The model only included major components, and the error was distributed normally along a straight line. The model points was not closed, and the data was presented in a strewn pattern in the vs fits plots, as seen in Figure 4.7 (c). No outliner was found in figure 4.7 (d). The histogram in Figure 4.7 (e) presented distribution of data within the limits and the data frequently lied on the central line. So the model was adequate for conducting this experimental study.

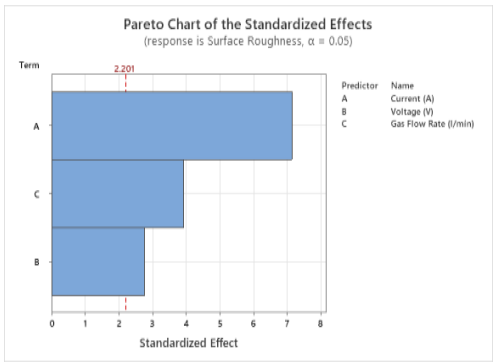

(a)

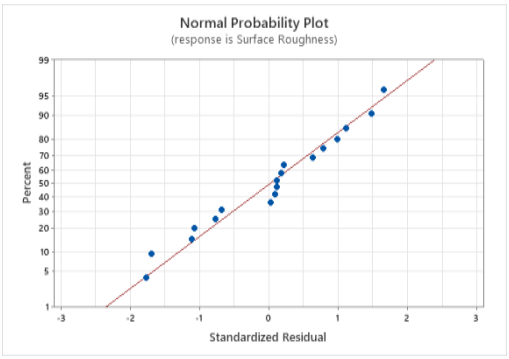

(b)

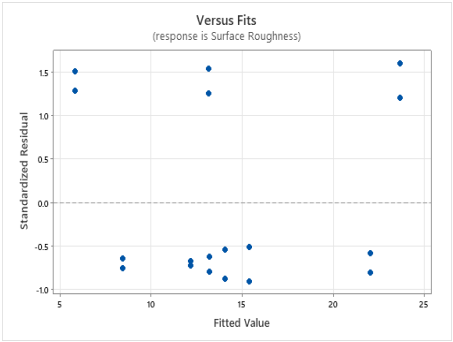

(c)

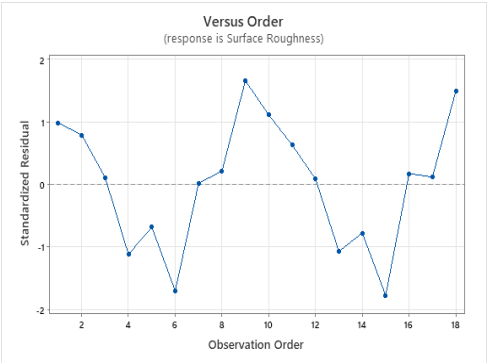

(d)

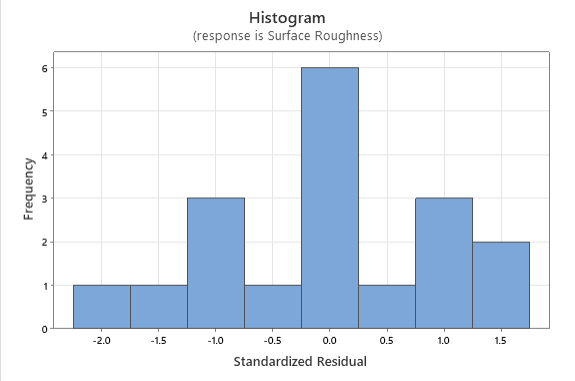

(e)

Figure 4-7: (a) Pareto Chart (b) Normal Probability Chart (c) Histogram (d) Residual VS Fitted (e) Versus Order

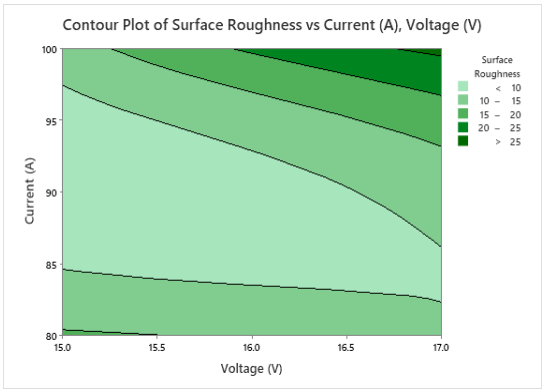

(a)

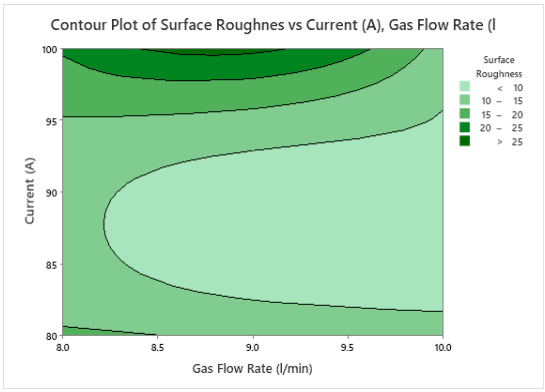

(b)

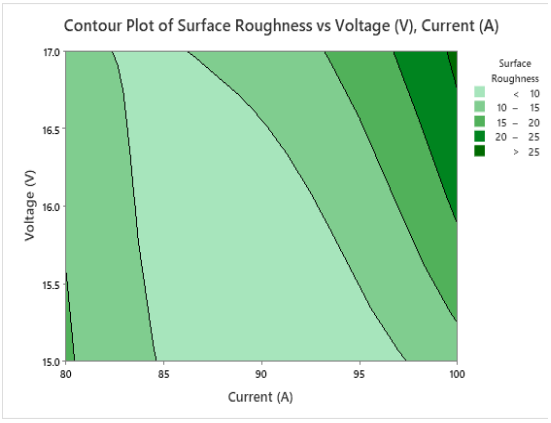

(c)

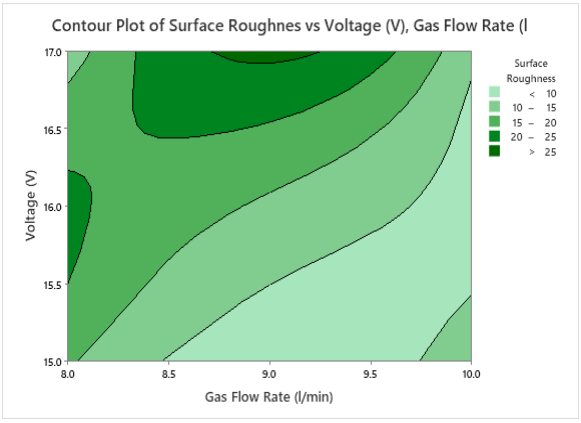

(d)

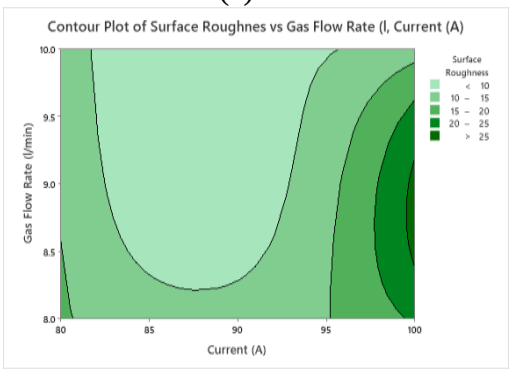

(e)

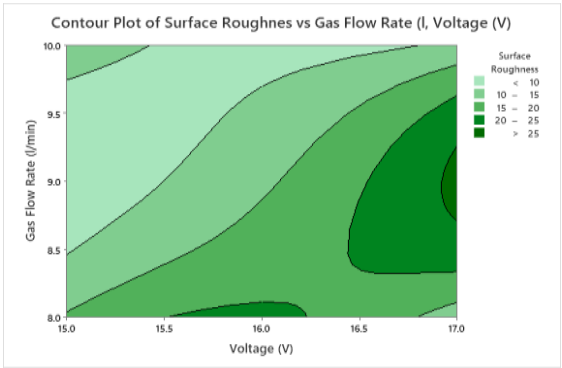

(f)

Figure 4-8: Surface plot of Surface Roughness (308L) (a) Current vs Voltage (b) Current vs Gas flow rate(c) Voltage vs current (d) Voltage vs Gas flow rate (e) Gas Flow rate vsCurrent (f) Gas Flow rate vs Voltage

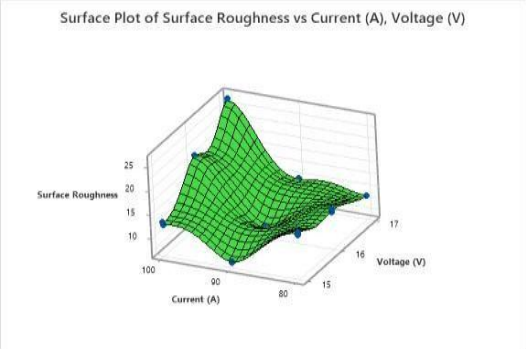

(a)

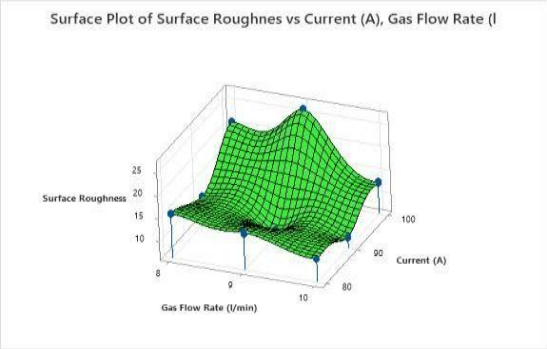

(b)

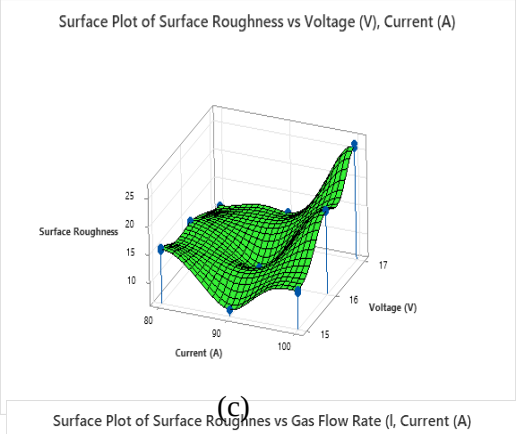

(c)

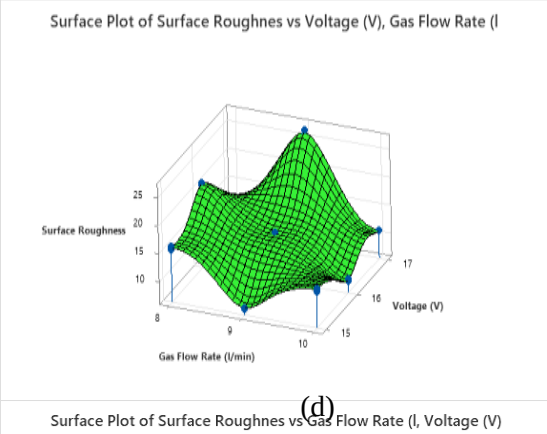

(d)

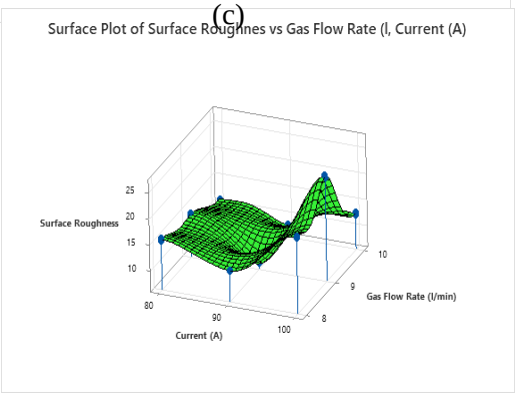

(e)

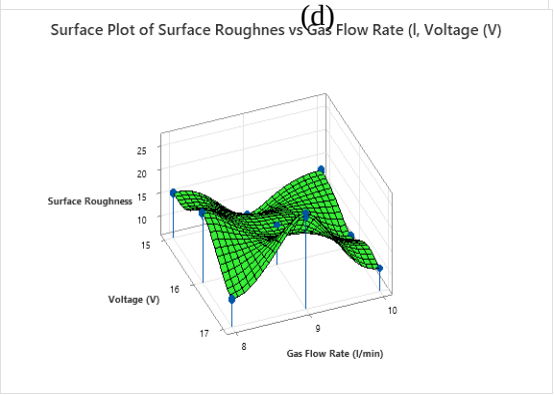

(f)

Figure 4-9: Surface plot of Surface Roughness (308L) (a) Current vs Voltage (b) Current vs Gas flow rate(c) Voltage vs current (d) Voltage vs Gas flow rate (e) Gas Flow rate vsCurrent (f) Gas Flow rate vs Voltage

4.4 HARDNESS (VICKERS) TEST

Hardness test is used to study the effect of welding parameters on material properties. It was measured at the interval of 0.5mm across the weld joint. Hardness test result of all the welded sample weld through ER316L filler and ER308L filler are enlisted in table 4.7 and table 4.8 respectively.

Table 4.7: Hardness Result of Welded Specimens with ER316L

Sample No	Current. (A)	Voltage. (V)	Gas. Flow Rate. (L/min)	Avg Hardness (HV)
S-1.	80	15	8	220
S-2.	80	16	9	215
S-3.	80	17	10	230
S-4.	90	15	9	330
S-5.	90	16	10	266
S-6.	90	17	8	260
S-7.	100	15	10	210
S-8.	100	16	8	230
S-9.	100	17	9	240

From the above table it is noted that 330 HV is maximum hardness for specimen No 4 and 210 HV is the minimum hardness for sample No 7. Table 4.8 shows the hardness results of samples when using 308L filler rod. It is observed from the above table that for sample no: H hardness is maximum and for the sample no.B hardness is minimum.

Table 4.8: Hardness Result of Welded Specimens with ER308L

Sample No.	Current (A)	Voltage (V)	Gas Flow Rate (L/min)	Avg Hardness (HV)
S-A	80	15	8	215
S-B	80	16	9	200
S-C	80	17	10	205
S-D	90	15	9	220
S-E	90	16	10	245
S-F	90	17	8	207
S-G	100	15	10	280
S-H	100	16	8	290
S-I	100	17	9	230

From table 4.7 and 4.8 it is noted that hardness values of nine welded samples weld through 316L filler and nine sample welded through 308L filler has weld zone hardness value greater than base metal.

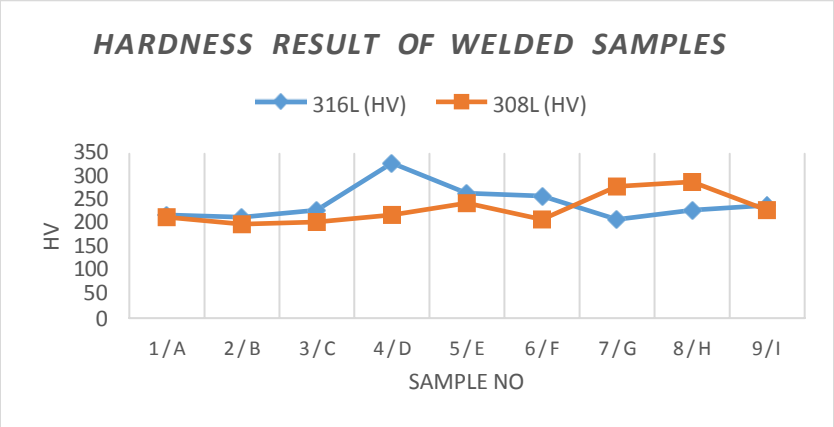

Figure 4-10: Graphical representation of Hardness (316L & 308L)

The hardness of welded joints AISI321/ER316L and AISI321/ER308L at weld joint is compared in Figure 4.10. It is to be observed in the graph that the welded joint AISI321/ER316L has a maximum hardness than AISI321/ER308L The hardness value of welded joint by using ER316L is higher than that of AISI321/ER308L.

4.4.1 EVALUATION OF HARDNESS OF AISI321/316L

4.4.1.1 Main Effect Plot for Hardness (316L)

Main effect plot was carried out by using Minitab 20 software. Effect of TIG welding parameters on hardness was studied in main effect plot. Figure 4.11 shows the main effect plot for hardness of nine samples welded by using 316L filler rod.

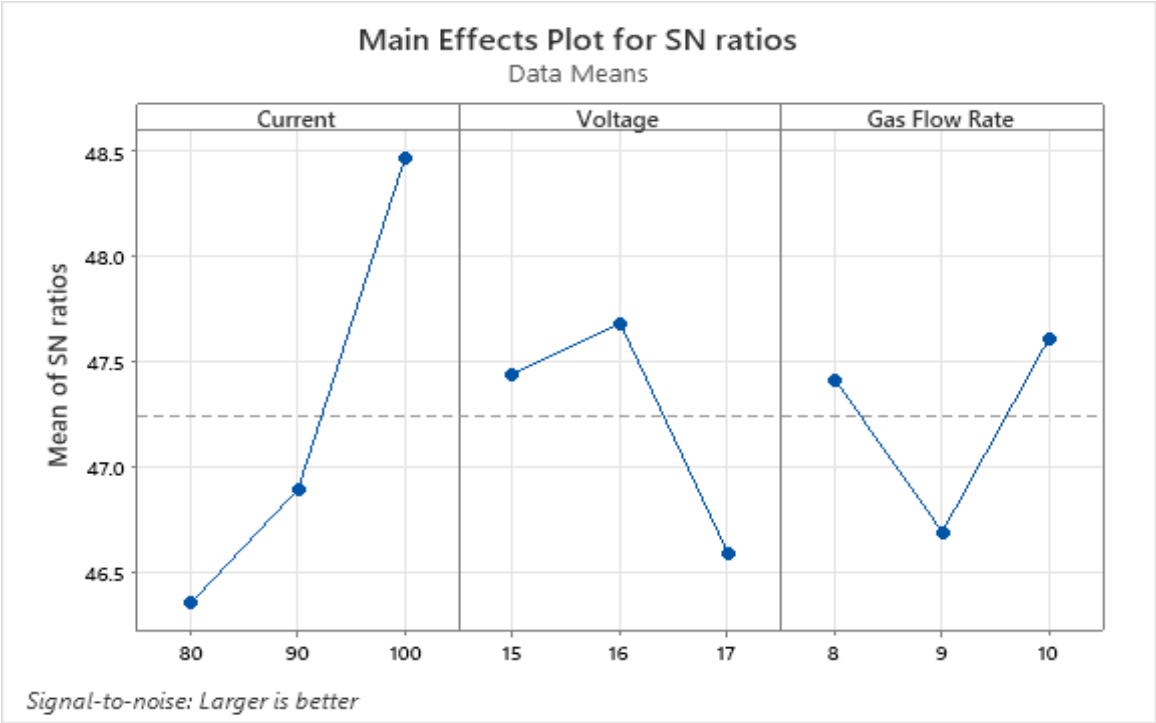

Figure 4-11:S/N ratio Mean Effect Plot

Table 4.9: Response table for Signal to Noise Ratio (ER316L)

Level	Current	Voltage	Gas Flow Rate
1	46.35	47.44	47.41
2	46.89	47.68	46.69
3	48.47	46.59	47.61
Delta	2.12	1.09	0.92
Rank	1	2	3

From the figure 4.11 it can be seen that current is the most contributing factor in hardness. The hardness of specimens will be increased when the current is at 90 A, the voltage at 15 V, and the gas flow rate is at 8 liter/min. We consider these settings to be the best for this experiment.

4.4.1.2 ANOVA Analysis for Hardness (316L)

ANOVA was used to determine statistically significant TIG welding parameters. experimental results for hardness are analyzed in table 4.10 using ANOVA.

Table 4.10: Analysis of variance for S/N ratio Hardness (ER316L)

Source	DF	Seq SS	Contribution	Adj SS	Adj MS	F-Value	P-Value
Gas Flow Rate	2	2883.1	12.73%	2883.1	1441.56	3.70	0.059
Voltage	2	840.1	3.71%	840.1	420.06	1.08	0.374
Current	2	14645.8	64.65%	14645.8	7322.89	18.80	0.000
Error	11	4285.3	18.92%	4285.3	389.57		
Lack-of-Fit	2	4216.8	18.61%	4216.8	2108.39	277.01	0.000
Pure Error	9	68.5	0.30%	68.5	7.61		
Total	17	22654.3	100.00%				

The results show that current is the most significant in effecting the hardness compared to least significant parameters i.e. gas flow rate and voltage because P value of current is less than 0.05 with contribution of 64.65%. Current is the most important factor which is shown in petro chart in figure 4.12(a). According to figure 4.12(b), the ANOVA analysis revealed that the data points were almost exactly in a straight line. The model only included major components, and the error was distributed normally along a straight line. The model points was not closed, and the data was presented in a strewn pattern in the vs fits plots, as seen in Figure 4.12 (c). No outliner

was found in figure 4.12 (d). The histogram in Figure 4.12 (e) presented distribution of data within the limits and the data frequently lied on the central line. So the model was adequate for conducting this experimental study.

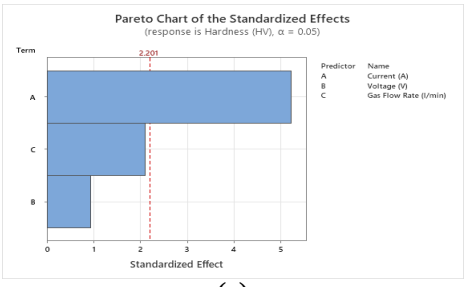

(a)

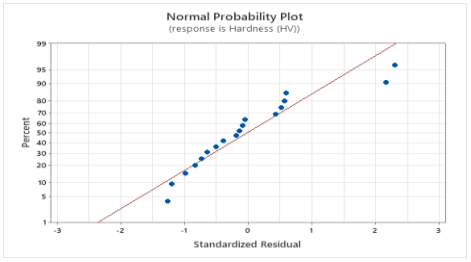

(b)

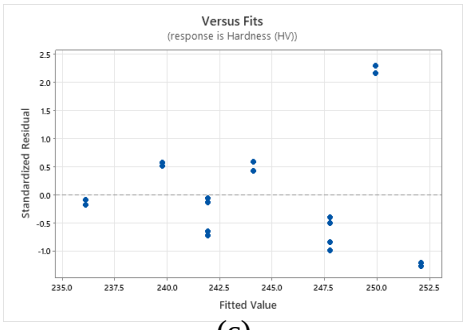

(c)

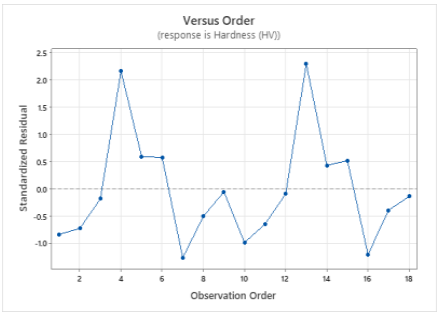

(d)

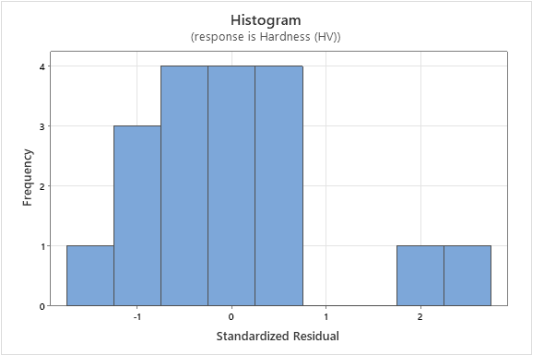

(e)

Figure 4-12: (a) Pareto Chart (b) Normal Probability Chart (c) Verses fit (d) Versus order (e) Histogram

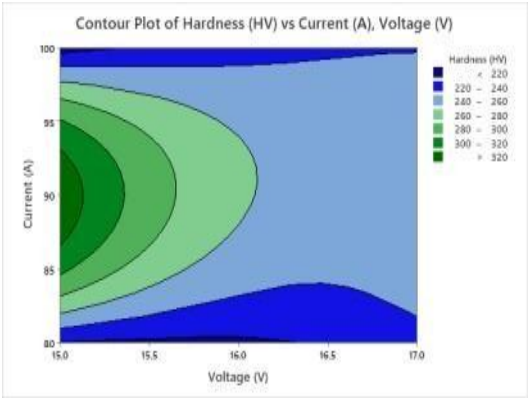

(a)

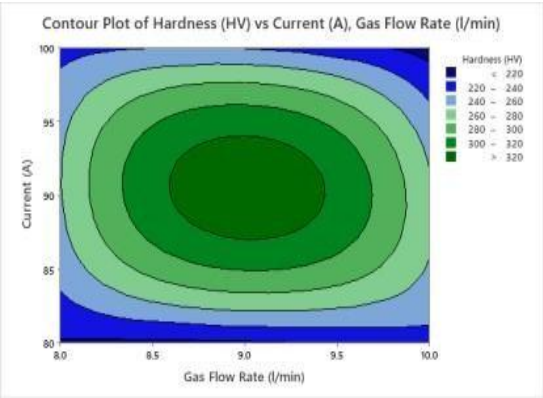

(b)

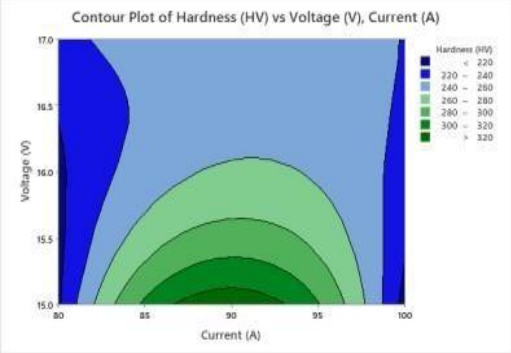

(c)

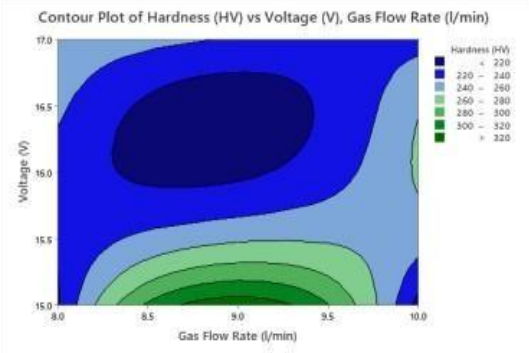

(d)

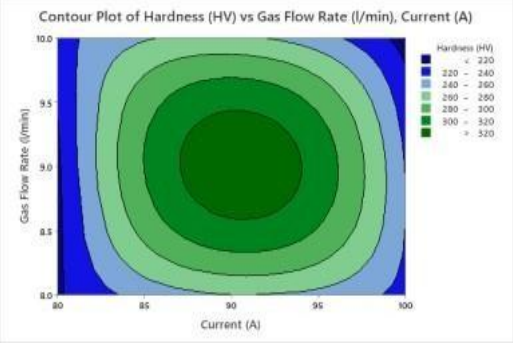

(e)

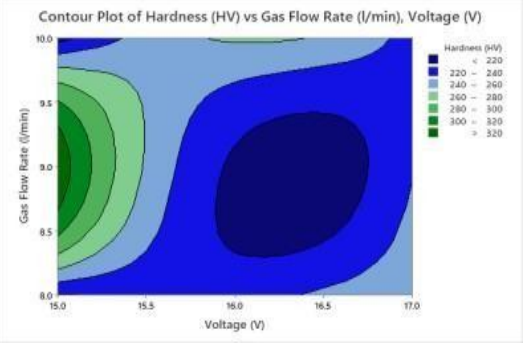

(f)

Figure 4-13: Contour plot of Hardness (316L) (a) Current vs Voltage (b) Current vs Gas flow rate(c) Voltage vs current (d) Voltage vs Gas flow rate (e) Gas Flow rate vs Current (f) Gas Flow rate vs Voltage

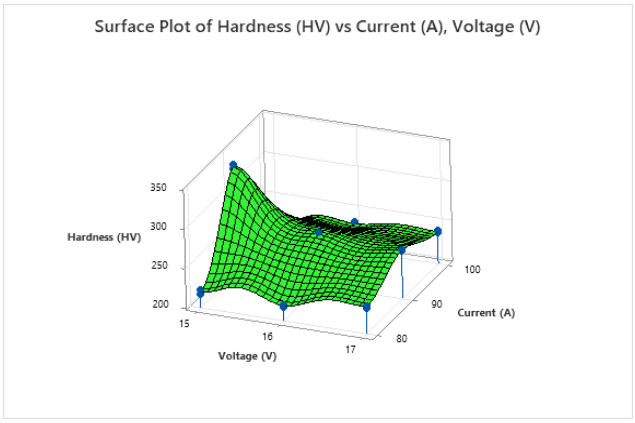

(a)

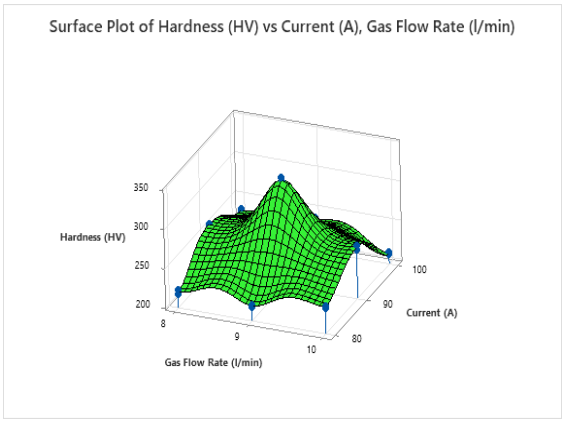

(b)

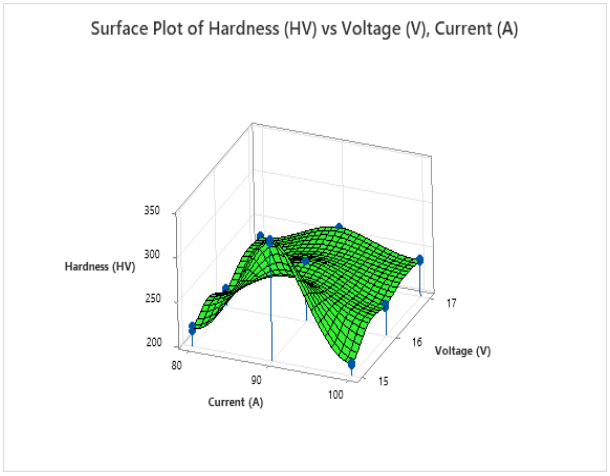

(c)

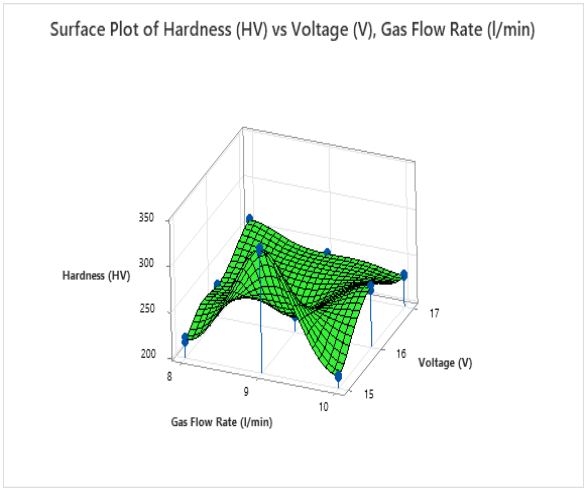

(d)

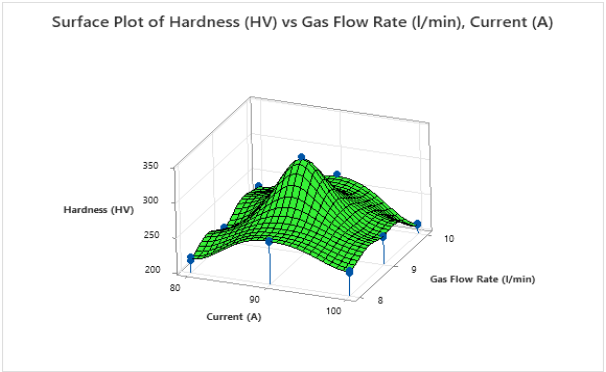

(e)

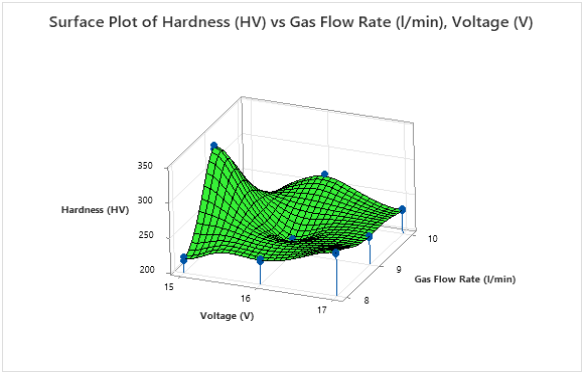

(f)

Figure 4-14: Surface plot of Hardness (316L) (a) Current vs Voltage (b) Current vs Gas flow rate(c) Voltage vs current (d) Voltage vs Gas flow rate (e) Gas Flow rate vs Current (f) Gas Flow rate vs Voltage

4.4.2 EVALUATION OF HARDNESS OF AISI321/308L

4.4.2.1 Main Effect Plot for Hardness (308L)

Main effect plot was carried out by using Minitab 20 software. Effect of TIG welding parameters on hardness was studied in main effect plot. Figure 4.15 shows the main effect plot for hardness of nine samples welded by using 308L filler rod. Main effect plot for S/N ratio is shown in figure 4.15 and response table for S/N ratio is shown in table 4.11.

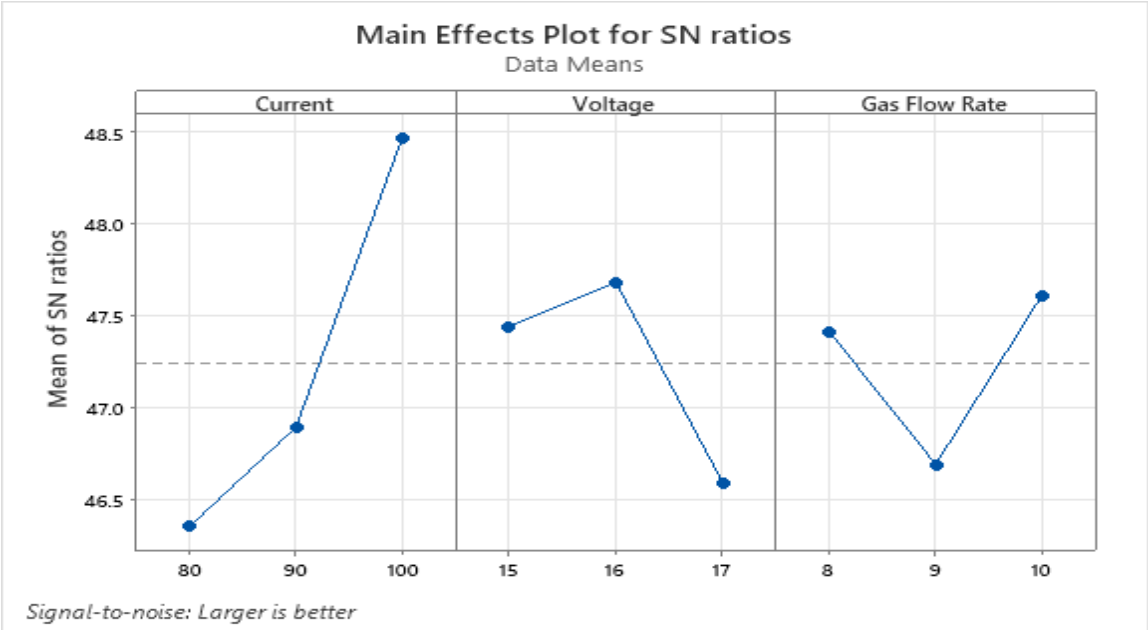

Figure 4-15: S/N ratio main effect plot of welding parameters

From the table 4.11 it is shown that hardness of selected welded sample is higher when welding current is 100A, voltage is at 16 V and gas flow rate is at 9 lit/min thus we find these welding parameters are optimal for this experiment.

Table 4. 11: Response Table for Signal to Noise Ratios

Level	Current	Voltage	Gas Flow Rate
1	46.35	47.44	47.41
2	46.89	47.68	46.69
3	48.47	46.59	47.61
Delta	2.12	1.09	0.92
Rank	1	2	3

4.4.2.2 ANOVA for Hardness (308L)

TIG welding parameters were statistically analyzed using analysis of variance (ANOVA). The current, with a contribution of 60.25 percent, is clearly the most influential parameter of the control factor on the hardness. Weld bead shape, weld quality, and hardness are all affected by current.

Table 4. 12: Analysis of variance for Hardness (308L)

Source	DF	Seq SS	Contribution	Adj SS	Adj MS	F-Value	P-Value
Current (A)	1	10325.3	60.25%	10325.3	10325.3	28.22	0.000
Voltage (V)	1	1633.3	9.53%	1633.3	1633.3	4.46	0.053
Gas Flow Rate (l/min)	1	56.3	0.33%	56.3	56.3	0.15	0.701
Error	14	5123.0	29.89%	5123.0	365.9		
Lack-of-Fit	5	5064.0	29.55%	5064.0	1012.8	154.49	0.000
Pure Error	9	59.0	0.34%	59.0	6.6		
Total	17	17138.0	100.00%				

Current is the most important factor which is shown in petro chart in figure 4.16(a). According to figure 4.16(b), the ANOVA analysis revealed that the data points were almost exactly in a straight line. The model only included major components, and the error was distributed normally along a straight line. The model points were not closed, and the data was presented in a strewn pattern in the vs fits plots, as seen in Figure 4.16 (c). No outliner was found in figure 4.16 (d). The histogram in Figure 4.16 (e) presented distribution of data within the limits and the data frequently lied on the central line. So the model was adequate for conducting this experimental study.

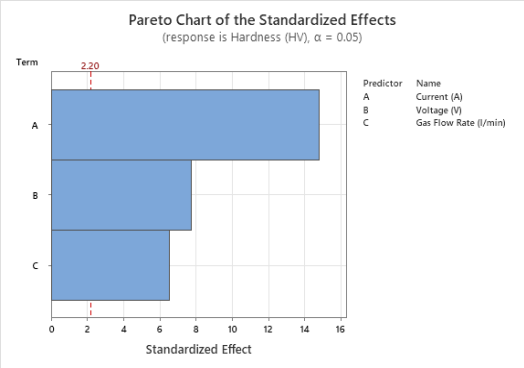

(a)

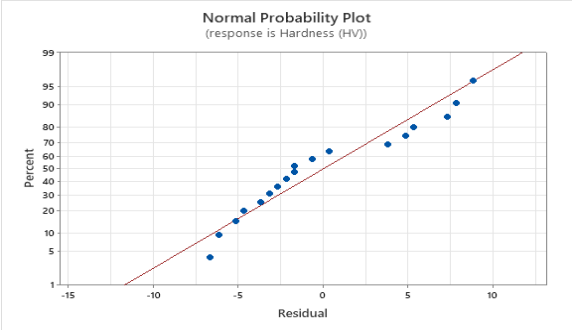

(b)

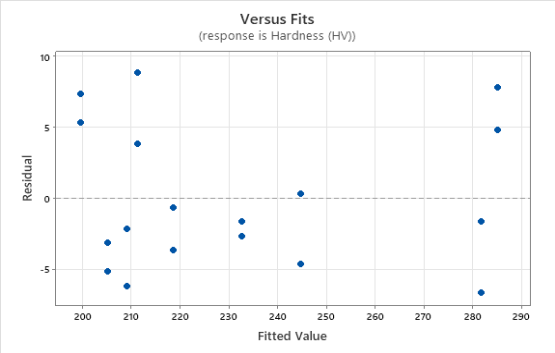

(c)

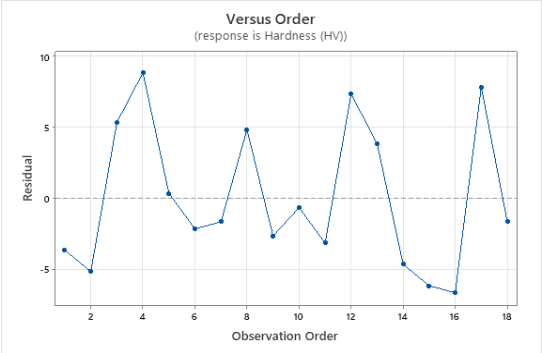

(d)

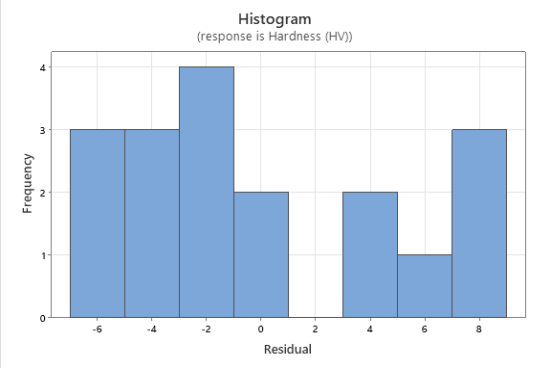

(e)

Figure 4-16: (a) Pareto Chart (b) Normal Probability Chart (c) Verses fit (d) Versus order (e) Histogram

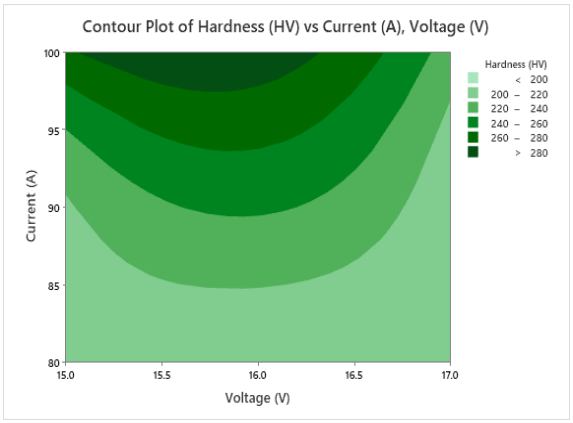

(a)

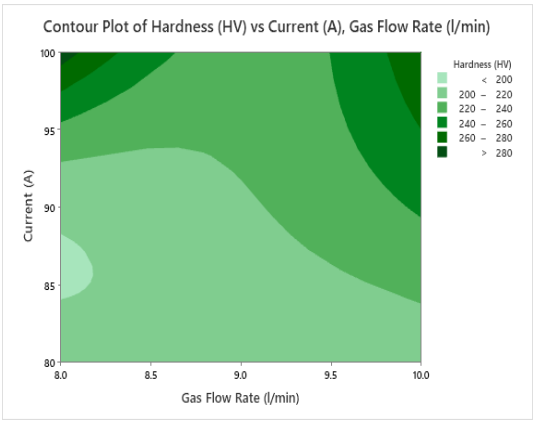

(b)

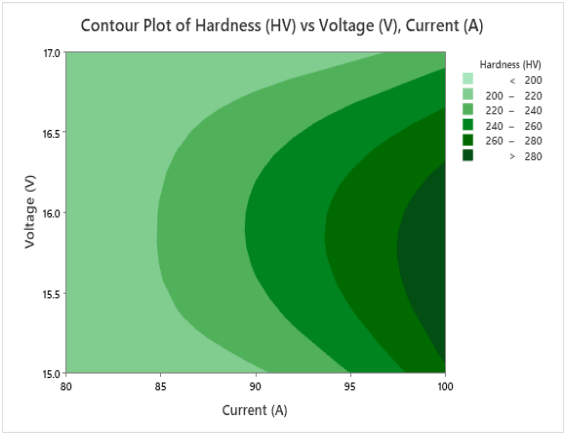

(c)

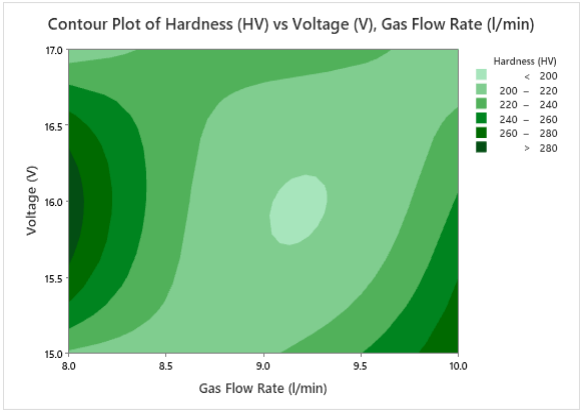

(d)

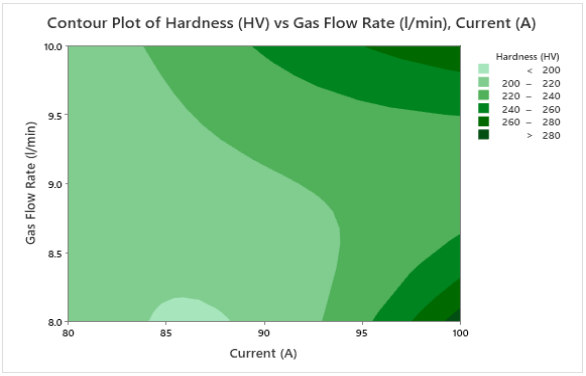

(e)

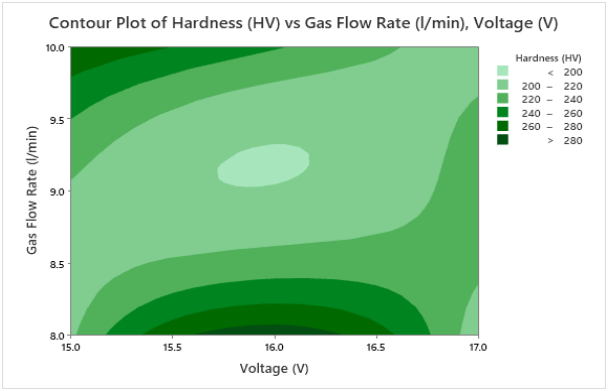

(f)

Figure 4-17: Contour plot of Hardness (308L) (a) Current vs Voltage (b) Current vs Gas flow rate(c) Voltage vs current (d) Voltage vs Gas flow rate (e) Gas Flow rate vs Current (f) Gas Flow rate vs Voltage

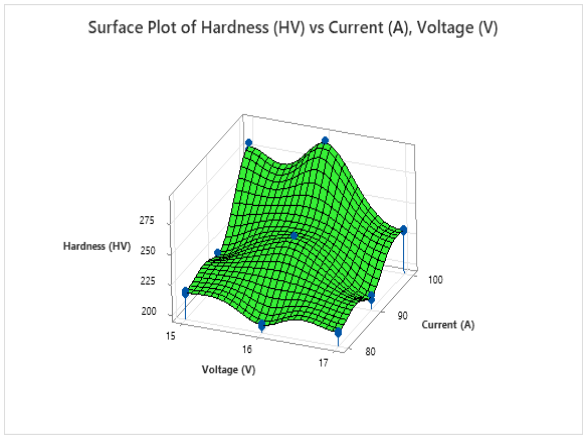

(a)

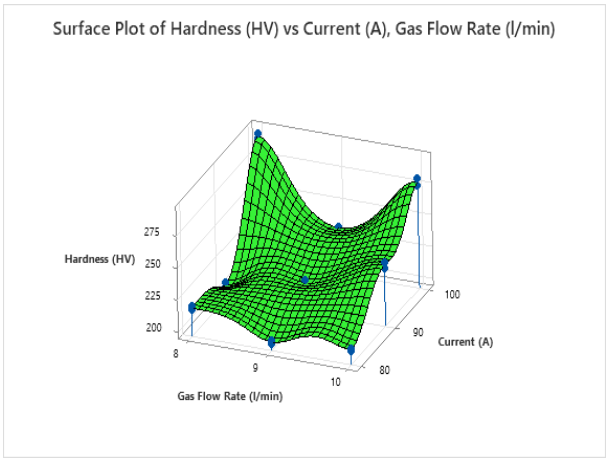

(b)

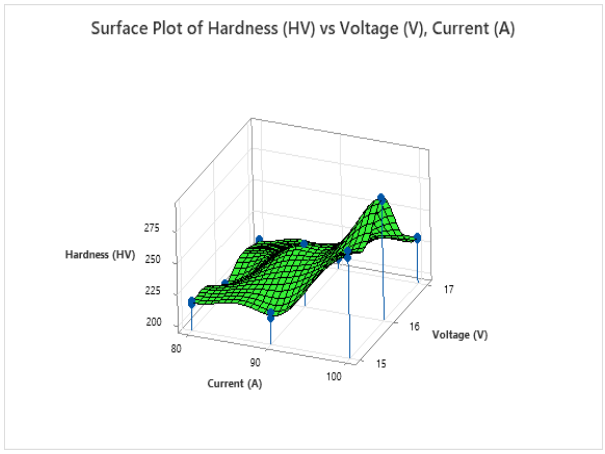

(c)

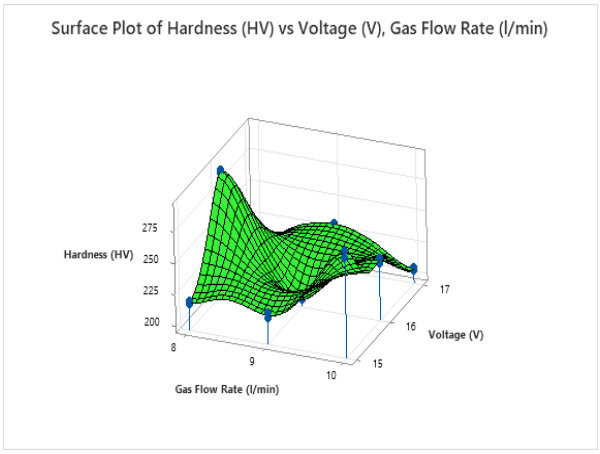

(d)

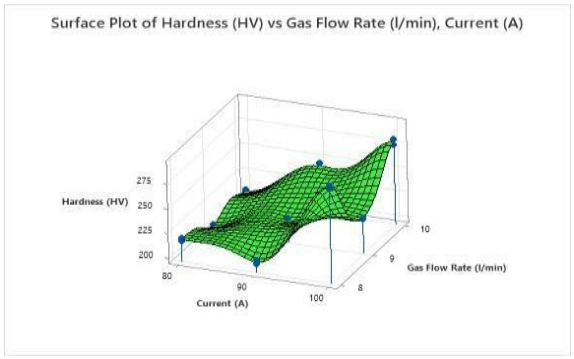

(e)

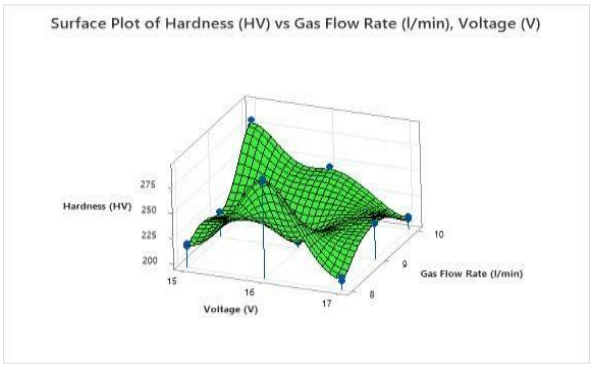

(f)

Figure 4-18:Surface plot of Hardness (308L) (a) Current vs Voltage (b) Current vs Gas flow rate(c) Voltage vs current (d) Voltage vs Gas flow rate (e) Gas Flow rate vs Current (f) Gas Flow rate vs Voltage

4.5 YEILD STRENGTH, UTS AND % ELONGATION

To quantify and evaluate the joint strength the welded samples were loaded until fracture is occurred. In the welding zone, the specimens cracked from weld zone. The breakdown happened at the parting region of the weld zone, indicating it the weakest point. Yield strength, Ultimate Tensile strength and % elongation was measured at room temperature by using universal testing machine. Experimental results of yield strength, ultimate tensile strength (UTS) and percentage elongation (% Elongation) are measured for nine welded specimens welded by using 316L filler wire and nine specimens are welded by using 308L filler wire are enlisted in table 4-11 and 4-12 respectively.

Table 4.11: Experimental Results of Welded Specimens AISI321/ER316L

Sample No	Current (A)	Voltage (V)	Gas Flow rate (lit/min)	Yield Strength (MPa)	UTS (MPa)	% Elongation
S-1	80	15	8	265	807	61.5
S-2	80	16	9	314	657	39.6
S-3	80	17	10	282	639	50.7
S-4	90	15	9	333	620	37.5
S-5	90	16	10	286	772	49.9
S-6	90	17	8	321	651	38.4
S-7	100	15	10	393	673	32.3
S-8	100	16	8	285	625	39.2
S-9	100	17	9	314	607	38.6

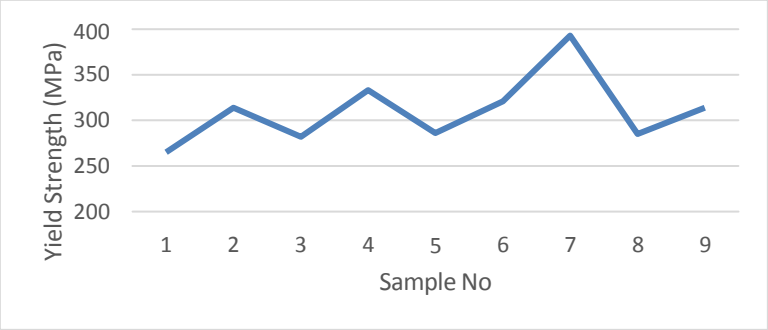

Figure 4-19: Yield Strength of Welded Specimens (AISI321/ER316L)

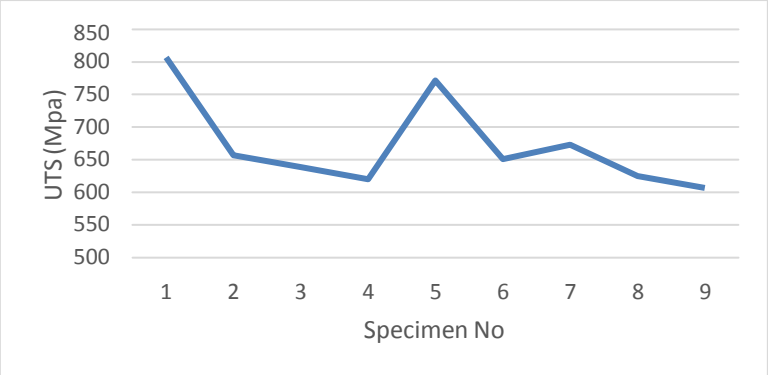

Figure 4-20: Ultimate Tensile Strength of Welded Specimens (AISI321/ER316L)

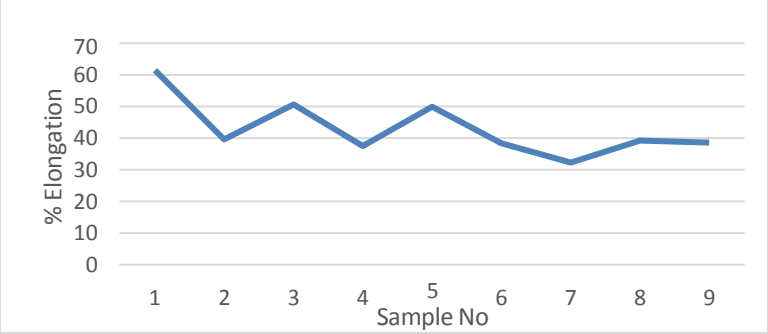

Figure 4-21: Percent Elongation of Welded Specimens (AISI321/ER316L)

In table 4.11 it is noted that changes in current, voltages and gas flow rate had clear effect on UTS, yield strength, and % elongation of welded specimens weld by using 316L filler rod. The

yield strength, UTS and % elongation results of nine welded samples are plotted in figure 4.19, 4.20 and 4.21. It is noted that specimen No 1 has maximum value of UTS (807MPa) and sample No 9 has minimum value of UTS (607 MPa). But in the case of % elongation and yield strength it is observed that sample 1 has maximum % elongation (61.5 %) and minimum yield strength (265MPa) whereas sample No 7 has minimum % elongation (32.3 %) and maximum value of yield strength (393MPa). It is also noted that UTS and % elongation is maximum at lower value of current, voltage, and gas flow rates but yield strength is minimum, whereas at higher values of current, voltage, and gas flow rate the UTS and % elongation is minimum and yield strength is maximum.

Table 4.12: Experimental Results of Welded Specimens AISI321/ER308L

Sample No	Current (A)	Voltage (V)	Gas Flow Rate (lit/min)	Yield Strength (MPa)	UTS (MPa)	% Elongation
S-A	80	15	8	313	610	35.5
S-B	80	16	9	306	628	41.5
S-C	80	17	10	288	606	42.0
S-D	90	15	9	338	661	41.2
S-E	90	16	10	311	620	44.0
S-F	90	17	8	379	713	50.9
S-G	100	15	10	349	644	40.0
S-H	100	16	8	310	669	36.7
S-I	100	17	9	337	667	38.8

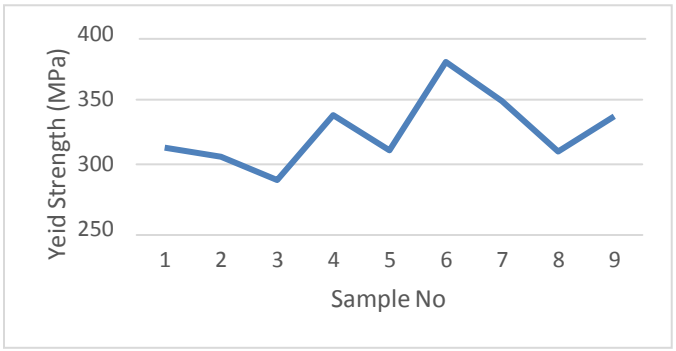

Figure 4-22: Yield Strength of Welded Specimens (AISI321/ER308L)

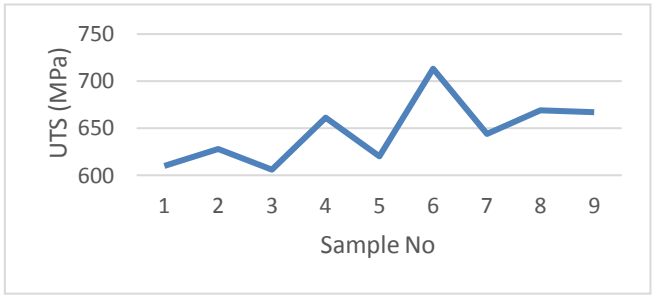

Figure 4-23: Ultimate Tensile Strength of Welded Specimens (AISI321/ER308L)

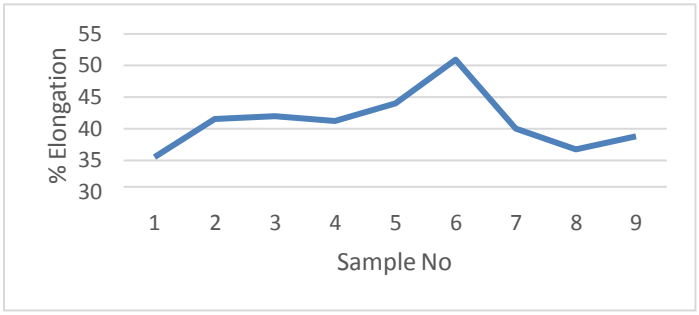

Figure 4-24: Ultimate Tensile Strength of Welded Specimens (AISI321/ER308L)

Changes in welding parameters, such as welding current, voltage, and gas flow rate, had a clear effect on the yield strength, UTS and % elongation of AISI321/ER308L, as shown in table 4.12 and figure 4.22, 4.23 & 4.24. It is observed that sample F has the highest UTS and Yield strength values of 713 MPa and 379 MPa respectively, whereas sample C has the lowest UTS

and yield strength values of 606 MPa and 288 MPa. Sample F has the highest percent elongation value 50.9 % while sample A achieved the lowest percent elongation value 35.5 %. The highest yield strength, UTS, and percent elongation were achieved at medium current and gas flow rate, whereas the minimum yield strength, UTS, and percent elongation were achieved at lower current and higher gas flow rate and voltage, as shown in table 4.12.

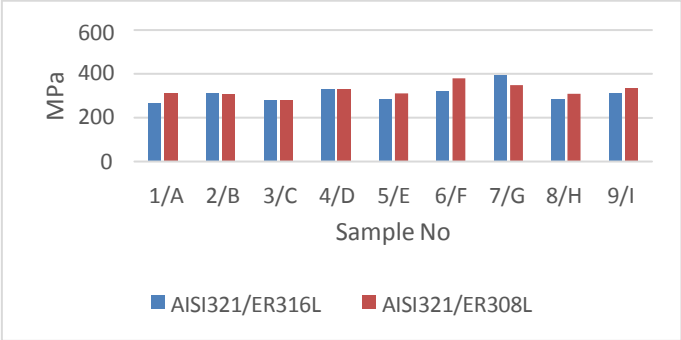

Figure 4-25: Comparison of Yield Strength between AISI321/ER316L & AISI321/ER308L

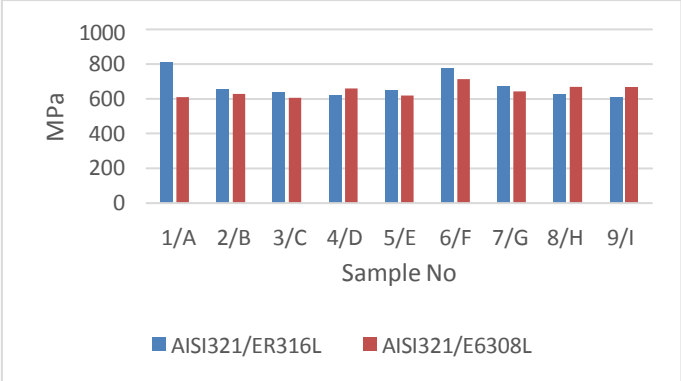

Figure 4-26: Comparison of UTS between AISI321/ER316L & AISI321/ER308L

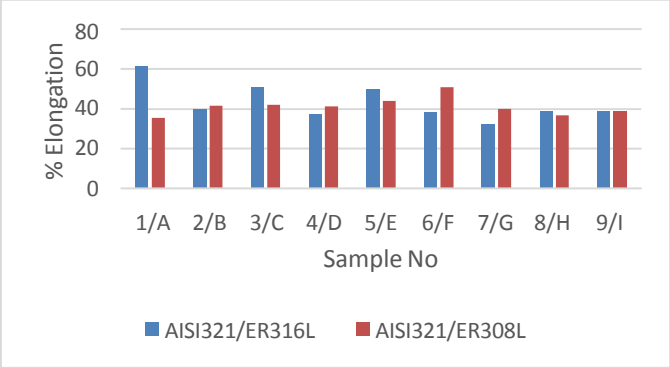

Figure 4-27: Comparison of % Elongation between AISI321/ER316L & AISI321/ER308L

The figure 4.25, 4.26 & 4.27 show bar chart comparison of yield strength, UTS and % elongation of nine samples weld by using 316L filler rod and nine samples welded by using 308L filler rod. From the bar charts it is clearly observed that sample welded through 316L has higher UTS and % elongation than the sample welded by using 308L filler wire, whereas the yield strength of 308L welded samples are higher. From the above comparison chart, yield strength, UTS and % elongation are much influenced by the filler rod used for welding. Of the two joint, sample welded through 316L filler wire has better results than sample welded through 308L filler wire.

4.5.1 EFFECT OF WELDING PARAMETRS ON YIELD STRENGTH, UTS AND % ELONGATION

- **Mean Effect plot and ANOVA Analysis**

The mean effect plot and ANOVA analysis was performed by using Minitab 20 software. In this software we are able to generate reaction graphs for the welding parameters effects on yield strength, UTS and % elongation. When the parameter value is changed from one level to another, response graphs for means of S/N ratios are plotted to know the variation and outcome of each parameter. The optimum level is the one with highest S/N ratio. Moreover, ANOVA is performed to evaluate percent contribution of each parameter on responses. It helps in evaluating importance of process parameters and to accurately determine optimum parameter levels

4.5.1.1 Mean Effect Plot for Yield Strength (ER316L)

Mean effect plot for yield strength of AISI 321/ER316L welded samples are calculated by using Minitab and their result is enlisted in table 4.13

Table 4.13: Signal to Noise ratio of yield strength

Sample No	Yield Strength MPa	S/N ratio dB
S-1	265	48.3814
S-2	314	50.0200
S-3	282	48.9740
S-4	333	50.4748
S-5	286	49.0343
S-6	321	50.1836
S-7	393	51.9208
S-8	285	49.0193
S-9	314	49.8826

The mean effect plot for the S/N ratio is displayed in figure 4.28, and the response table for the S/N ratio is presented in table 4.14.

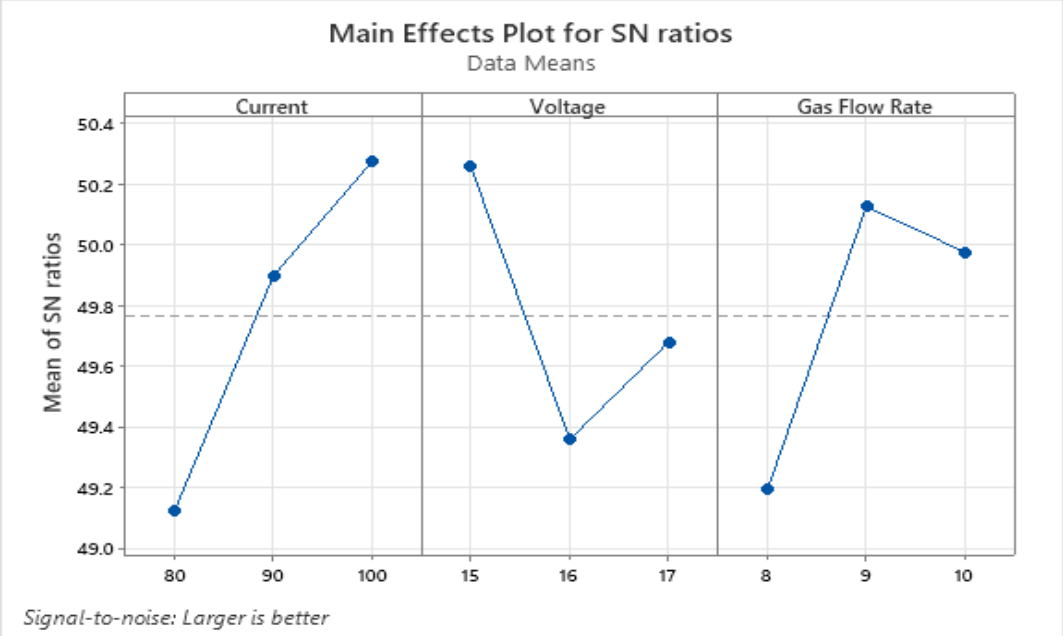

Figure 4-28: Main Effect Plot for S/N ratio

Table 4.14: Response Table for S/N Ratios

Level	Current	Voltage	Gas Flow Rate
1	49.13	50.26	49.19
2	49.90	49.36	50.13
3	50.27	49.68	49.98
Delta	1.15	0.90	0.93
Rank	1	3	2

According to the Taguchi approach, the best parameter is the one that generates the highest S/N ratio. The yield strength of the resulting specimens is maximum when the arc current is kept at 100 A, the voltage is kept at 15 V, and the gas flow rate is kept at 10 l/min, as shown in table 4.14 and figure 4.28, therefore we estimate these parameters to be the optimum for this experiment.

4.5.1.2 ANOVA Analysis for Yield Strength (ER316L)

The results of the analysis of variance on the data for Yield Strength is shown in table 4.15.

Table 4.15: Analysis of Variance for S/N ratio (ER316L)

Source	DF	Seq SS	Contribution	Adj SS	Adj MS	F-Value	P-Value
Current	2	5607.4	22.32%	5607.4	2803.72	2.66	0.114
Voltage	2	4115.4	16.38%	4115.4	2057.72	1.96	0.188
Gas Flow Rate	2	3830.1	15.24%	3830.1	1915.06	1.82	0.208
Error	11	11573.9	46.06%	11573.9	1052.18		
Lack-of-Fit	2	11488.4	45.72%	11488.4	5744.22	604.65	0.000
Pure Error	9	85.5	0.34%	85.5	9.50		
Total	17	25126.9	100.00%				

According to ANOVA table 4.15, the most influential factor for yield strength is current, which has a 22.32 percent contribution factor. The next most influential aspect is voltage, which has a 16.38 percent contribution, followed by gas flow rate, which has 15.24 percent contribution.

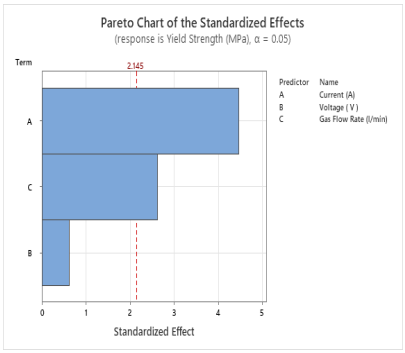

(a)

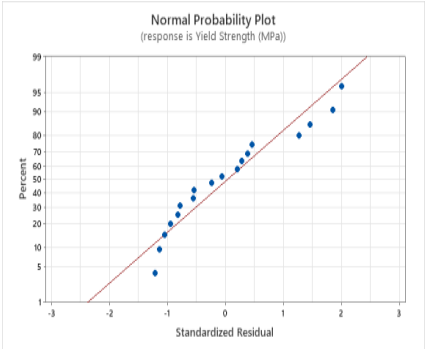

(b)

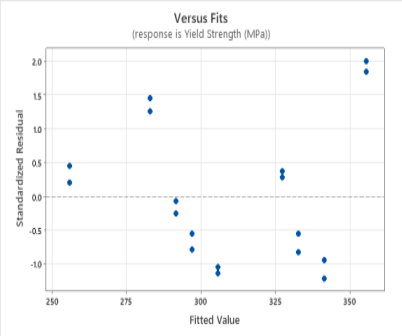

(c)

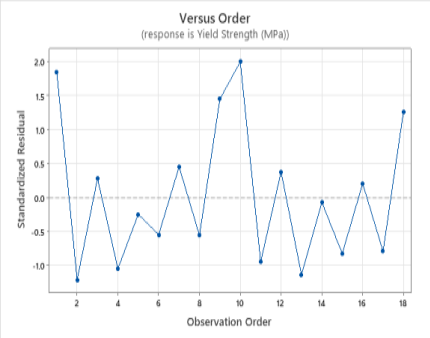

(d)

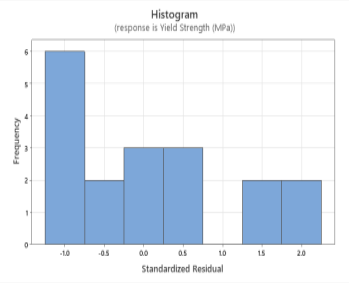

(e)

Figure 4-29:(a) Pareto Chart (b) Normal Probability Chart (c) Verses fit (d) Versus order (e) Histogram

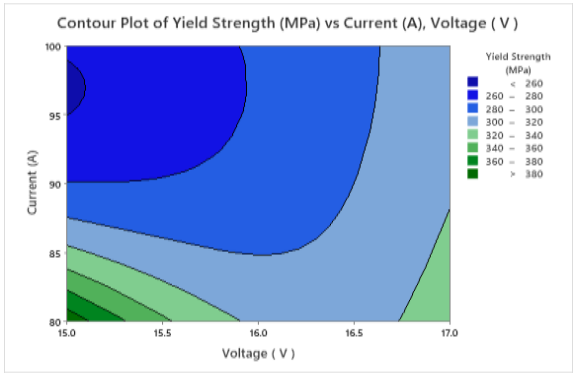

(a)

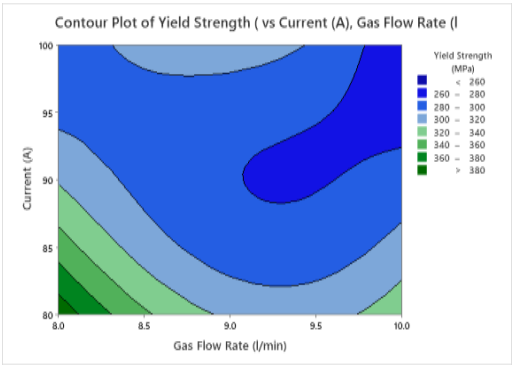

(b)

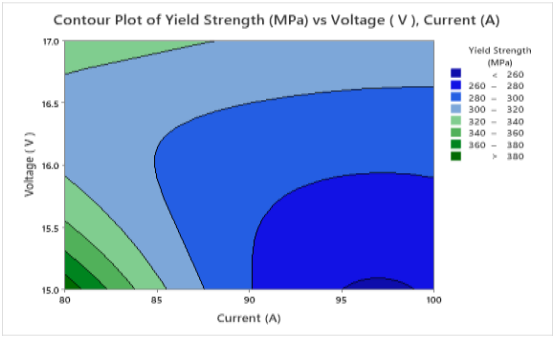

(c)

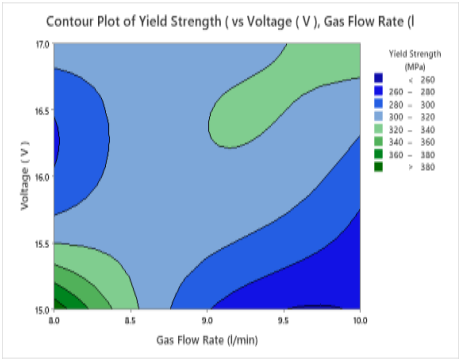

(d)

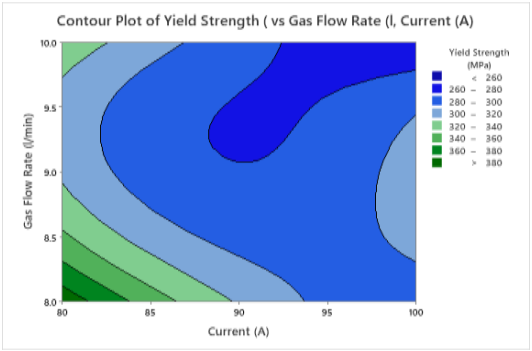

(e)

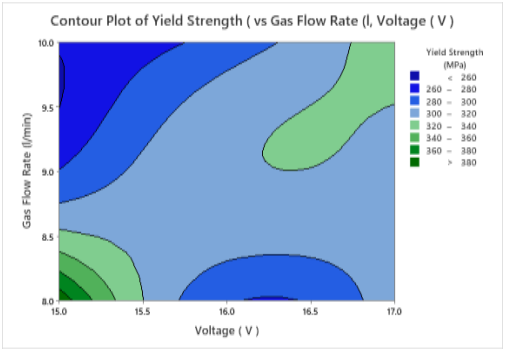

(f)

Figure 4-30: Contour plot of Yield strength(316L) (a) Current vs Voltage (b) Current vs Gas flow rate(c) Voltage vs current (d) Voltage vs Gas flow rate (e) Gas Flow rate vs Current (f) Gas Flow rate vs Voltage

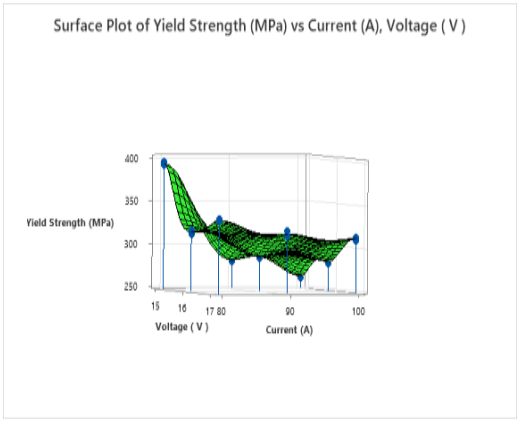

(a)

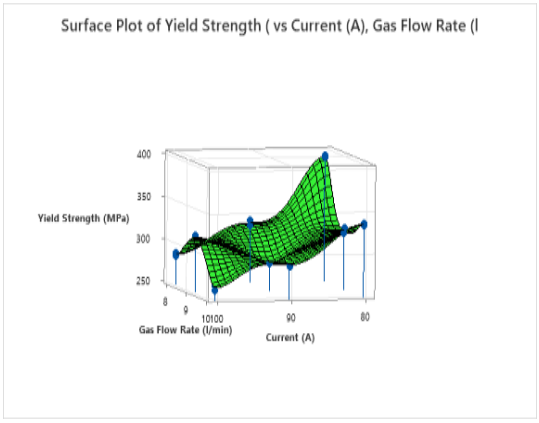

(b)

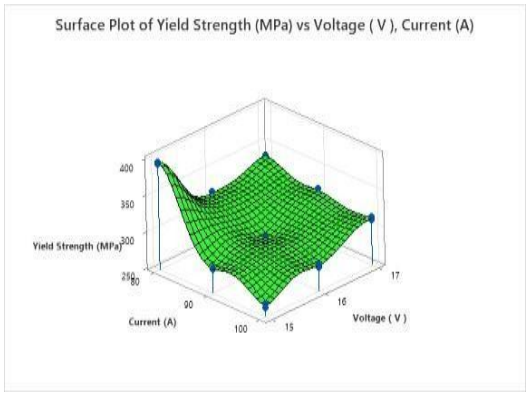

(c)

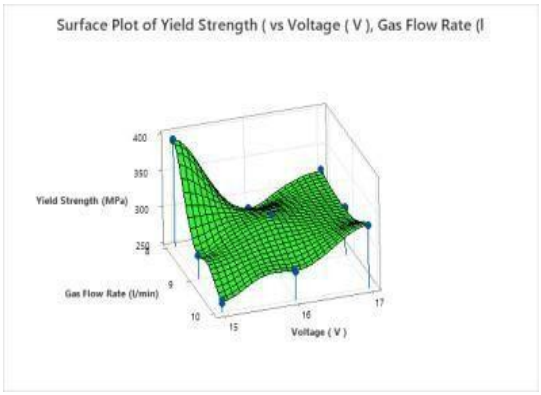

(d)

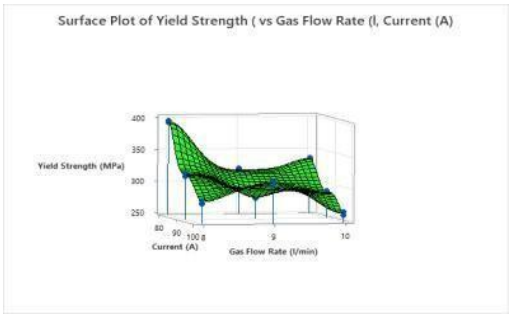

(e)

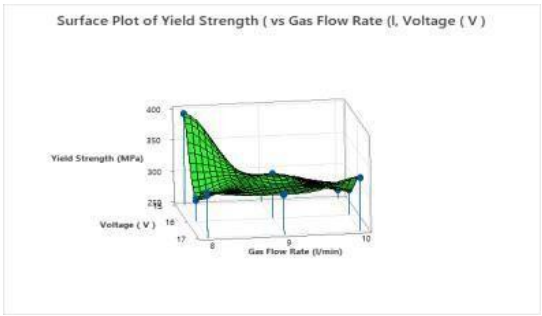

(f)

Figure 4-31: Surface plot of Yield strength (316L) (a) Current vs Voltage (b) Current vs Gas flow rate(c) Voltage vs current (d) Voltage vs Gas flow rate (e) Gas Flow rate vs Current (f) Gas Flow rate vs Voltage

4.5.1.3 Main Effect Plot of UTS (ER316L)

The signal to noise ratio of UTS of AISI 321/ER316L welded samples was calculated using Minitab, and the results are shown in table 4.16.

Table 4.16: Signal to Noise ratio of UTS (ER316L)

Sample No	UTS MPa	S/N ratio dB
S-1.	807	58.1536
S-2.	657	56.3180
S-3.	639	56.1168
S-4.	620	55.8618
S-5.	772	57.7411
S-6.	651	56.2582
S-7.	673	56.5732
S-8.	625	55.9521
S-9.	607	55.6566

S/N ratio main effect plot is shown in figure 4.32 response table for S/N ratio is shown in table 4.17.

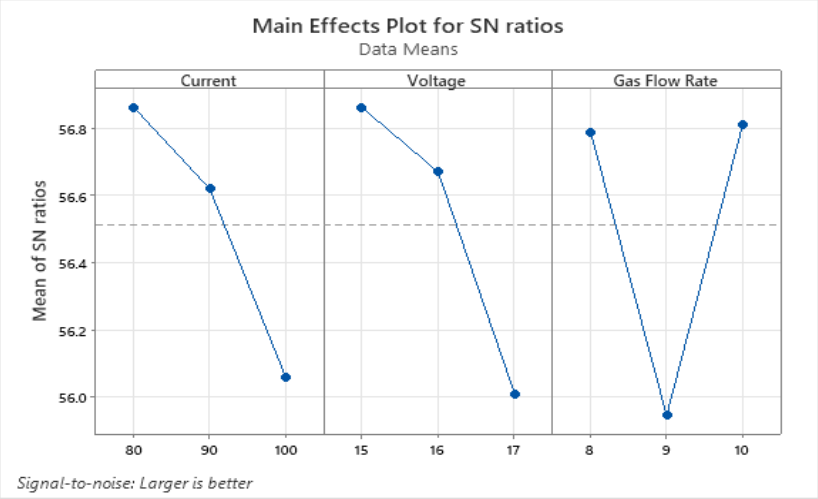

Figure 4-32: Main Effect Plot for S/N ratio

Table 4.17: Response Table for S/N Ratios (ER316L)

Level	Current	Voltage	Gas Flow Rate
1	56.86	56.86	56.79
2	56.62	56.67	55.95
3	56.06	56.01	56.81
Delta	0.80	0.85	0.86
Rank	3	2	1

The ideal parameter will yield the maximum S/N ratio, according to the taguchi technique. Table 4.17 and figure 4.32 demonstrate that the UTS of the created specimens is highest when the arc current is kept at 80 A, the voltage is kept at 15 V, and the gas flow rate is kept at 8 l/min, thus we consider these parameters are the optimum for this experiment.

4.5.1.4 ANOVA Analysis for UTS (ER316L)

The results of the analysis of variance (ANOVA) on the data for UTS are shown in Table 4.18.

Table 4.18: Analysis of Variance for S/N ratio (ER316L)

Source	DF	Seq SS	Contribution	Adj SS	Adj MS	F-Value	P-Value
Current (A)	2	9923.4	15.81%	9923.4	4961.7	2.18	0.159
Voltage (V)	2	12232.1	19.49%	12232.1	6116.1	2.69	0.112
Gas Flow Rate (l/min)	2	15568.8	24.81%	15568.8	7784.4	3.42	0.070
Error	11	25031.3	39.89%	25031.3	2275.6		
Lack-of-Fit	2	24980.8	39.81%	24980.8	12490.4	2226.01	0.000
Pure Error	9	50.5	0.08%	50.5	5.6		
Total	17	62755.6	100.00%				

The most influential element for UTS, according to ANOVA table 4-18 is gas flow rate, which has a 24.81 % and 0.070 impact factor. Voltage is the second most significant factor which has a 19.49% and the current, which has a 15.81 %.

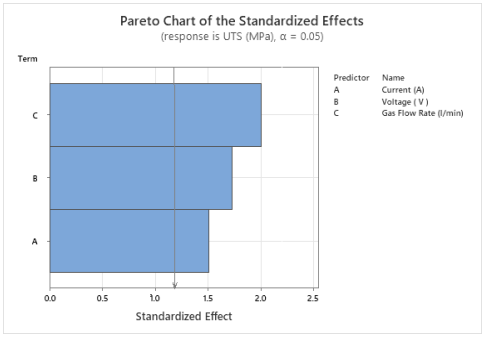

(a)

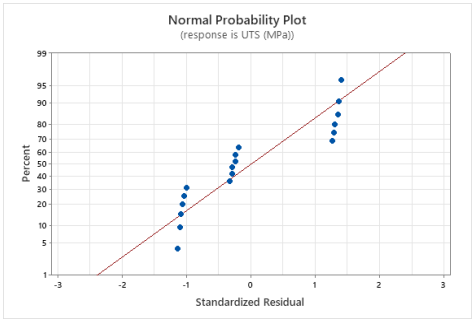

(b)

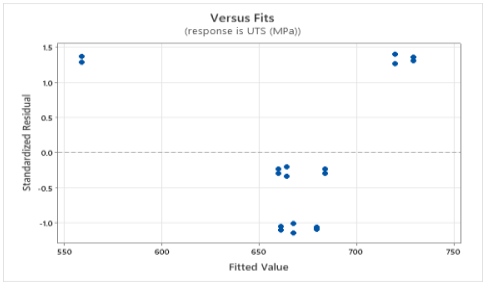

(b)

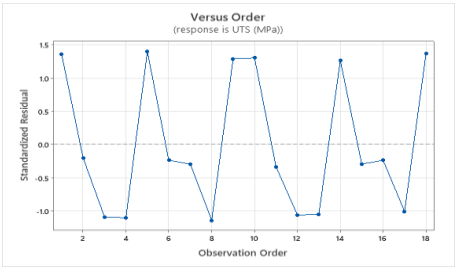

(d)

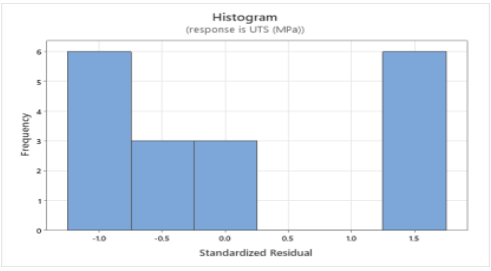

(e)

Figure 4-33 (a) Pareto Chart (b) Normal Probability Chart (c) Verses fit (d) Versus order (e) Histogram

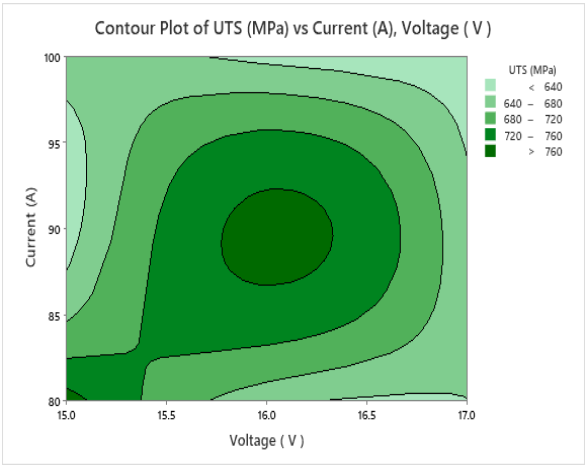

(a)

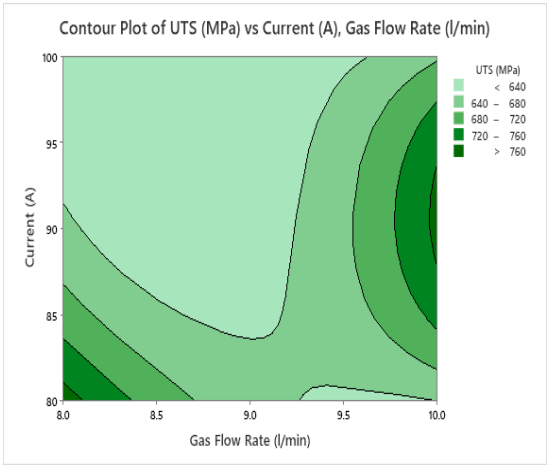

(b)

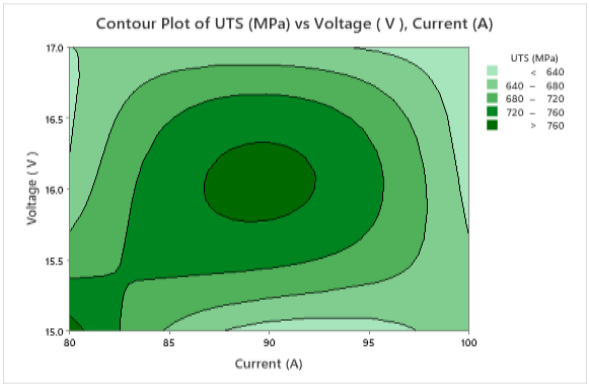

(c)

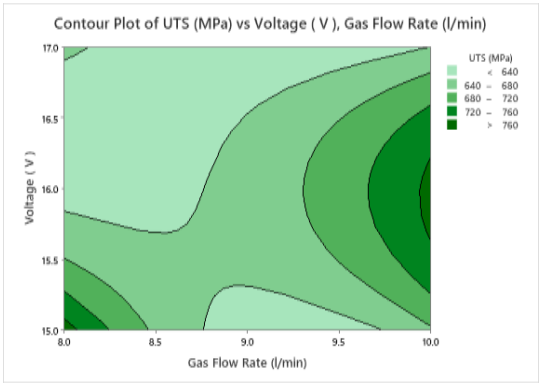

(d)

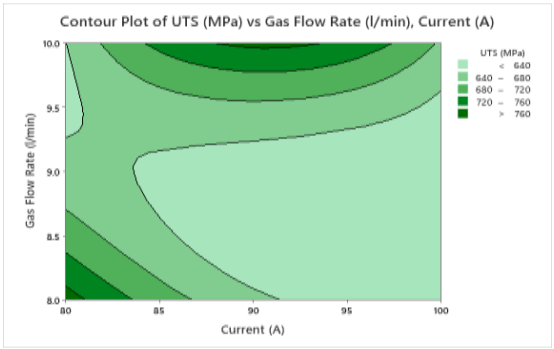

(e)

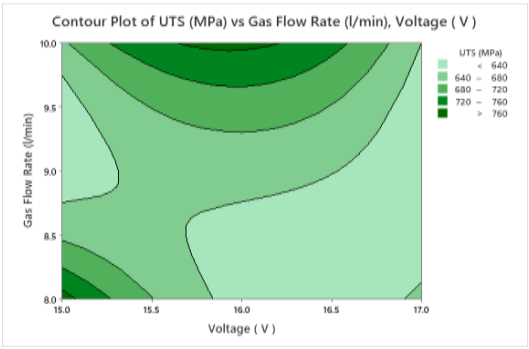

(f)

Figure 4-34: Contour plot of UTS(316L) (a) Current vs Voltage (b) Current vs Gas flow rate(c) Voltage vs current (d) Voltage vs Gas flow rate (e) Gas Flow rate vs Current (f) Gas Flow rate vs Voltage

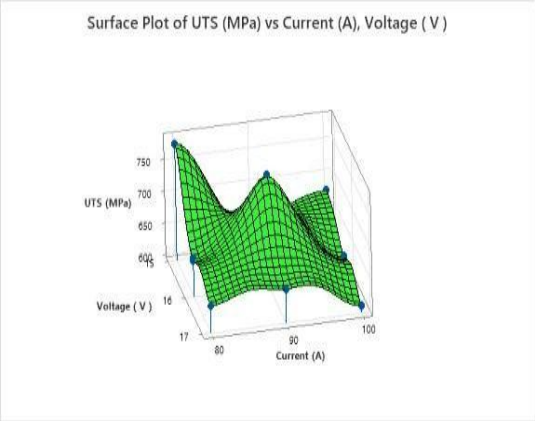

(a)

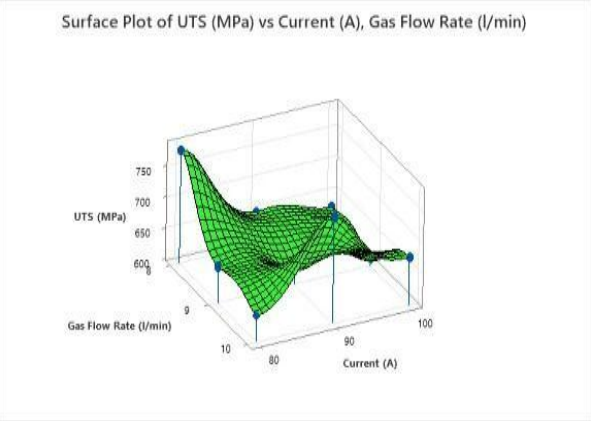

(b)

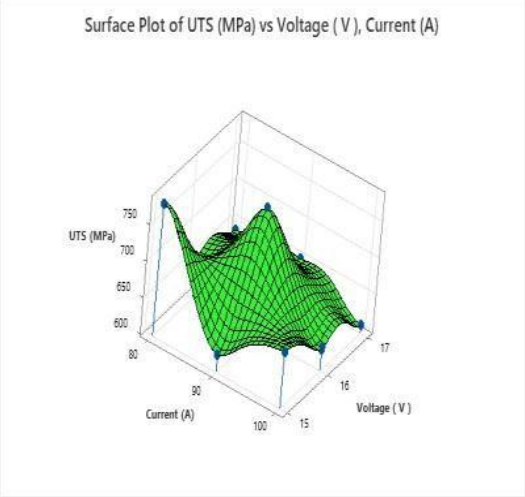

(c)

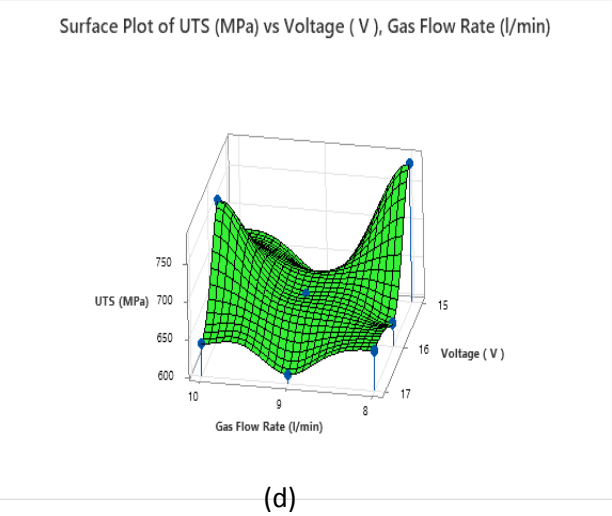

(d)

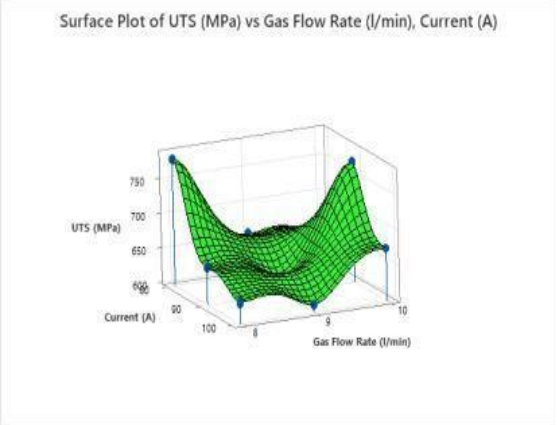

(e)

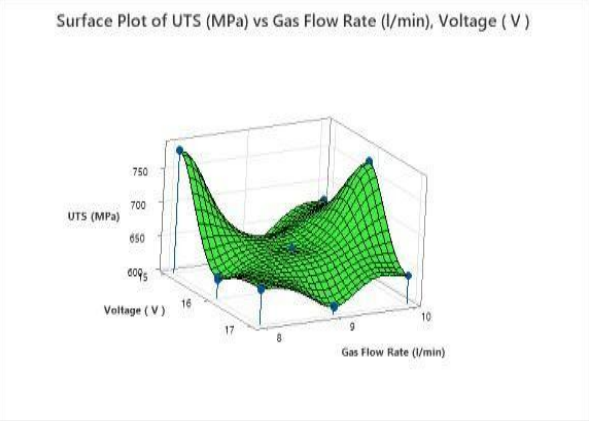

(f)

Figure 4-35: Contour plot of UTS (316L) (a) Current vs Voltage (b) Current vs Gas flow rate(c) Voltage vs current (d) Voltage vs Gas flow rate (e) Gas Flow rate vs Current (f) Gas Flow rate vs Voltage

4.5.1.5 Main Effect Plot of % Elongation (ER316L)

MINTAB was used to determine the signal to noise ratio of percent elongation of AISI 321/ER316L welded samples, and the findings are reported in table 4.19.

Table 4.19: Signal to Noise ratio of % Elongation (ER316L)

Sample No	% Elongation MPa	S/N ratio dB
S-1	61.5	35.8333
S-2	39.6	32.0609
S-3	50.7	34.1426
S-4	37.5	31.3738
S-5	49.9	33.8459
S-6	38.4	31.7534
S-7	32.3	30.2890
S-8	39.2	31.8322
S-9	38.6	31.5683

The mean effect plot for the S/N ratio is displayed in figure 4.36, and the response table for the S/N ratio is presented in table 4.20.

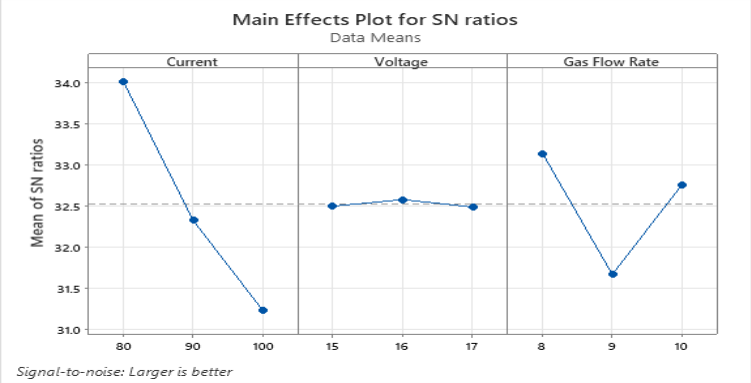

Figure 4-36: Main Effect Plot for S/N ratio

Table 4.20: Response Table for S/N Ratios (ER316L)

Level	Current	Voltage	Gas Flow Rate
1	34.01	32.50	33.14
2	32.32	32.58	31.67
3	31.23	32.49	32.76
Delta	2.78	0.09	1.47
Rank	1	3	2

According to the Taguchi technique, the optimum parameter is the one that generates the largest S/N ratio. The % elongation of the produced specimens is largest when the arc current is held at 80 A, the voltage is kept at 15 V, and the gas flow rate is maintained at 8 L/min, as shown in table 4.26 and figure 4.31, therefore these settings are the best for this experiment.

4.5.1.6 ANOVA Analysis of % Elongation (316L)

Table 4.21 shows the results of an analysis of variance (ANOVA) on the dataset for percent elongation.

Table 4.21: Analysis of Variance for S/N ratio (ER316L)

Source	DF	Seq SS	Contribution	Adj SS	Adj MS	F-Value	P-Value
Current	2	642.60	47.86%	642.603	321.302	7.39	0.009
Voltage	2	6.24	0.47%	6.243	3.122	0.07	0.931
Gas Flow Rate	2	215.41	16.04%	215.410	107.705	2.48	0.129
Error	11	478.34	35.63%	478.343	43.486		
Lack-of-Fit	2	474.62	35.35%	474.623	237.312	574.14	0.000
Pure Error	9	3.72	0.28%	3.720	0.413		
Total	17	1342.60	100.00%				

According to ANOVA Table 4.21, the most influencing factor for percent elongation is current, which has contribution of 47.86 % and 0.009 impact factor. As P value of current is less than 0.05.

4.5.1.7 Main Effect Plot of Yield Strength (ER308L)

Signal to noise ratio of yield strength of AISI 321/ER308L welded samples are calculated by using MINTAB and their result is enlisted in table 4.22.

Table 4.22: Signal to Noise ratio of yield strength (ER308L)

Sample No	Yield Strength MPa	S/N ratio dB
S-A	313	49.8689
S-B	306	49.7426
S-C	288	49.1727
S-D	338	50.5911
S-E	311	49.8967
S-F	379	51.5842
S-G	349	50.8689
S-H	310	49.8412
S-I	337	50.5782

S/N ratio main effect plot is shown in figure 4.37 response table for S/N ratio is shown in table 4.23.

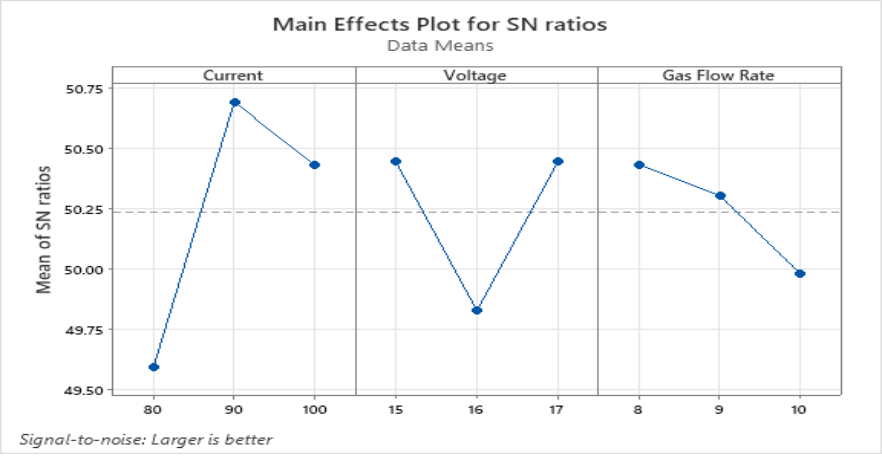

Figure 4-37: **Main Effect Plot for S/N ratio (ER308L)**

Table 4.23: Response Table for S/N Ratios (ER308L)

Level	Current	Voltage	Gas Flow Rate
1	49.59	50.44	50.43
2	50.69	49.83	50.30
3	50.43	50.45	49.98
Delta	1.10	0.62	0.45
Rank	1	2	3

The optimum parameter, according to the Taguchi technique, is the one that produces the maximum S/N ratio. We can see from table 4-23 and figure 4-37 that the yield strength of the obtained specimens is highest when the arc current is kept at 90 A, the voltage is kept at 17 V, and the gas flow rate is held at 8 l/min, thus we consider these settings to be the best for this experiment.

4.5.1.8 ANOVA Analysis of Yield Strength (ER308L)

Table 4.24 shows the results of the analysis of variance on the data for Yield Strength.

Table 4.24: Analysis of Variance for S/N ratio

Source	DF	Seq SS	Contribution	Adj SS	Adj MS	F-Value	P-Value
Current	2	5560.1	44.85%	5560.11	2780.06	8.55	0.006
Voltage	2	2330.1	18.80%	2330.11	1165.06	3.58	0.04
Gas Flow Rate	2	929.8	7.50%	929.78	464.89	1.43	0.281
Error	11	3576.9	28.85%	3576.94	325.18		
Lack-of-Fit	2	3561.4	28.73%	3561.44	1780.72	1033.97	0.000
Pure Error	9	15.5	0.13%	15.50	1.72		
Total	17	12396.9	100.00%				

According to ANOVA table 4.24, the most influential factor for yield strength is current, which has a 44.85 percent with significance of 0.006. The next most influential aspect is voltage, which has a 18.80 percent contribution with significance of 0.04, followed by gas flow rate, which has an 7.50 percent contribution.

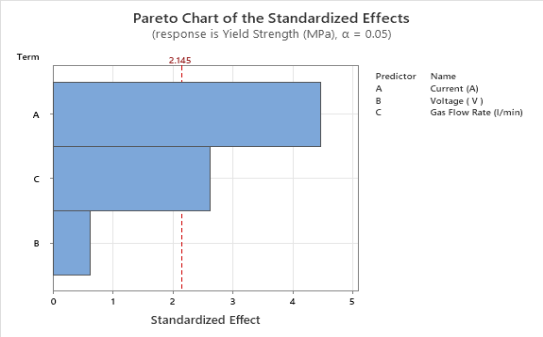

(a)

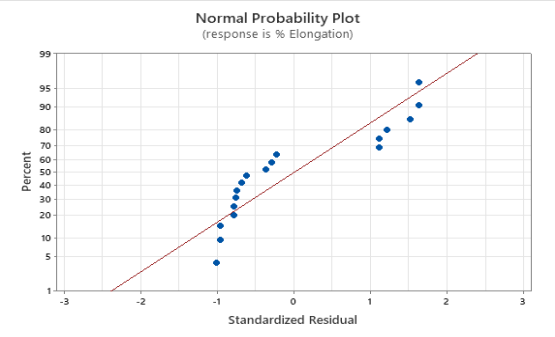

(b)

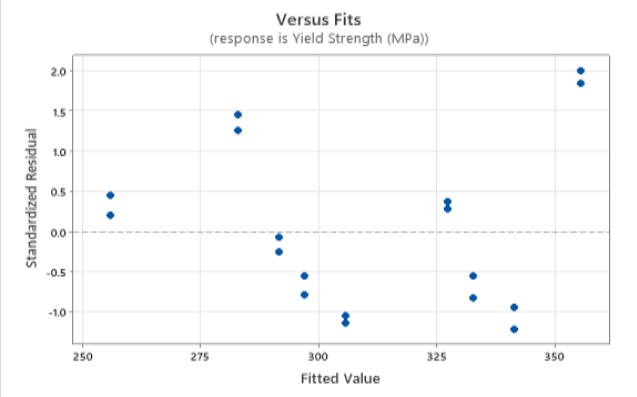

(c)

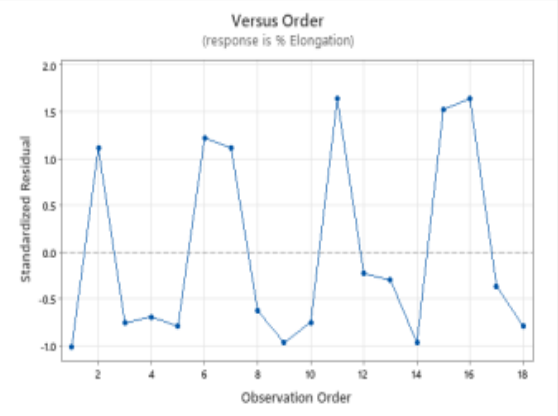

(d)

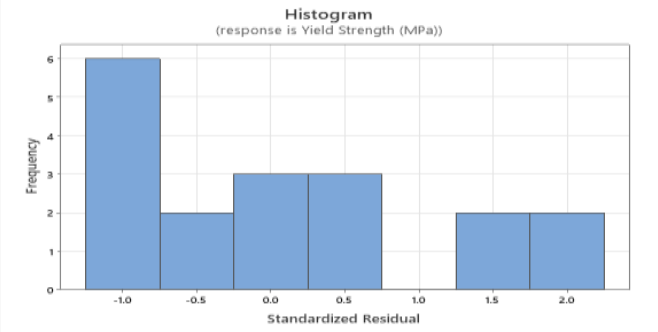

(e)

Figure 4-38 (a) Pareto Chart (b) Normal Probability Chart (c) Verses fit (d) Versus order (e) Histogram

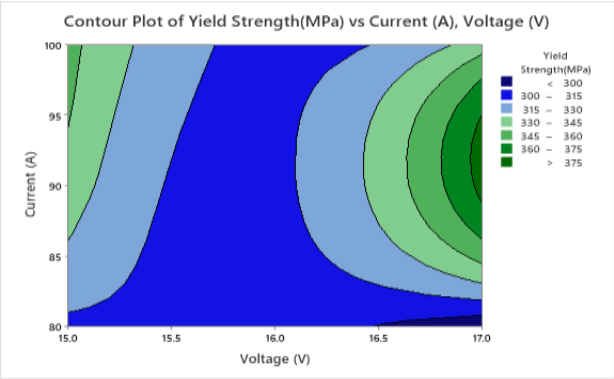

(a)

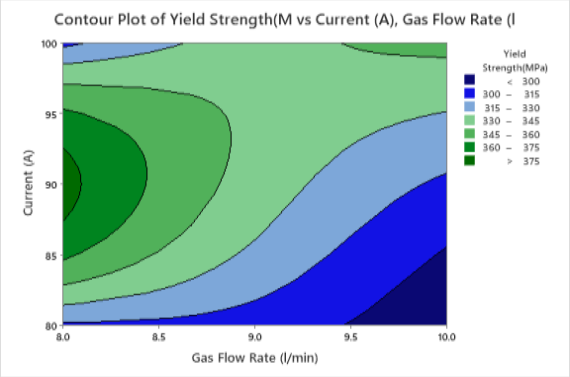

(b)

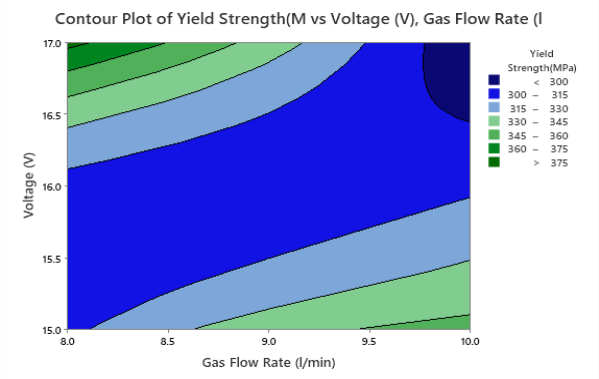

(c)

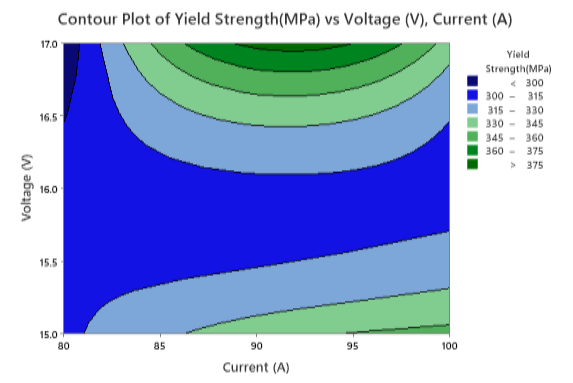

(d)

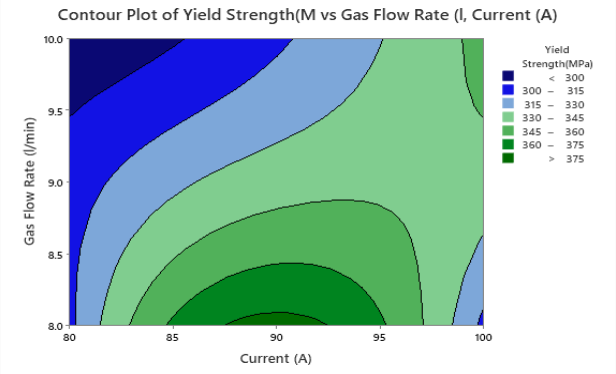

(e)

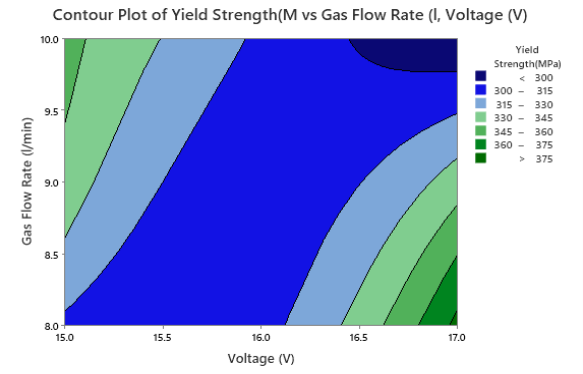

(f)

Figure 4-39: Contour plot of Yield strength (308L) (a) Current vs Voltage (b) Current vs Gas flow rate(c) Voltage vs current (d) Voltage vs Gas flow rate (e) Gas Flow rate vs Current (f) Gas Flow rate vs Voltage

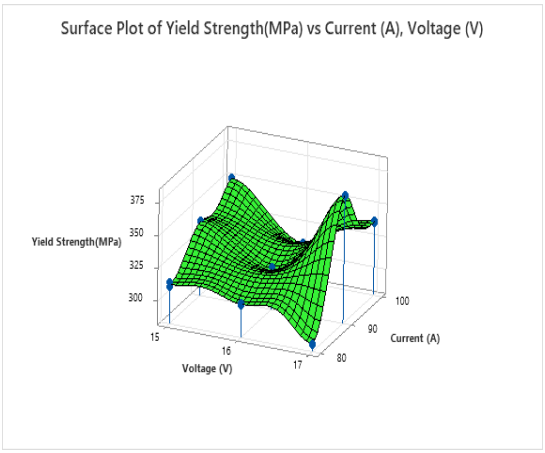

(a)

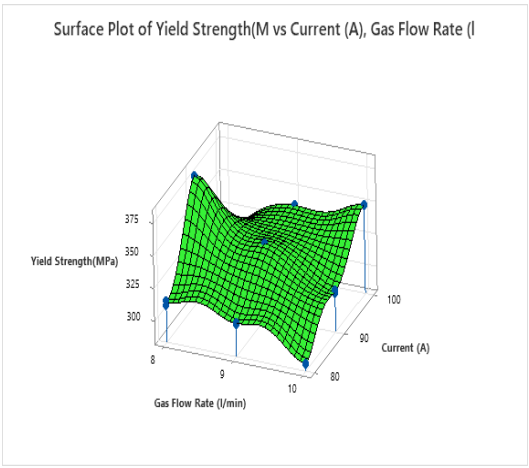

(b)

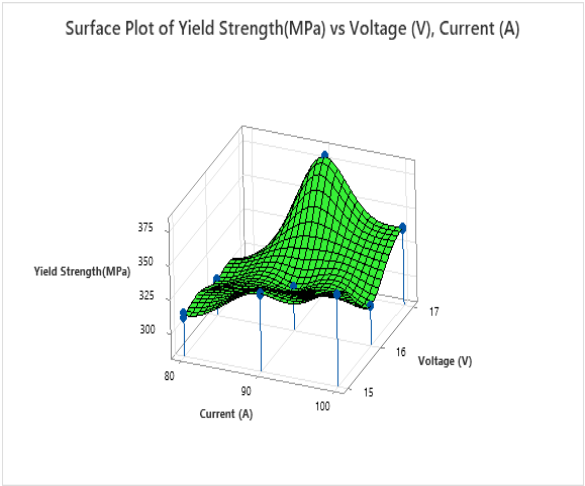

(c)

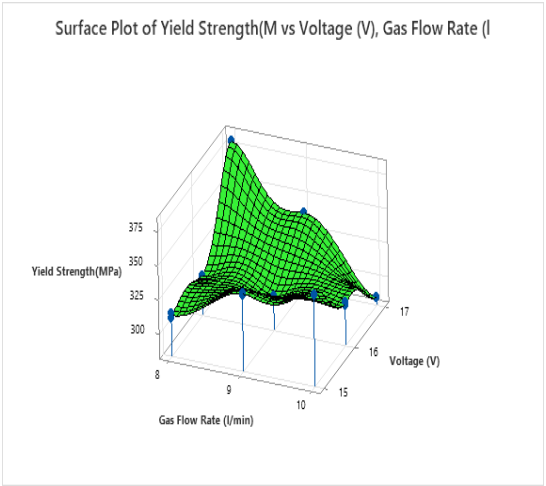

(d)

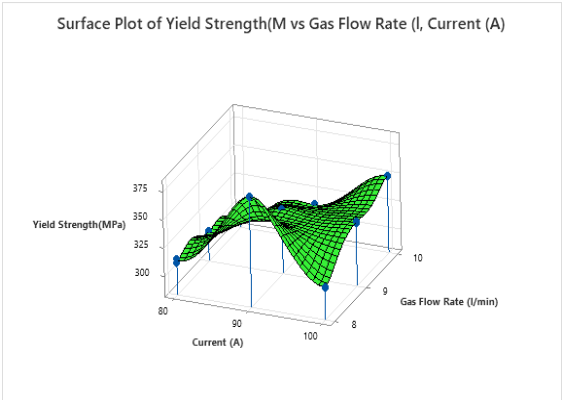

(e)

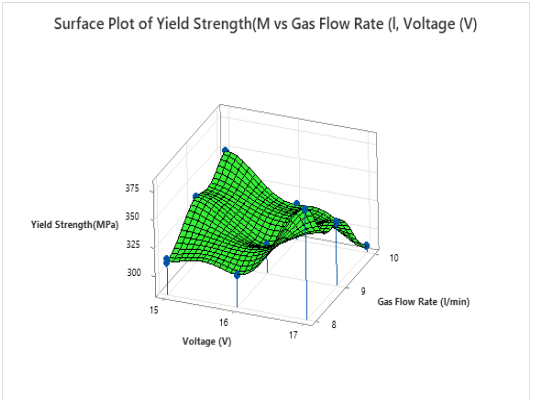

(f)

Figure 4-40: Surface plot of Yield strength (308L) (a) Current vs Voltage (b) Current vs Gas flow rate(c) Voltage vs current (d) Voltage vs Gas flow rate (e) Gas Flow rate vs Current (f) Gas Flow rate vs Voltage

4.5.1.9 Main Effect Plot of UTS (ER308L)

The signal to noise ratio of UTS of AISI 321/ER308L welded samples was calculated using MINTAB, and the results are shown in table 4.25.

Table 4.25: Signal to Noise ratio of UTS (ER308L)

Sample No	UTS MPa.	S/N ratio. dB
S-A	610	55.7066
S-B	628	55.9592
S-C	606	55.6495
S-D	661	56.4040
S-E	620	55.8478
S-F	713	57.0618
S-G	644	56.1777
S-H	669	56.5085
S-I	667	56.4825

S/N ratio main effect plot is shown in figure 4.41 response table for S/N ratio is shown in table 4.26.

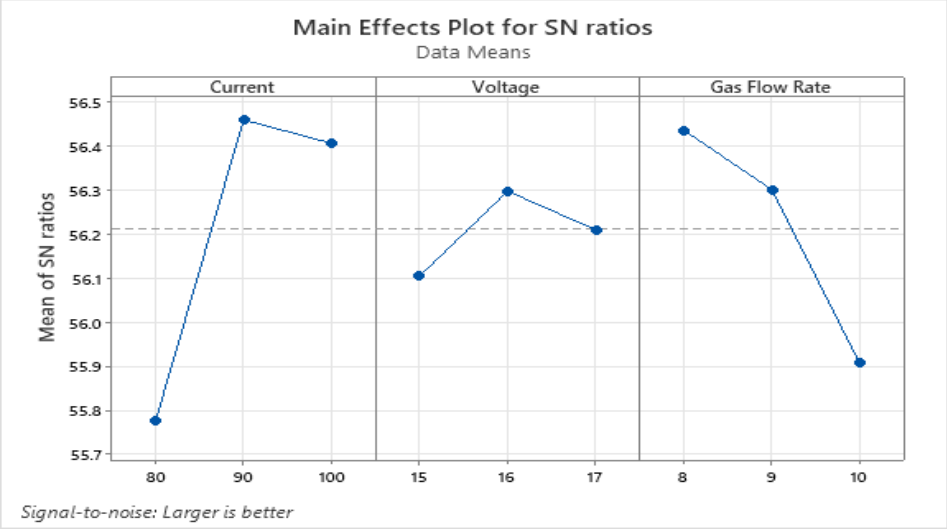

Figure 4-41: Main Effect Plot for S/N ratio

Table 4.26: Response Table for S/N Ratios (ER308L)

Level	Current	Voltage	Gas Flow Rate
1	55.78	56.10	56.43
2	56.46	56.30	56.30
3	56.40	56.21	55.91
Delta	0.68	0.19	0.53
Rank	1	3	2

According to the Taguchi approach, the best parameter will produce the highest S/N ratio. Table 4.26 and figure 4.41 show that when the arc current is kept at 90 A, the voltage is kept at 17 V, and the gas flow rate is maintained at 8 l/min, the UTS of the generated specimens is maximum, so we believe these parameters to be the best for this experiment.

4.5.2 ANOVA Analysis of UTS (308L)

Table 4.27 shows the results of the analysis of variance (ANOVA) on the data for UTS.

Table 4.27: Analysis of Variance for S/N ratio (ER308L)

Source	DF	Seq SS	Contribution	Adj SS	Adj MS	F-Value	P-Value
Current	2	9548.8	48.84%	9420.5	4710.2	11.77	0.002
Voltage	2	209.3	1.07%	407.8	203.9	0.51	0.614
Gas Flow Rate	2	5390.9	27.57%	5390.9	2695.4	6.73	0.012
Error	11	4403.5	22.52%	4403.5	400.3		
Total	17	19552.4	100.00%				

The most influential element for UTS, according to ANOVA table 4.27 is current, which has a 48.84 % contribution and current is most significant factor. Gas flow rate is the second most important factor which has a 27.57% contribution and the voltage which has a 1.07 % contribution.

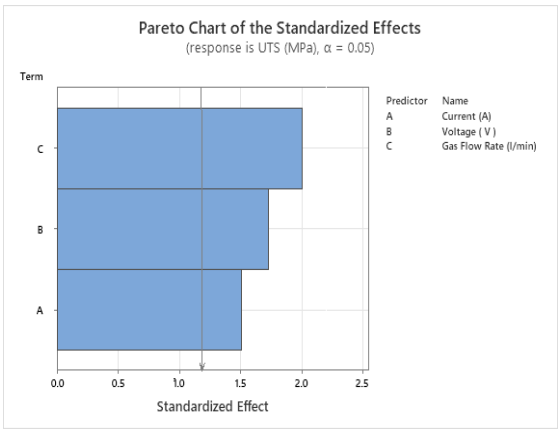

(a)

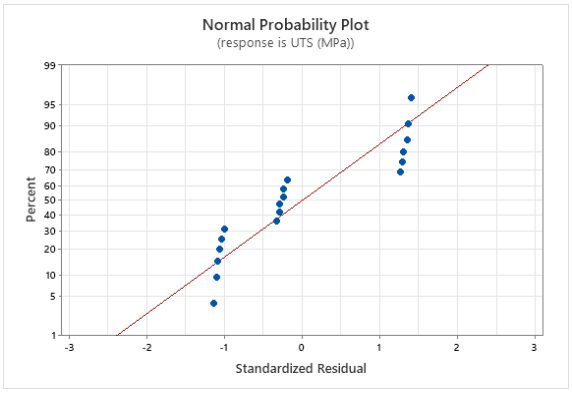

(b)

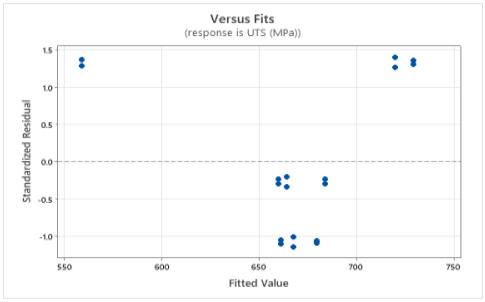

(c)

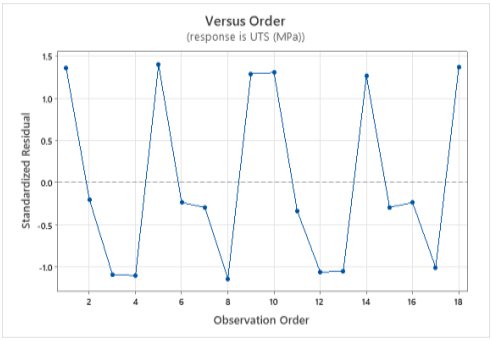

(d)

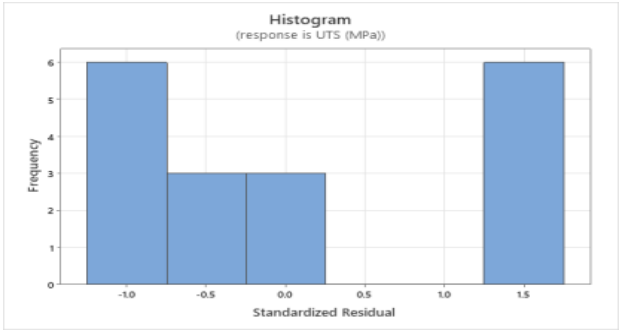

(e)

Figure 4-42: (a) Pareto Chart (b) Normal Probability Chart (c) Verses fit (d) Versus order (e) Histogram

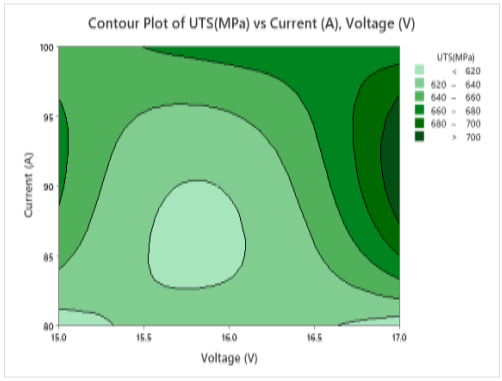

(a)

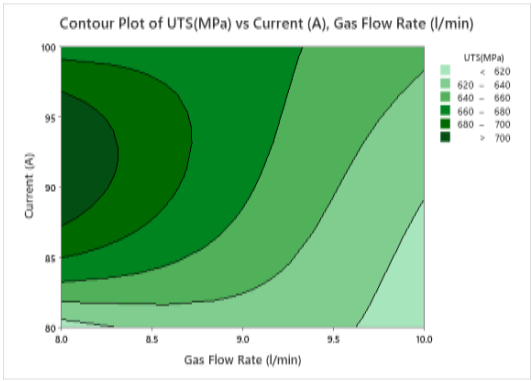

(b)

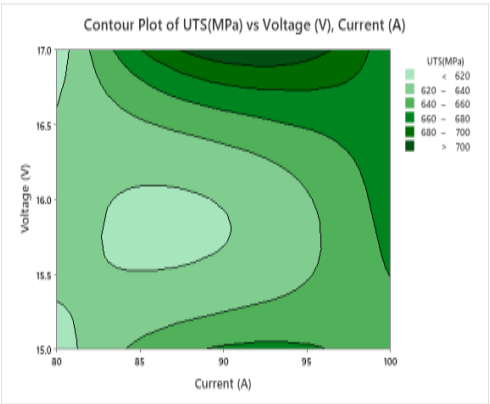

(c)

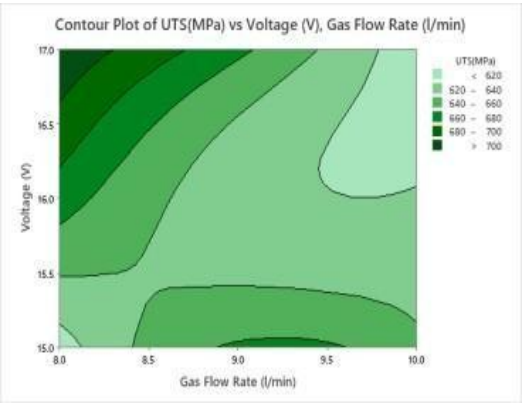

(d)

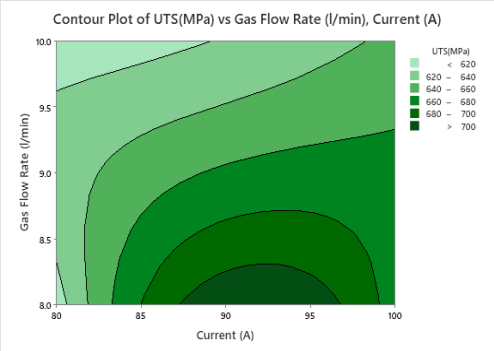

(e)

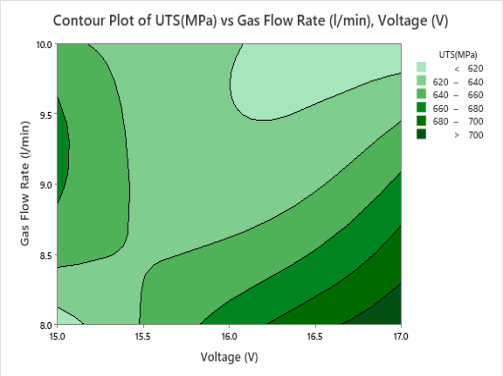

(f)

Figure 4-43: Contour plot of UTS (308L) (a) Current vs Voltage (b) Current vs Gas flow rate (c) Voltage vs current (d) Voltage vs Gas flow rate (e) Gas Flow rate vs Current (f) Gas Flow rate vs Voltage

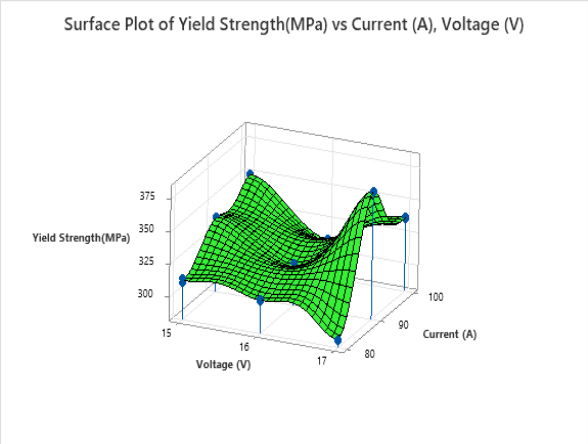

(a)

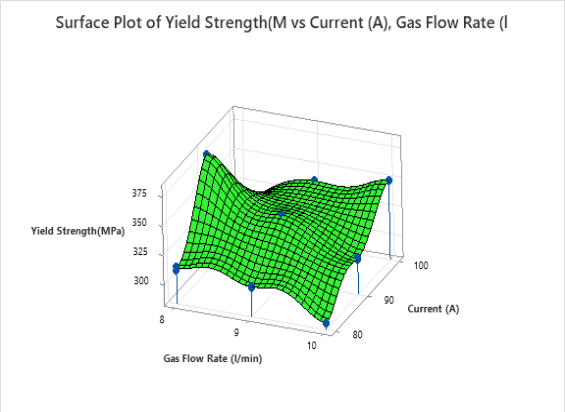

(b)

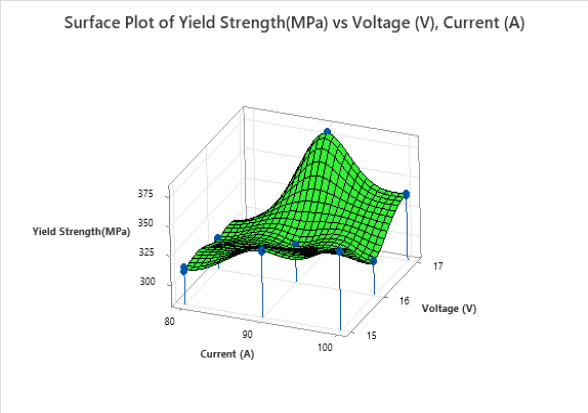

(c)

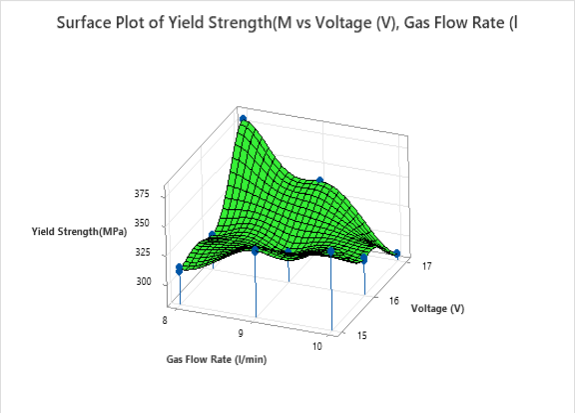

(d)

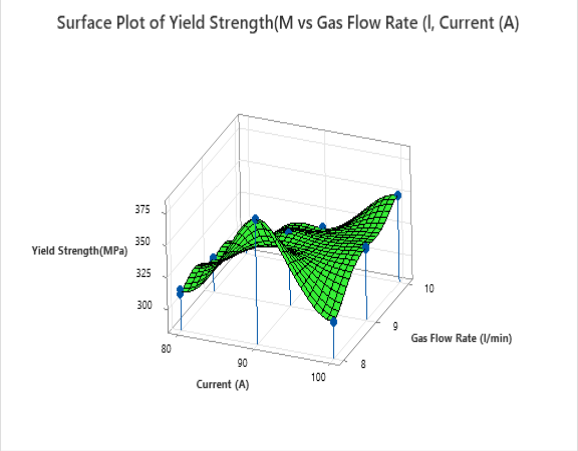

(e)

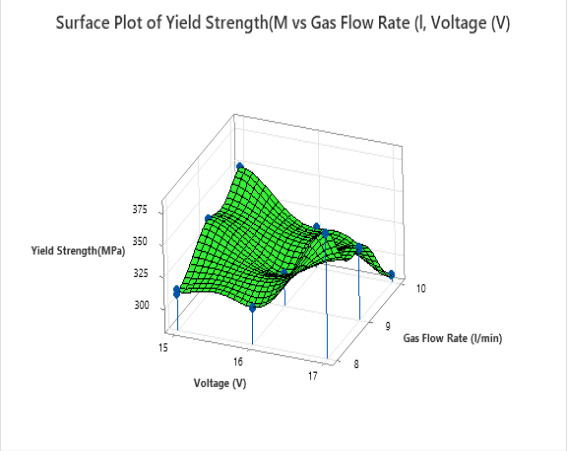

(f)

Figure 4-44: Surface plot of UTS (308L) (a) Current vs Voltage (b) Current vs Gas flow rate (c) Voltage vs current (d) Voltage vs Gas flow rate (e) Gas Flow rate vs Current (f) Gas Flow rate vs Voltage

4.5.2.1 Mean Effect Plot for % Elongation (ER308L)

The signal to noise ratio of % elongation of AISI 321/ER308L welded samples was calculating by using MINTAB, and the results are shown in table 4.28.

Table 4.28: Signal to Noise ratio of % Elongation (ER308L)

Sample No	% Elongation MPa	S/N ratio dB
S-A	35.5	31.0767
S-B	41.5	32.4127
S-C	42.0	32.5856
S-D	41.2	32.3908
S-E	44.0	32.8292
S-F	50.9	34.2016
S-G	40.0	32.1677
S-H	36.7	31.3632
S-I	38.8	31.8209

The mean effect plot for the S/N ratio is displayed in figure 4.45, and the response table for the S/N ratio is presented in table 4.29.

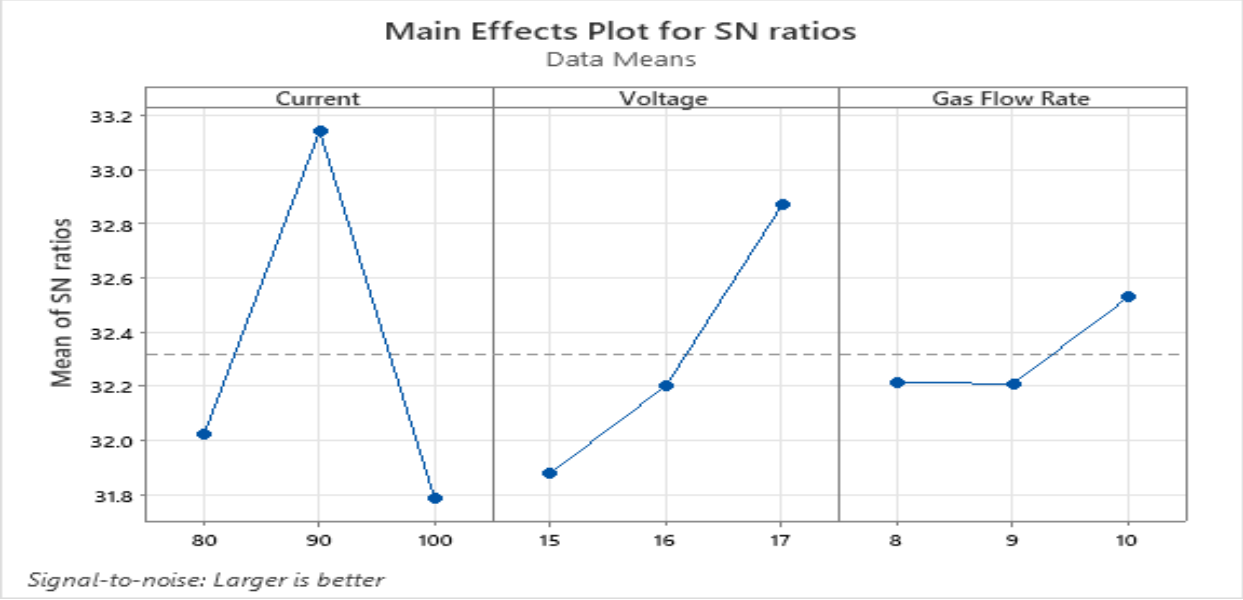

Figure 4-45: Main Effect Plot for S/N ratio

Table 4.29: Response Table for S/N Ratios (ER308L)

Level	Current	Voltage	Gas Flow Rate
1	32.03	31.88	32.21
2	33.14	32.20	32.21
3	31.78	32.87	32.53
Delta	1.36	0.99	0.32
Rank	1	2	3

The best parameter, with respect to to the Taguchi method, is the one that yields the maximum S/N ratio. Table 4.29 & figure 4.45 demonstrate that the percent elongation of the manufactured specimens is greatest when the arc current is kept at 90 A, the voltage is kept at 17 V, and the gas flow rate is held at 8 L/min, therefore we believe these settings are the optimum for this experiment.

4.5.2.2 ANOVA Analysis for % Elongation (308L)

The results of ANOVA on the data for % elongation are illustrated in Table 4.30.

Table 4.30: Analysis of Variance for S/N ratio (ER308L)

Source	DF	Seq SS	Contribution	Adj SS	Adj MS	F-Value	P-Value
Current	2	154.263	47.08%	154.263	77.1317	9.55	0.004
Voltage	2	77.310	23.59%	77.310	38.6550	4.78	0.032
Gas Flow Rate	2	7.213	2.20%	7.213	3.6067	0.45	0.651
Error	11	88.873	27.12%	88.873	8.0794		
Lack-of-Fit	2	86.063	26.27%	86.063	43.0317	137.82	0.000
Pure Error	9	2.810	0.86%	2.810	0.3122		
Total	17	327.660	100.00%				

According to ANOVA Table 4.30, the most influencing factor for percent elongation is current, which has contribution of 47.08 % The second most important aspect is voltage, which has contribution of 23.59 %,.

4.6 Responses Regression Modeling

ANOVA responses with respect to process parameters presented the significant variables. The Regression analysis method give quadratic equation for each response. These model equations are presented below

4.6.1 Predicted Model Equation for Surface Roughness (ER316L)

The equation (1) shows the predicted model for surface roughness when 316L filler wire is used.

$$\text{Surface Roughness} = 982.9 - 19.323\,X1 - 21.69\,X2 + 9.26\,X3 + 0.07600\,X1^2 - 0.300\,X2^2 - 0.562\,X3^2 + 0.3725\,X1*X2 \quad (1)$$

X1: Current (A) X2: Voltage (V) X3: Gas Flow Rate

4.6.2 Predicted Model Equation for Hardness (ER316L)

The equation (2) shows the predicted model for hardness

$$\text{Hardness (HV)} = -4826 + 184.61\,X1 - 460.2\,X2 + 116.7\,X3 - 0.7858\,X1^2 + 11.17\,X2^2 - 39.67\,X3^2 - 2.567\,X1*X2 + 36.50\,X2*X3 \quad (2)$$

X1: Current (A) X2: Voltage (V) X3: Gas Flow Rate

4.6.3 Predicted Model Equation for Yield Strength (ER316L)

The equation (3) shows the predicted model for yield strength

$$\text{Yield Strength (MPa)} = 14420 - 93.42\,X1 - 964.0\,X2 - 471.8\,X3 + 0.2142\,X1^2 + 21.17\,X2^2 + 26.08\,X3^2 + 3.233\,X1*X2 \quad (3)$$

X1: Current (A) X2: Voltage (V) X3: Gas Flow Rate

4.6.4 Predicted Model Equation for Ultimate Tensile Strength (ER316L)

The equation (4) shows the predicted model for yield strength

UTS (MPa)=12613 - 148.22 X1 + 136.6 X2 - 1382.2 X3 - 21.83 X2^2 + 106.91 X3^2 + 8.998 X1*X2 - 30.79 X2*X3 (4)

X1: Current (A) X2: Voltage (V) X3: Gas Flow Rate

4.6.5 Predicted Model Equation for % Elongation (ER316L)

The equation (5) shows the predicted model for yield strength

% Elongation=2725.9 - 12.405 X1 - 112.23 X2 - 270.85 X3 + 10.803 X3^2 + 0.7456 X1*X2 + 4.938 X2*X3 (5)

X1: Current (A) X2: Voltage (V) X3: Gas Flow Rate

4.6.6 Predicted Model Equation for Surface Roughness (ER308L)

The equation (6) shows the predicted model for surface roughness when 308L filler wire is used.

Surface Roughness=1755.9 - 19.485 X1 - 104.62 X2 - 10.91 X3 + 0.08922 X1^2 + 2.525 X2^2 + 0.2188 X1*X2 + 0.656 X2*X3 (6)

X1: Current (A) X2: Voltage (V) X3: Gas Flow Rate

4.6.7 Predicted Model Equation for Hardness (ER308L)

The equation (7) shows the predicted model for hardness

Hardness (HV)= -4826 + 184.61 X1 - 460.2 X2 + 116.7 X3 - 0.7858 X1^2 + 11.17 X2^2 - 39.67 X3^2 - 2.567 X1*X2 + 36.50 X2*X3 (7)

X1: Current (A) X2: Voltage (V) X3: Gas Flow Rate

4.6.8 Predicted Model Equation for Yield Strength (ER308L)

The equation (8) shows the predicted model for yield strength

Yield Strength (MPa)=2317 + 3.53 X1 - 547.8 X2 + 497.7 X3 - 0.09583 X1^2 + 24.083 X2^2 + 1.583 X3^2 + 0.8500 X1*X2 - 33.167 X2*X3 (8)

X1: Current (A) X2: Voltage (V) X3: Gas Flow Rate

4.6.9 Predicted Model Equation for Ultimate Tensile Strength (ER308L)

The equation (9) shows the predicted model for yield strength

UTS(MPa)= 114 + 12.52 X1 - 554.6 X2 + 995.3 X3 - 0.0583 X1^2 + 25.75 X2^2 + 1.567 X1*X2 - 3.017 X1*X3 - 46.00 X2*X3 (9)

X1: Current (A) X2: Voltage (V) X3: Gas Flow Rate

4.6.10 Predicted Model Equation for % Elongation (ER308L)

The equation (10) shows the predicted model for yield strength

% Elongation=-976.4 + 10.37 X1 + 49.07 X2 + 33.0 X3 - 0.04633 X1^2 - 0.2198 X1*X2 + 0.1419 X1*X3 - 2.900 X2*X3 (10)

X1: Current (A) X2: Voltage (V) X3: Gas Flow Rate

4.7 Model Adequacy for Quadratic Model

4.8 Experimental Validation Study

Responses optimization was done with help of Minitab software. This procedure was carried out considering the importance and desirability of the responses. To optimize the response the software provides combination of optimal parameters.

For the response of surface roughness of 316L the optimal solution provided by software is shown in figure 4.45

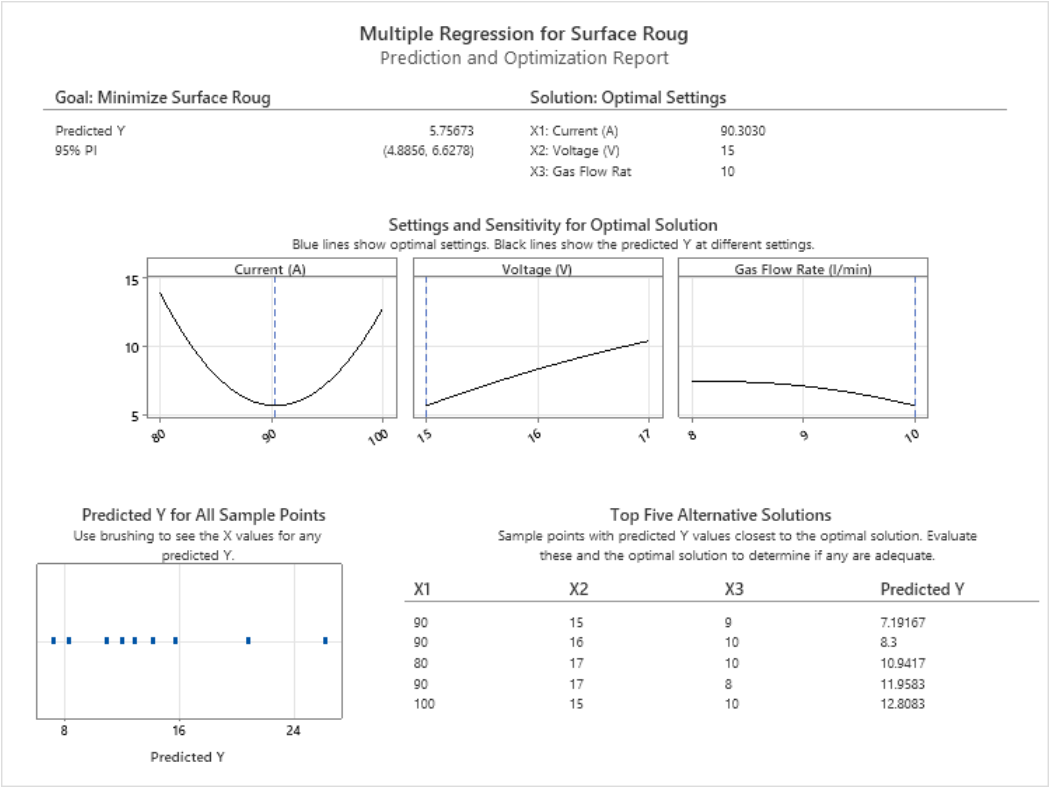

Figure 4-46: Predicted and Optimal Solution of Surface Roughness (316L)

The minimization of response variables can be represented in the form of plot, where setting of parameters for lowest responses are shown with dotted line. The plot represents the minimum value of surface roughness.

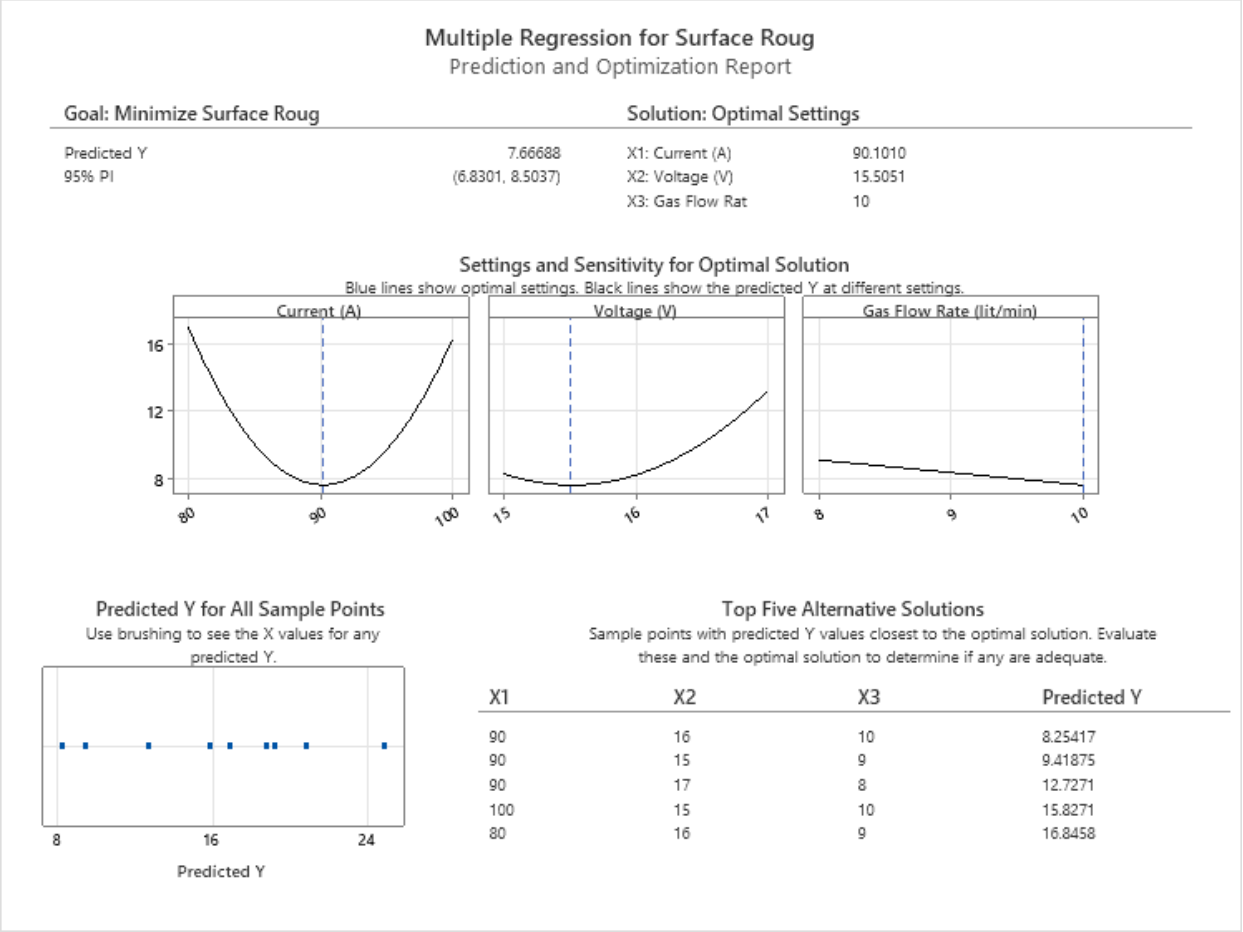

Figure 4-47: Predicted and Optimal Solution of Surface Roughness (308L)

The minimization of response variables can be represented in the form of plot, where setting of parameters for lowest responses are shown with dotted line. The plot represents the minimum value of surface roughness.

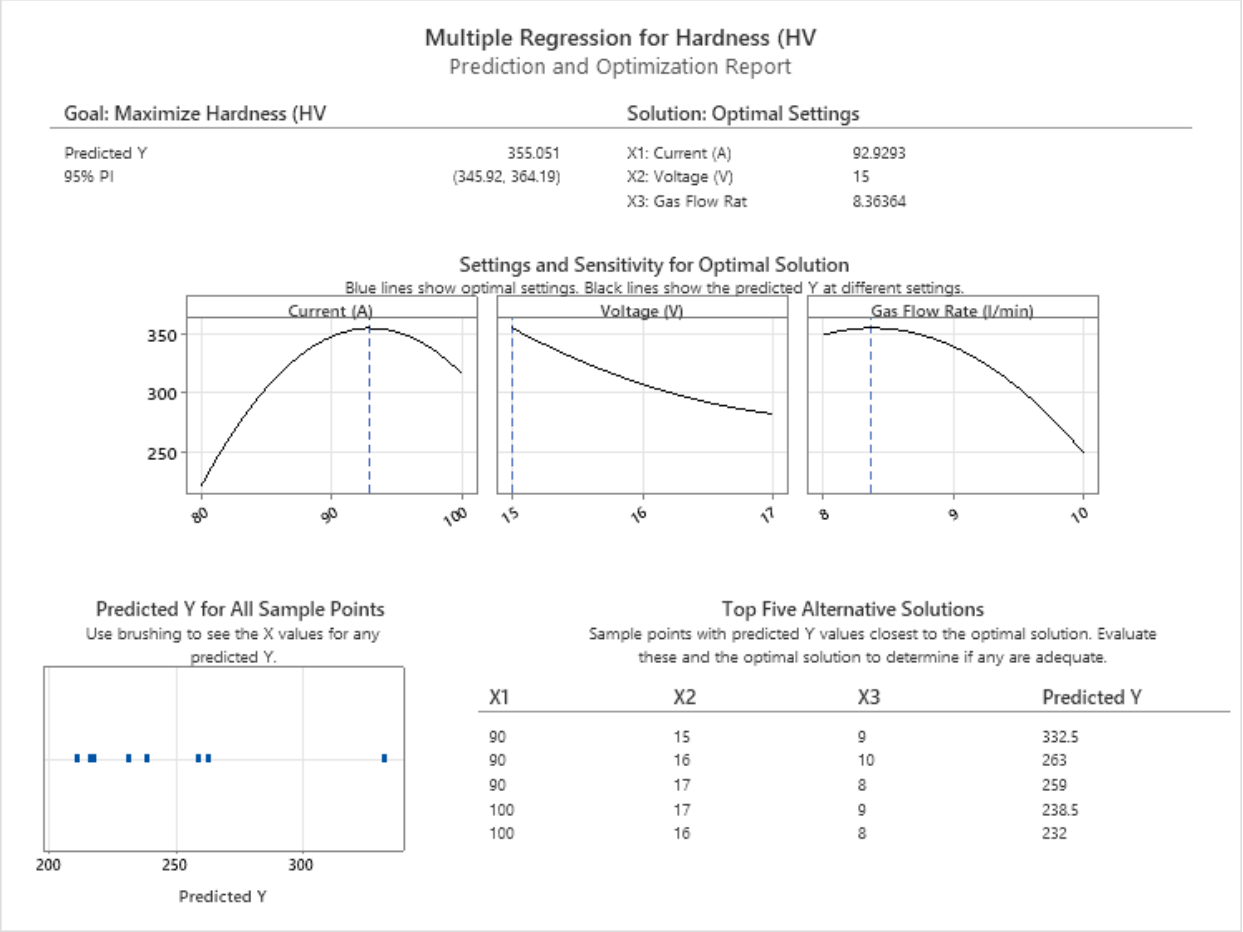

Figure 4-48: Predicted and Optimal Solution of Hardness (316L)

The maximization of response variables can be represented in the form of plot, where setting of parameters for highest responses are shown with dotted line. The plot represents the maximum value of hardness.

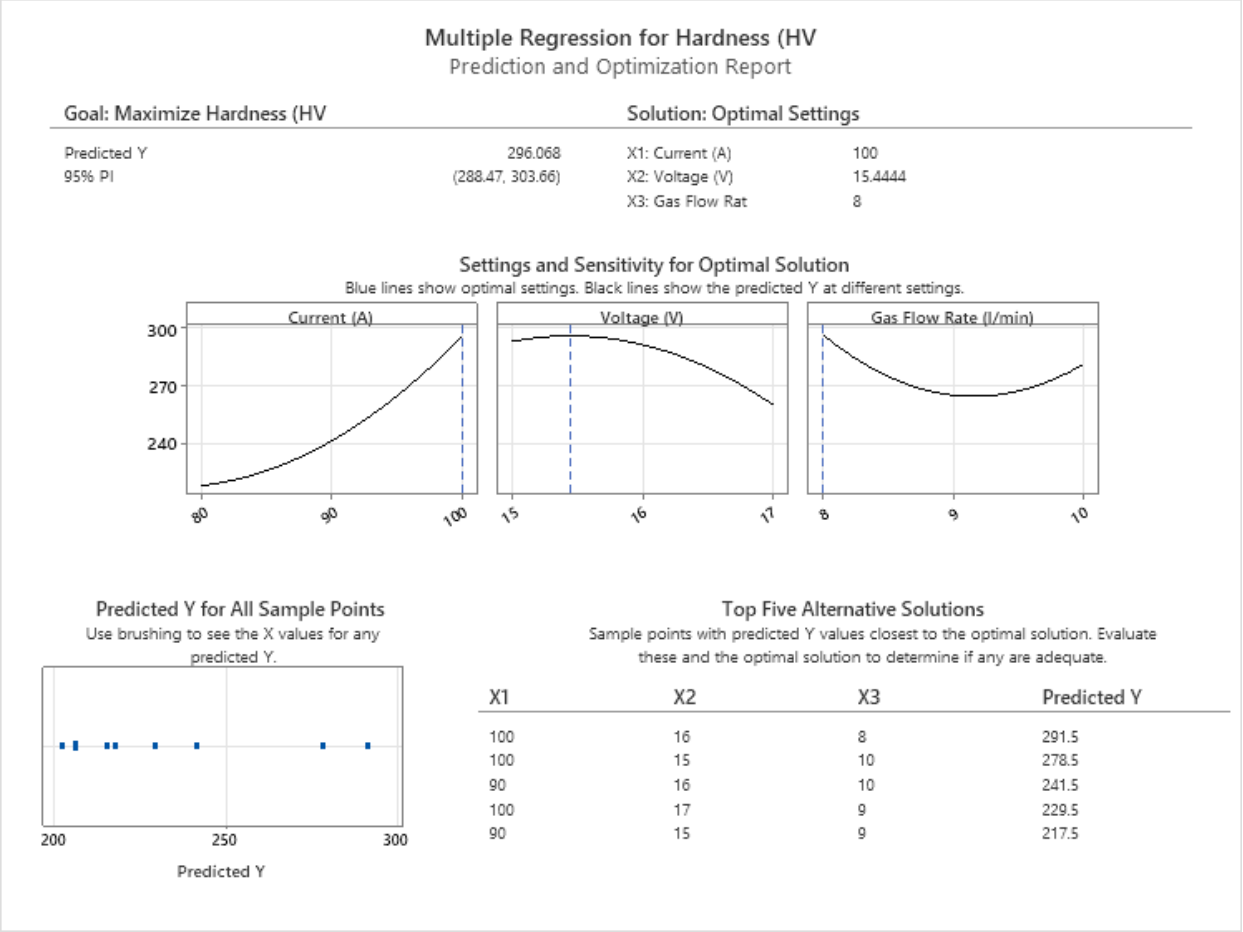

Figure 4-49: Predicted and Optimal Solution of Hardness (308L)

The maximization of response variables can be represented in the form of plot, where setting of parameters for highest responses are shown with dotted line. The plot represents the maximum value of hardness.

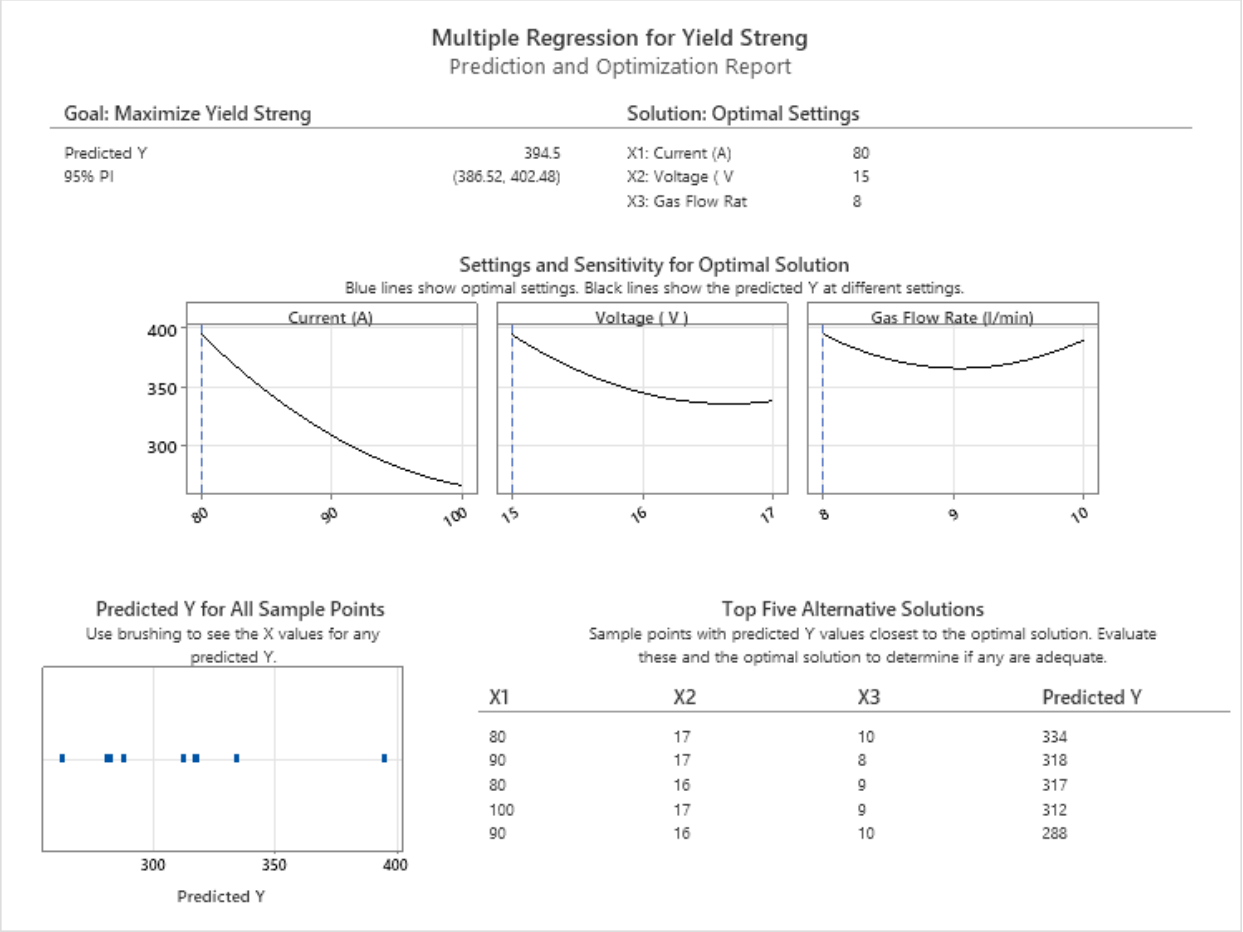

Figure 4-50: Predicted and Optimal Solution of Yield Strength (316L)

The maximization of response variables can be represented in the form of plot, where setting of parameters for highest responses are shown with dotted line. The plot represents the predicted maximum value of Yield strength.

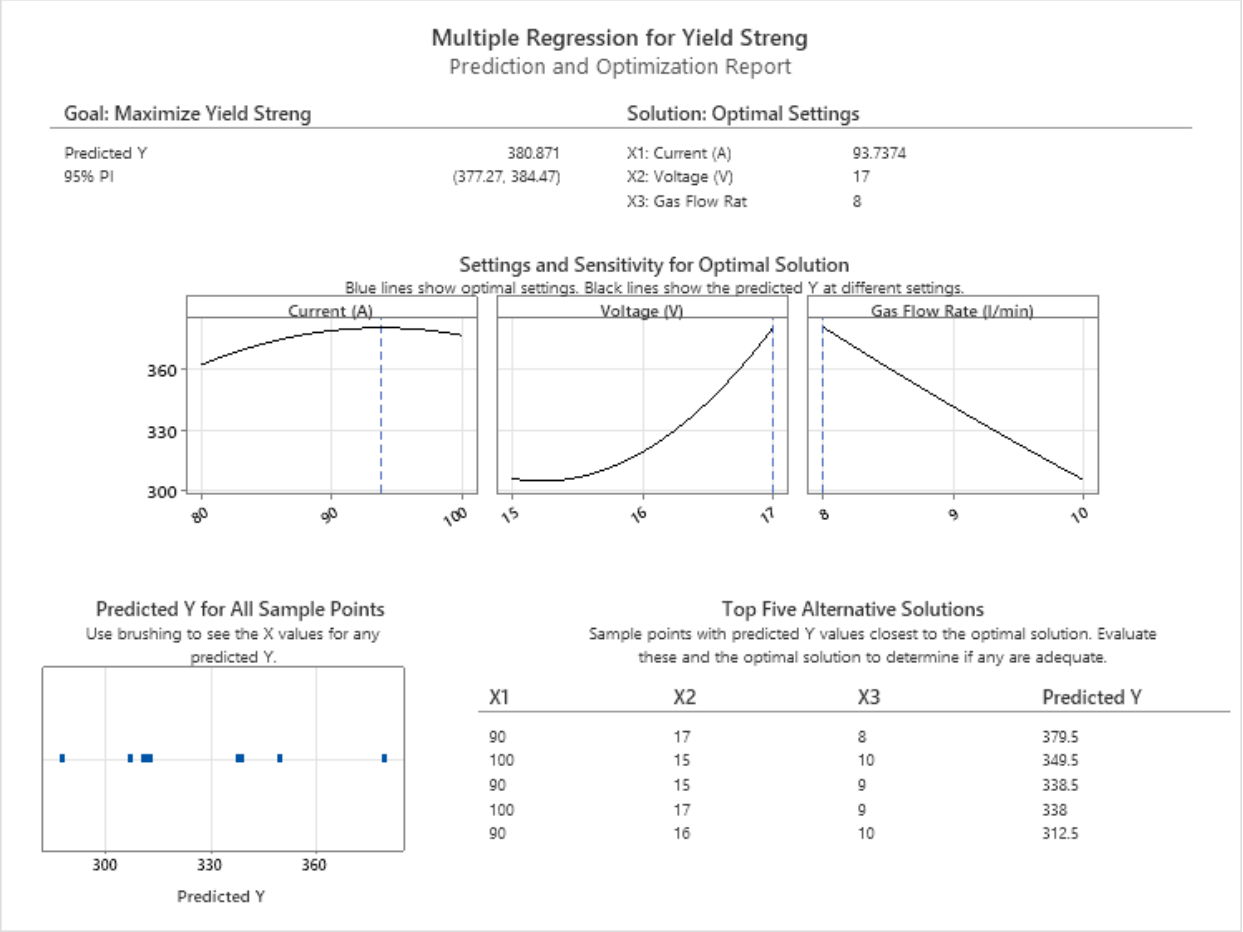

Figure 4-51: Predicted and Optimal Solution of Yield Strength (308L)

The maximization of response variables can be represented in the form of plot, where setting of parameters for highest responses are shown with dotted line. The plot represents the predicted maximum value of Yield strength.

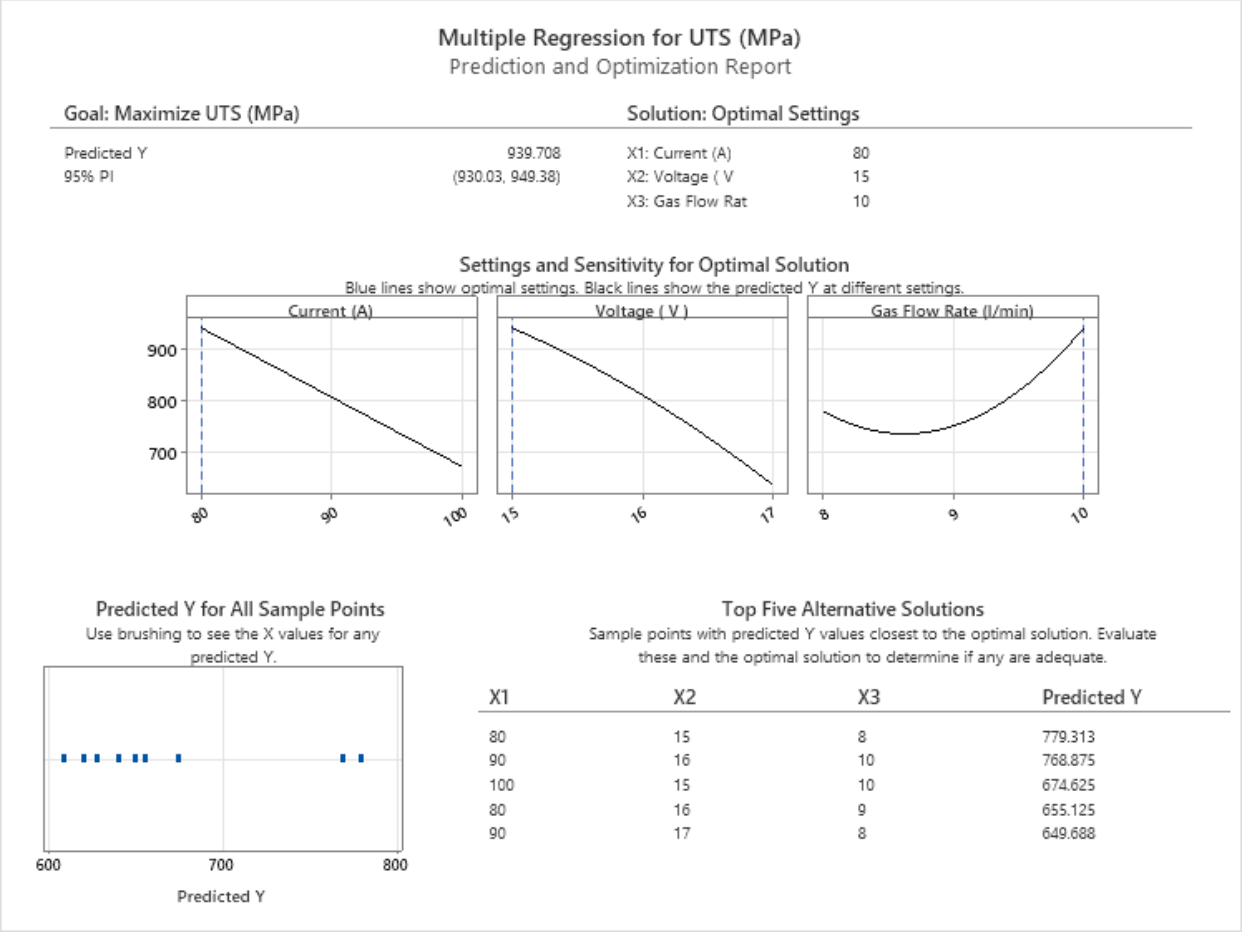

Figure 4-52: Predicted and Optimal Solution of UTS (316L)

The maximization of response variables can be represented in the form of plot, where setting of parameters for highest responses are shown with dotted line. The plot represents the predicted maximum value of UTS.

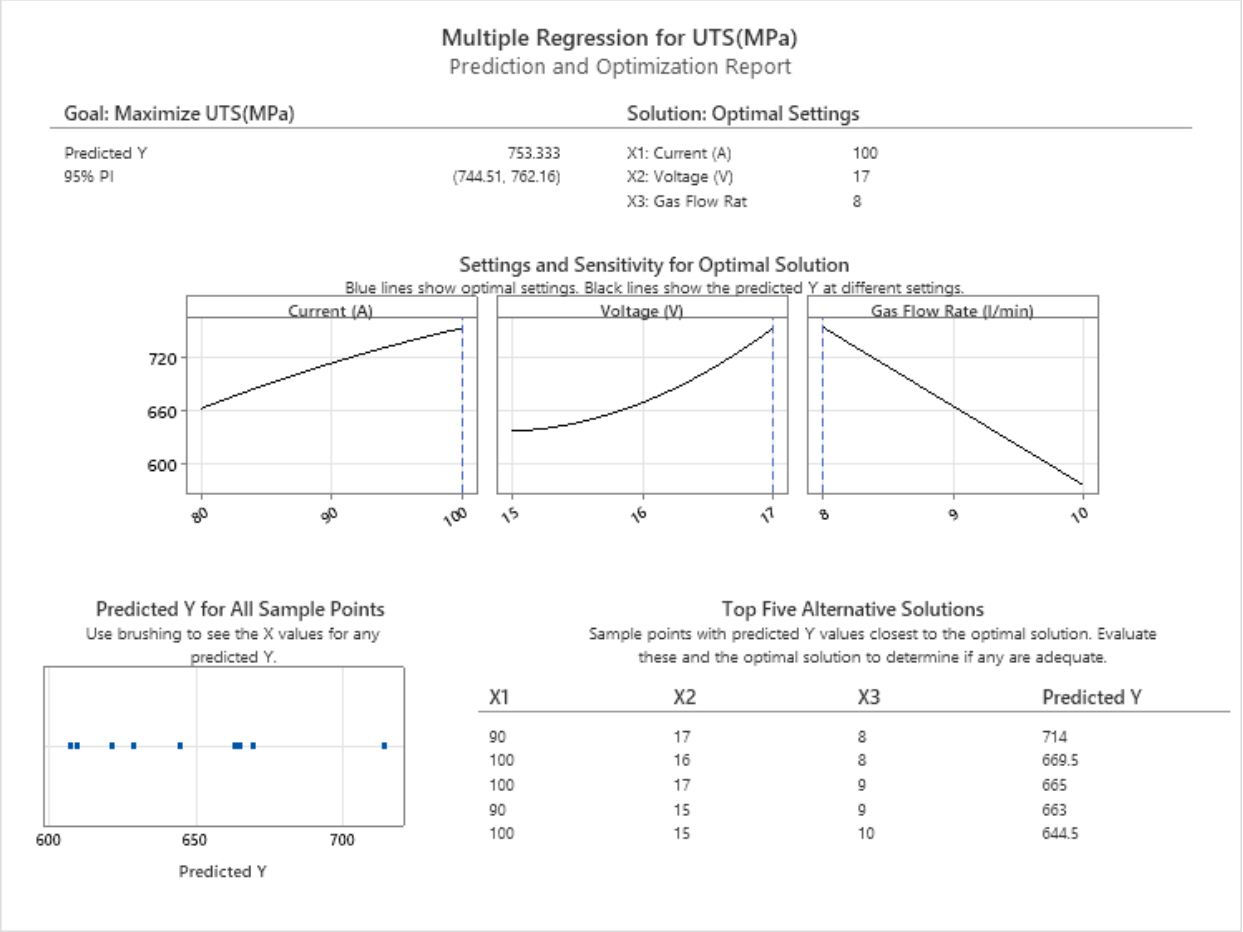

Figure 4-53: Predicted and Optimal Solution of UTS (308L)

The maximization of response variables can be represented in the form of plot, where setting of parameters for highest responses are shown with dotted line. The plot represents the predicted maximum value of UTS.

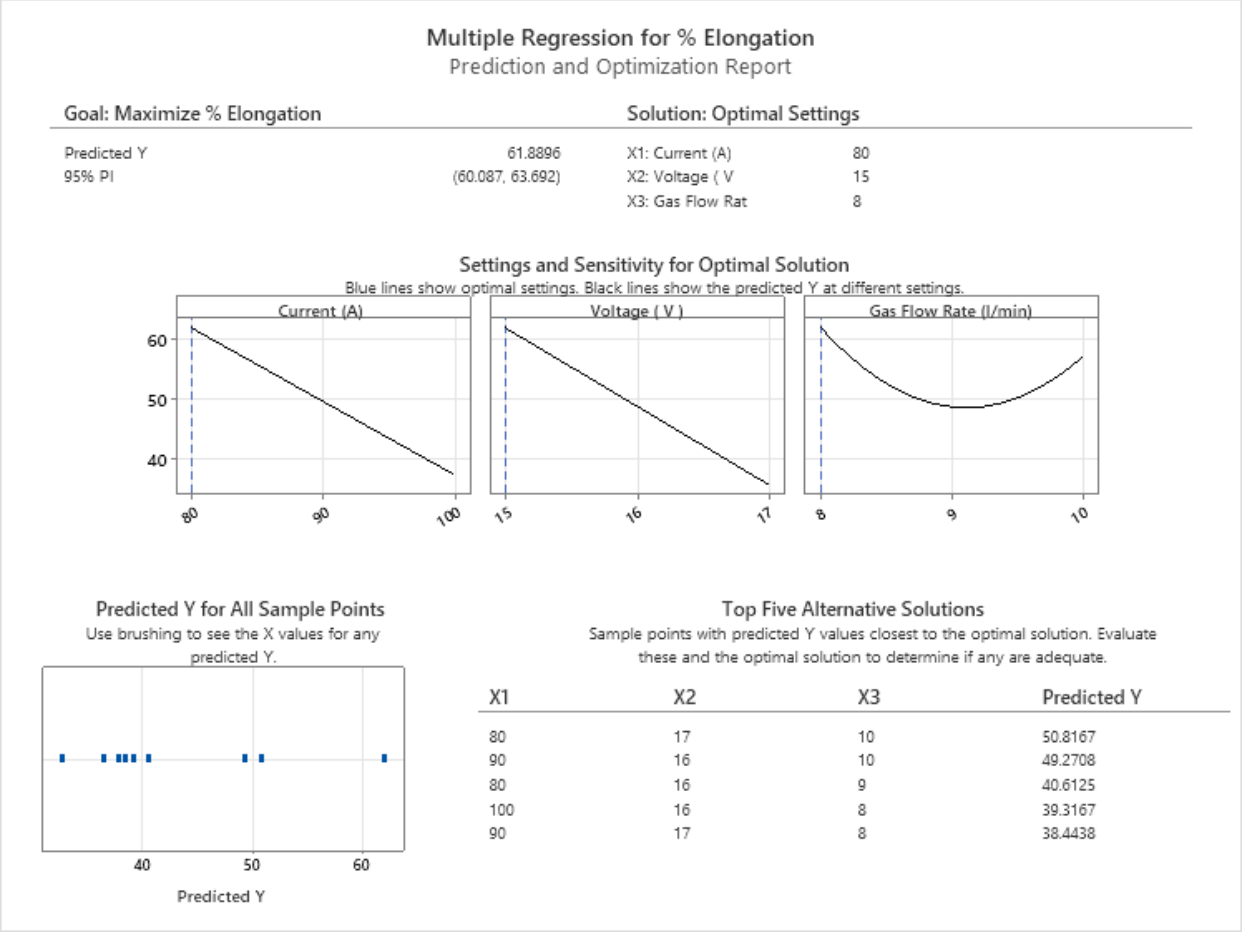

Figure 4-54: Predicted and Optimal Solution of % elongation (316L)

The maximization of response variables can be represented in the form of plot, where setting of parameters for highest responses are shown with dotted line. The plot represents the predicted maximum value of % elongation.

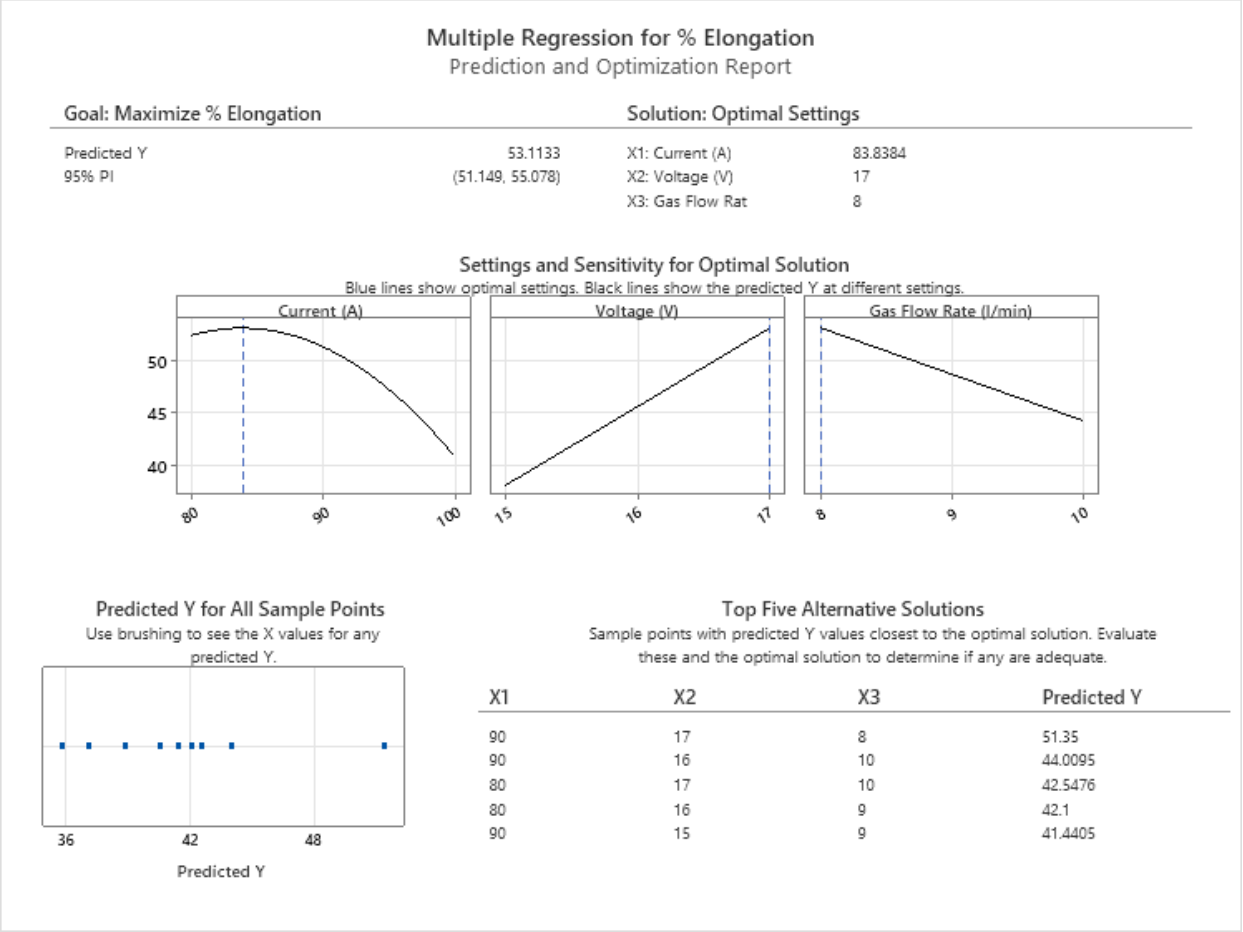

Figure 4-55: Predicted and Optimal Solution of % elongation (308L)

The maximization of response variables can be represented in the form of plot, where setting of parameters for highest responses are shown with dotted line. The plot represents the predicted maximum value of % elongation.

4.9 MICROSTRUCTURE ANALYSIS

Weldments made of stainless steel usually feature an austenitic matrix with variable grades of delta ferrite. The quantity of delta ferrite in a weld diminishes toughness, ductility, and corrosion resistance [25]. It is necessary to examine the mechanical features and microstructural studies of the joint produced by an ideal set of input parameters. The microstructural characterization of the welded samples was carried out using optical microscopic analysis after thorough metallographic preparation (Olympus BX51).The microstructure of the butt joint was captured with a 200x magnification optical microscope. The microstructures of the fusion zone, heat affected zone, and base metal zone of tungsten inert gas weld-ments (AISI321/ER316L and AISI321/ER308L) are analyzed in Figures 4.56 and 4.57 to confirm metallurgical bonding after welding. It is simple to distinguish between the f u s i o n zone (FZ), heat affected zone (HAZ) and base metal (BM). The austenite (white- γ) is a base metal, with ferrite stringers (black-δ) at the grain boundary and intermetallic compounds such as titanium carbides [26]. The heat produced through the welding process causes metallurgical alterations in welded material, particularly in the fusion zone (FZ). In welding, several characteristics like as current, voltage, speed, and temperature affect the solidification mode. These variables are the primary sources of microstructural changes in the fusion zone during welding. The Schaeffer diagram[27] is used to calculate the (Creq/Nieq) ratio. The fusion zone solidification mode may be explained by the (Creq/Nieq) ratio. This suggests that solidification begins with the creation of primary δ-ferrite, followed by the solid-state transition of ferrite into austenite. At normal temperature, the austenite in the microstructure is the result of direct solidification of the liquid metal and solid-state transition of ferrite into austenite. Furthermore, because the TIG welding process cools so quickly, the final transformation is left incomplete. There isn't enough time for δ ferrite to fully convert into austenite. Because of the high cooling rates, the samples created with low input parameters and therefore low heat input consist of skeletal δ-ferrite in plain austenitic matrix and dendritic lathy δ-ferrite at the dendrite core encircled by inter dendritic γ phase.

4.9.1 AISI321 welding with 316L at different parameters

The welded AISI321 samples have varied structures due to varying welding parameters. The AISI321 welded with 316L filler rod samples were examined. Figure 4-56 illustrate the (BM) base metal,.(HAZ) heat affected zone, and (FZ) fusion zone. The fusion area is the region between the weld and the BM, also known as the semi melting area. The weld metal transfers to the heat-affected zone at this point in the welding junction. In microstructural analysis the base metal (BM) indicates microstructure of ferrite and pearlite. In comparison to the BM and the FZ, which represents extra ferritic and low pearlite, the heat-affected zone (HAZ) exhibits coarse grains. The coarse grains have no influence on AISI321' tensile or bend characteristics. [28] The fusion zone contains austenite, ferrite, and martensite laths. This mixed mode microstructure of the weld metal is likely due to dissimilar welding junction.

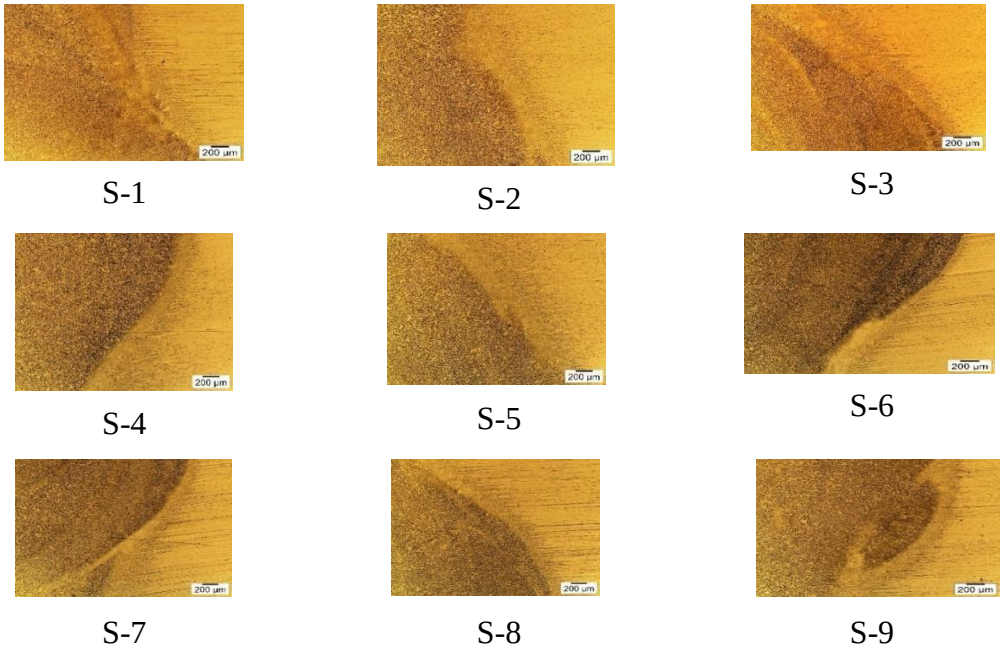

Figure 4-56: Microstructures of AISI321/ER316L

4.9.2 AISI321 welding with 308L

The different structure of the welded AISI321 samples are due to different welding parameter. Specimens of the AISI321/ER308L were analyzed. (BM) Base metal, (HAZ) Heat affected zone and (FZ) Fusion zone are illustrated in figure 4.36. In microstructure analysis of BM, ferrite and pearlite are shown. In comparison to the BM and the FZ, grain roughening had no influence on tensile and bend characteristics.[29] The finer grains in the fusion zone reflect extra ferritic and a lesser amount of pearlite. Due to the rapid solidification of the weld. Austenite, ferrite, and martensite laths are seen in the fusion zone; this combination mode microstructure of weld is due to different filler wire.

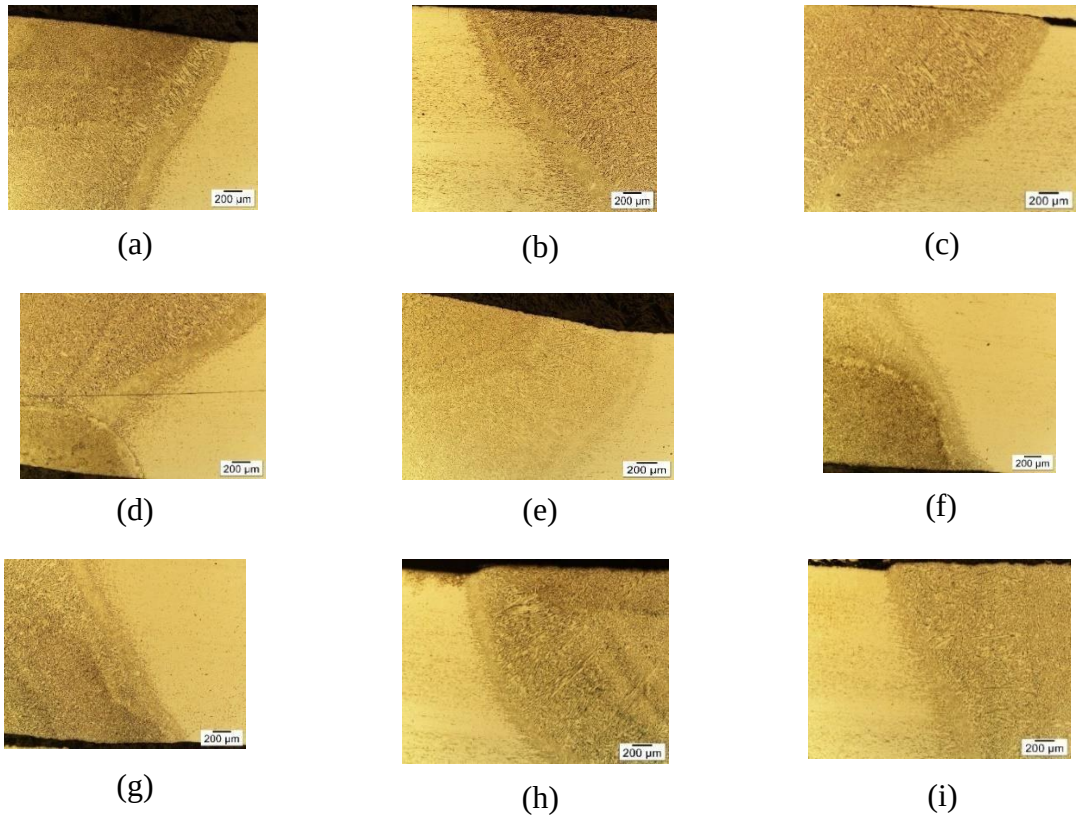

Figure 4-57: Microstructures of AISI321/ER308L

CHAPTER 5: CONCLUSION AND.RECOMMENDATION

5.1 INTRODUCTION

In current chapter optimization of welding parameter for welding of austenitic steel (AISI321) with two different filler wire was analyzed and discussed. Based on the analysis conclusion and recommendation for future work were drawn.

5.2 CONCLUSION

Surface roughness, hardness, tensile strength, yield strength and percentage elongation of AISI321 with ER316L & ER308L welded specimens was evaluated. Based on the finding it was determined that above mentioned parameters are mainly dependent on the weld current, gas flow and voltage. On the source of experimental statistics and analysis, the following outcomes are formed.

- The main factors that influence the quality of a weld joint are current, gas flow rate and voltage.
- Surface roughness of AISI321/ER316L welded specimens is good at moderate current and gas flow rates, as well as lower voltage (90A, 15V, and 9 l/min). Good surface roughness is attained for AISI 321/ ER308L welded specimens at moderate current, higher voltage, and gas flow rate (i.e. 90A, 17V, and 10 l/min). AISI321/ER316L samples had a lower surface roughness value than AISI321/ER308L welded samples, implying that AISI321/ER316L has a better surface roughness.
- Hardness of welded samples AISI321/ER316L is maximum at moderate current and gas flow and low voltage value (i.e 90A, 15V and9 l/min) whereas max. hardness of samples AISI321/ER308L is at higher value of current and lower value of voltage (i.e 100A, 16V and 8 l/min).

- AISI321/ER316L welded specimens have higher UTS and % elongation value at lower current, voltage and gas flow. Whereas, AISI321/ER308L welded specimens have higher UTS and % elongation value at moderate value of current, voltage and gas flow.
- Welded specimens AISI321/ER316L ultimate tensile strength (UTS) is found significantly greater than AISI321/ER308L, which proposes that welded specimens AISI321/ER316L has better ultimate tensile strength than that of welded specimens AISI321/ER308L.
- Welded specimens of AISI321/ER316L have much higher yield strength than those of AISI321/ER308L, implying that sample AISI321/ER316L has higher yield strength than the AISI321/ER308L samples.
- Based on the findings, 316L filler metal is the best welding material for welding of austenitic steel AISI321 at low current, voltage, and gas flow rates.

5.3 RECOMMENDATION AND FUTURE WORK

The goals of this research project have been met. However, past research suggests that more effort is needed in the future to enhance on what has already been accomplished. The following ideas have been proposed:

- To further optimize the welding parameters, the Charpy impact test should be performed on AISI 321 samples.
- Bend test should be performed on AISI321 sample to optimize the welding parameters.
- SEM will be used on every sample to evaluate the welded sample's chemistry, which may then be linked to the material's microstructure and hardness.

References

[1] American Iron and Steel Institute, „Welding of Stainless Steels and Other Joining Methods“, *NiDI Aisi*, pp. 1–46, 1988.

[2] Ö. ÇINAR, M. C. YARALI, E. ERDEMİR, B. N. ÇETİNER, A. MERGEN, and A. N. GÜLLÜOĞLU, „The Similar and Dissimilar TIG Welding of 316L and 321 Austenitic Stainless Steels“, *ALKÜ Fen Bilim. Derg.*, vol. 1, no. 3, pp. 148–155, 2019, doi: 10.46740/alku.622016.

[3] „welding types (Unit 3) 解答“, no. Unit 3, pp. 3–4.

[4] Millerwelds, „Gas Tungsten Arc Welding (GTAW)“, *Shock*, 2013. .

[5] „WHAT DIFFERENT TYPES OF ARC WELDINGS? [ADVANTAGES & APPLICATIONS]“. .

[6] „Gas Metal Arc“. .

[7] „ERW“. .

[8] *Welding Processes Handbook byK Weman*. .

[9] „The fundamentals of gas tungsten-arc welding: ; consumables; and equipment necessary for the process“. .

[10] *TIG welding booklet*. .

[11] M. Saha, „Effect of Welding Parameter of Welded Joint of Stainless Steel 304 by TIG Welding“, *SSRN Electron. J.*, vol. 201009, 2020, doi: 10.2139/ssrn.3643709.

[12] P. K. Singh, „Optimization of Tig Welding Process Parameters Using Taguchi ‟ S Anal Ysis‟‟, no. November 2017, 2018.

[13] A. Singh and R. Mittal, „Experimental Analysis on TIG welding process parameters of dissimilar metals SS304-SS202 using Taguchi Method‟‟, *Int. J. Eng. Manuf. Sci.*, vol. 7, no. 2, pp. 249–258, 2017.

[14] N. Karunakaran, „Effect of Pulsed Current on Temperature Distribution and Characteristics of GTA Welded Magnesium Alloy‟‟, *IOSR J. Mech. Civ. Eng.*, vol. 4, no. 6, pp. 1908–1916, 2013, doi: 10.9790/1684-0460108.

[15] G. B. Joseph and T. N. Valarmathi, „Improve the welding parameters for aisi 304L by TIG welding‟‟, *Int. J. Mech. Prod. Eng. Res. Dev.*, vol. 10, no. 3, pp. 633–644, 2020, doi: 10.24247/ijmperdjun202058.

[16] A. Durgutlu, „Experimental investigation of the effect of hydrogen in argon as a shielding gas on TIG welding of austenitic stainless steel‟‟, *Mater. Des.*, vol. 25, no. 1, pp. 19–23, 2004, doi: 10.1016/j.matdes.2003.07.004.

[17] N. Ghosh, P. K. Pal, and G. Nandi, „Parametric Optimization of MIG Welding on 316L Austenitic Stainless Steel by Grey-based Taguchi Method‟‟, *Procedia Technol.*, vol. 25, no. Raerest, pp. 1038–1048, 2016, doi: 10.1016/j.protcy.2016.08.204.

[18] A. Kumar and S. Sundarrajan, „Effect of welding parameters on mechanical properties and optimization of pulsed TIG welding of Al-Mg-Si alloy‟‟, *Int. J. Adv. Manuf. Technol.*, vol. 42, no. 1–2, pp. 118–125, 2009, doi: 10.1007/s00170-008-1572-8.

[19] K. Sittichai, N. Santirat, and P. Sompong, „A Study of Gas Metal Arc Welding Affecting Mechanical Properties of Austenitic Stainless‟‟, *World Acad. Sci. Eng. Technol.*, vol. 6, no.1, pp. 402–405, 2012.

[20] K. Nakata, M. Ozawa, and K. Kamo, „Temper-bead repair welding of neutron-irradiated reactor (pressure) vessels by low-heat-input TIG and YAG laser welding“, *Weld. Int.*, vol. 21, no. 7, pp. 482–495, 2007, doi: 10.1080/09507110701579621.

[21] S. Mamat, „Effect of welding heat input on microstructure and mechanical properties at coarse grain heat affected zone of ABS grade a steel EFFECT OF WELDING HEAT INPUT ON MICROSTRUCTURE AND MECHANICAL PROPERTIES AT COARSE GRAIN HEAT“, no.
December, 2015.

[22] International ASTM, „Standard Test Method for Microidentation Hardness (Knoop and Vickers) of Materials“, *E384*, pp. 1–43, 2016.

[23] S. Moore *et al.*, „Sample preparation methods for optimal HS-AFM analysis: Duplex stainless steel“, *Ultramicroscopy*, vol. 222, no. November 2020, p. 113210, 2021, doi: 10.1016/j.ultramic.2021.113210.

[24] A. E. / E8M, „E8/E8M - 15a: Standard Test Methods for Tension Testing of Metallic Materials“, *ASTM International, West Conshohocken, PA, United States*, no. C. American Society for Testing and Materials, 2015.

[25] S. Mohan Kumar, S. Sankarapandian, and N. Siva Shanmugam, „Investigations on mechanical properties and microstructural examination of activated TIG-welded nuclear grade stainless steel“, *J. Brazilian Soc. Mech. Sci. Eng.*, vol. 42, no. 6, pp. 1–21, 2020, doi: 10.1007/s40430-020-02393-4.

[26] S. Mohan Kumar and N. Siva Shanmugam, „Effect of heat input and weld chemistry on mechanical and microstructural aspects of double side welded austenitic stainless steel

321 grade using tungsten inert gas arc welding process", *Materwiss. Werksttech.*, vol. 51, no. 3, pp. 349–367, 2020, doi: 10.1002/mawe.201900063.

[27] L. Beres, „Proposed modification to Schaeffler diagram for chrome equivalents and carbon for more accurate prediction of martensite content", *Weld. J. (Miami, Fla)*, 1998.

[28] „Defects and discontinuities– ESC defects training QA/QC.", 2016. .

[29] C. Zhang, X. Song, P. Lu, and X. Hu, „Effect of microstructure on mechanical properties in weld-repaired high strength low alloy steel", *Mater. Des.*, vol. 36, no. April 2012, pp. 233– 242, 2012, doi: 10.1016/j.matdes.2011.11.016.

[30] "A Text book of Welding Technology", O.P.Khanna, Dhanpat Rai Publications, Edition 2005.

[31] "Welding processes and technology", R. S. Parmar, Khanna Publishers, ISBN No. 81-7409- 126-2.

[32] Manufacturing Technology", P. N. Rao, Tata mc-graw hill publishers, ISBN-1: 978-0-07-008798-9.

[33] "Welding Technology & Design", V.M. Radhakrishnan, New Age International publishers, ISBN: 81-224-1672-1.

[34] Kumar S. and Shahi A.S. (2011) "Effect of heat input on the microstructure andmechanical properties of gas tungsten arc welded AISI 304 stainless steel joints", Materials and Design, vol. 32, pp. 3617-3623.

[35] Choi B.H. and Choi B.K. (2008) "The effect of welding conditions according tomechanical properties of pure titanium", Journal of Materials Processing Technology", vol.201,pp. 526-530.

[36] Sivashanmugam M., Shanmugam C., Kumar. T and Kumar M. (2010), "Investigation ofMicrostructure and Mechanical properties of GTAW and GMAW Joints on AA7075 Aluminum Alloy", IEEE (978-1-4244-9082-0), pp. 241-246.

[37] Gulnec B., Develi K., Kahraman N., Durgutlu A. (2005), "Experimental study of the effect of hydrogen in argon as a shielding gas in MIG welding of austenitic stainless steel",International Journal of Hydrogen Energy, vol. 30, pp. 1475-1481.

[38] Bang Hee Seon, Bang Han Sur, Kim You chul and Oh Ik Hyun (2011), "A study on mechanical and microstructure characteristics of the STS304L butt joints using hybrid CO_2 laser-gas metal arc welding", Materials and Design, vol.32, pp. 2328-2333.

[39] Cao R., Zhu S.S., Feng W., Peng Y., Jiang F., DU W.S., Tian Z.L. and Chen J.H. (2011), " Effects of weld metal property and fraction on the toughness of welding joints of a 8% Ni 980 MPa high strength steel", Journal of Materials Processing Technology, vol. 211, pp. 759-772.

[40] Chenbin Li & Liming Liu (2012), "Investigation on weldability of magnesium alloy thin sheet T-joints: arc welding, laser welding, and laser-arc hybrid welding", International Journal of Advanced Manufacturing Technology, ref. no. DOI 10.1007/s00170-012-4145-9.

[41] Durgutlu Ahmet (2004) "Experimental investigation of the effect of hydrogen in argon as a shielding gas on TIG welding of austenitic stainless steel", Materials and Design, vol. 25, pp.19–23.

[42] Tarng Y.S. and Yang W.H. (1998), "Optimisation of the Weld Bead Geometry in GasTungsten Arc Welding by the Taguchi Method", International Journal of Advanced Manufacturing Technology, vol. 14, pp. 549-554.

[43] Kumar A. & Sundarrajan S. (2009), "Effect of welding parameters on mechanical properties and optimization of pulsed TIG welding of Al-Mg-Si alloy", International Journal

of Advanced Manufacturing Technology, vol. 42, pp. 118-125.

[44] Gharibshahiyan E., Honarbakhsh A.R., Parvin N., Rehimian M. (2011), "The effect of microstructure on hardness and toughness of low carbon welded steel using inert gas welding", Materials and Design, vol. 32, pp. 2042-48.

[45] Lothongkuma G., Chaumbaib P., Bhandhubanyong P. (1999), "TIG pulse welding of 304L austenitic stainless steel in at, vertical and overhead positions", Journal of Materials Processing Technology, vol. 89-90, pp. 410-414.

[46] ASTM E 8M-04, Standard Practice for Preparation Tension Testing of Metallic Materials (Philadelphia, PA, 2004)

[47] D. Bhattacharyya, J. Davis, M. Drew, R.P. Harrison, and L. Edwards, Characterization of Complex Carbide-Silicide Precipitates in a Ni-Cr-Mo-Fe-Si

[48] F. Huang, X.L. Hu, The Reason of Corrosion of Austenitic Stainless Steel Pressure Vessels and Prewention[J], GuangZhou Chemical Industry, 38(4) (2010) 180-181.

[49] J. Ji, Austenite Stainless Steel Weldability Brief Analysis[J], Coal Mine Machinery, 29(7) (2008) 85-86.

[50] Ramkumar KD, Patel SD, Praveen S, et al. Influence offiller metals and welding techniques on the structure–property relationships of Inconel 718 and SS 316L dissimilar weldments. Mater Des 2014; 62: 175–188